Targeting endoplasmic reticulum stress and autophagy in cancer

Thesis submitted for the degree of Doctor of Philosophy

2015

Charlotte Emily Johnson

(1264971)

Summary of thesis

SECTION A:

Student ID Number:	**1264971**
Title:	**MISS**
Surname:	**JOHNSON**
First Names:	**CHARLOTTE EMILY**
School:	**MEDICINE**
Title of Degree:	**PhD**
Full Title of Thesis	**Targeting endoplasmic reticulum stress and autophagy in cancer**

Student ID Number:	1264971

Summary of Thesis:

Mammalian/mechanistic target of mTOR complex 1 (mTORC1) regulates multiple cellular processes, including *de novo* protein synthesis, autophagy and apoptosis. mTORC1 overactivation occurs in a range of cancers and benign tumour dispositions as a result of mutations which increase mitogenic stimulus or cause malfunction of the tuberous sclerosis complex, the prime regulator of mTORC1 activity. mTORC1 overactivation results in elevated endoplasmic reticulum (ER) stress which, at low levels, elicits a pro-survival response. However, prolonged or excessive ER stress causes cell death. The present study utilised clinically relevant drug combinations to simultaneously enhance levels of ER stress and inhibit compensatory survival pathways in *in vitro* models of mTORC1 overactivity in order to cause non-genotoxic cell death. The main drugs used in this study were nelfinavir, an ER stress-inducer, chloroquine, an autophagy inhibitor, and bortezomib, a proteasome inhibitor. The key findings of this study include identification of drug combinations nelfinavir and chloroquine, nelfinavir and mefloquine, or nelfinavir and bortezomib to induce significant and selective cell death in mTORC1-driven cells, as measured by flow cytometry with DRAQ7 staining and western blot analysis for cleavage of apoptotic markers. Cell death is likely mediated through ER stress signalling, as shown by increased ER stress markers at both the level of mRNA and protein. Of interest, this study found cell death as a result of combined treatment with nelfinavir was not dependent on proteasome inhibition by nelfinavir, or autophagy inhibition by chloroquine. Additionally, nelfinavir-chloroquine-mediated cell death was completely rescued by inhibition of the vacuolar ATPase by bafilomycin-A1. In conclusion, mTORC1 overactive cells have higher basal levels of ER stress which can be manipulated with drug treatment beyond a survivable threshold, whereas cells capable of reducing mTORC1 signalling are able to survive. This study ascertained a combination of nelfinavir and chloroquine, nelfinavir and mefloquine, or nelfinavir and bortezomib, to cause effective cytotoxicity in mTORC1-driven cells.

Declaration

This work has not been submitted in substance for any other degree or award at this or any other university or place of learning, nor is being submitted concurrently in candidature for any degree or other award.

Signed …… (candidate) Date ……

STATEMENT 1

This thesis is being submitted in partial fulfillment of the requirements for the degree of **PhD**

Signed …… (candidate) Date ……

STATEMENT 2

This thesis is the result of my own independent work/investigation, except where otherwise stated.
Other sources are acknowledged by explicit references. The views expressed are my own.

Signed …… (candidate) Date ……

STATEMENT 3

I hereby give consent for my thesis, if accepted, to be available online in the University's Open Access repository and for inter-library loan, and for the title and summary to be made available to outside organisations.

Signed …… (candidate) Date ……

Acknowledgements

I would like to thank the following:

Dr Andrew Tee and Dr D. Mark Davies, for project supervision, technical and moral support.

Professor Rachel Errington and Marie Wiltshire, for the use of equipment (flow cytometer and time lapse microscope), training and help with software analysis (FlowJo and Metamorph).

Dr Elaine Dunlop for technical advice and assistance.

Dr Laura Thomas, for proof reading, moral support and friendship.

Dr Robert Thomas and Camille Fairbairn, for assistance using R software and writing scripts for generation of statistics.

I would also like to acknowledge Bethany Moody, whom I supervised for the duration of her undergraduate final project. Figures 3.1A, 4.1A, and appendices III, IV, and VIII were performed by Bethany Moody under direct supervision.

List of abbreviations

3-MA, 3-methyladenine, 4E-BP1, eukaryotic translation initiation factor 4E-binding protein 1, ACC, acetyl co-A carboxylase, AIDS, aquired immune deficiency syndome, AML, angiomyolipoma, AMP, adenosine monophosphate, AMPK, AMP-activated protein kinase, ARE, antioxidant response element, ART, antiretroviral therapy, ATF, activating transcription factor, ATG, autophagy protein, ATP, adenosine triphosphate, BAF, bafilomycin-A1, Bcl-2, B cell lymphoma 2, BTZ, bortezomib, CAMKKβ, calcium/calmodulin-dependent kinase kinase β, CEL, celecoxib, CHOP, C/EBP homologous protein, CMA, chaperone-mediated autophagy, CQ, chloroquine, DEPTOR, DEP domain-containing mTOR interacting protein, DIG, dogoxin, DMEM, Dulbecco's modified Eagle's medium, DMSO, dimethyl sulfoxide, DR5, death receptor 5, DTT, dithiothreitol, ECL, enhanced chemiluminescent, EDEM1, ER degradation enhancer mannosidase-like 1, EGFR, epidermal growth factor receptor, eIF2α, eukaryotic initiation factor 2α, ELT, Eker rat leiomyoma, ER, endoplasmic reticulum, ERAD, ER-associated degradation pathways, ERK, extracellular signal-related kinase, ETO, etoposide, FBS, fetal bovine serum, FDA, Food and Drug Administration, FKBP12, FK506-binding protein 12, RICTOR, FRB, FKBP12-rapamycin binding domain, GADD34, growth arrest and DNA damage protein 34, GAP, GTPase activating protein, GATOR, GAP activity towards Rags, GDP, guanosine diphosphate, GEF, guanine exchange factor, GRP78/BiP, glucose-regulated protein of molecular mass 78, GTP, guanine triphosphate, H2AX, H2A histone family member X, HERP, homocysteine-induced ER protein, HHV, human herpesvirus, HIF, hypoxia-inducible factor, HIV, human immunodeficiency virus, HSP, heat shock protein, IκB, Inhibitory κ B, IKK, IκB kinase, IRE1α, inositol-requiring enzyme 1α, JNK, c-jun N-terminal kinase, KS, Kaposi sarcoma, LAM, lymphangioleiomyomatosis, LAMP-2A, lysosome-associated membrane protein type 2A, LC3, microtubule-associated proteins 1A/1B light chain 3, LPV, lopinavir, MAPK, mitogen-activated protein kinase, MEF, mouse embryonic fibroblast, MDM2, mouse double minute 2 homologue, mLST8, mammalian lethal with sec-13 protein 8, MMP, matrix metalloprotease, mSIN1, stress-activated protein kinase-interacting protein 1, mTORC1/2, mammalian/mechanistic target of rapamycin complex 1/2, MQ, mefloquine, NAC, N-acetyl cysteine, NF-κB, nuclear factor-κ B, NFV, nelfinavir, Nrf2, nuclear factor (erythroid-derived 2)-like 2, NSCLC, non-small cell lung carcinoma, PARP,

poly-ADP ribose polymerase, PBMC, peripheral blood mononucleocytes, PBS, phosphate buffered saline, PERK, protein kinase-like ER kinase, PI, protease inhibitor, PI3K, phosphoinositide-3 kinase, PLD1, phospholipase D1, PP1, protein phosphatase 1, PRAS40, proline-rich Akt substrate 40 kDa, PROTOR-1, protein observed with RICTOR-1, PTEN, phosphatase and tensin homologue, PVDF, polyvinyl difluoride, Q-PCR, quantitative PCR, Rag, Ras-related GTPase, RAP, rapamycin, RAPTOR, regulatory-associated protein of mTOR, RER, rough ER, Rheb, Ras homologue enriched in brain, REDD1, regulated in DNA damage and development 1, RICTOR, rapamycin-insensitive companion of mTOR, RIPA, radio immunoprecipitation assay, ROS, reactive oxygen species, rpS6, ribosomal protein S6, RTV, ritonavir, S6K1, P70 S6 kinase 1, SEGA, subependymal giant cell astrocytoma, SEN, subependymal nodule, SER, smooth ER, SESN2, sestrin 2, SQSTM1, sequestosome 1, TAE, tris acetate EDTA, TBS, tris buffered saline, TBS-T, TBS-tween20, TNF, tumour necrosis factor, TPG, thapsigargin, TRAF2, TNF associated factor 2, TRB3, tribbles 3, TSC1/2, tuberous sclerosis complex 1/2, UPR, unfolded protein response, VEGF, vascular endothelial growth factor, v-ATPase, vacuolar ATPase, XBP1, X box-binding protein 1, XBP1s, spliced XBP1.

Contents

List of figures

List of tables

List of appendices

Chapter 1. Introduction

Cancer is a leading cause of death worldwide. Current therapies are not curative, cause high levels of patient toxicity, and generally lack a targeted approach. Identifying cancer biomarkers allows stratified treatment which produces a higher therapeutic index and a higher response rate. It is common for cancerous cells to be host to elevated levels of cellular stress due to increased proliferative rates, signalling imbalances, nutrient deprivation and DNA damage (Hanahan and Weinberg, 2011). One of the drivers of cell proliferation is mammalian target of rapamycin complex 1 (mTORC1), which is frequently upregulated in multiple cancer types due to upstream oncogenic mutation in mitogenic pathways or loss-of-function mutation in regulatory proteins, such as tuberous sclerosis complex 2 (TSC2). Rather than reducing levels of cellular stress, this study explored what effect increasing cellular stress beyond a tollerated threshold would have in genetically defined cell lines with overactive mTORC1.

1.1 mTOR

1.1.1 mTORC1

mTORC1 senses energy, oxygen and amino acid status, and is downstream of both mitogen-activated protein kinase (MAPK) and phosphoinositide-3 kinase (PI3K) mitogenic inputs. Protein and lipid synthesis, glucose metabolism, cell cycle, growth and autophagy are all regulated by mTORC1 (Fig 1.1). mTORC1 consists of the mTOR catalytic subunit, mammalian lethal with sec-13 protein 8 (mLST8), DEP domain-containing mTOR interacting protein (DEPTOR), Tti/Tel2, regulatory-associated protein of mTOR (RAPTOR) and proline-rich Akt substrate 40 kDA (PRAS40) (Laplante and Sabatini, 2012).

Amino acid accumulation within the lysosome causes the lysosomal vacuolar ATPase (v-ATPase) to undergo a conformational change which stimulates the coupled Ragulator complex to guanine-nucleotide exchange factor (GEF) activity (Zoncu *et al.*, 2011). This activates the Ras-related GTPases (Rags) and binds them to the lysosome membrane where they recruit mTORC1, bringing mTORC1 into proximity with Ras homologue enriched in brain (Rheb) GTPase (Groenewoud and Zwartkruis, 2013).

$Rheb^{GTP}$ activates mTORC1 - the exact mechanism for Rheb-mediated mTORC1 activation has not been confirmed but theories involve direct activation, whereby Rheb is bound to mTOR, and indirect activation, whereby Rheb binds to phospholipase D1 (PLD1) which then hydrolises phosphatidyl choline to phosphatidic acid (and chlorine) which binds to mTOR at the FK506-binding protein 12 (FKBP12)-rapamycin binding (FRB) domain. Both methods result in a conformational change in mTORC1, allowing binding of substrates. Primarily, the inhibitory PRAS40 is bound to RAPTOR until phosphorylation encourages its dissociation, allowing competitive binding of other substrates, including eukaryotic translation initiation factor 4E-binding protein 1 (4E-BP1).

The intracellular location of both mTORC1 and lysosomes is highly dynamic and is critical for mTORC1 activation. In nutrient abundant conditions, lysosomes migrate along microtubules adjacent to the nucleus, towards the cell periphery in order to accommodate upstream mitogenic signalling activation of mTORC1 (Pous and Codogno, 2011).

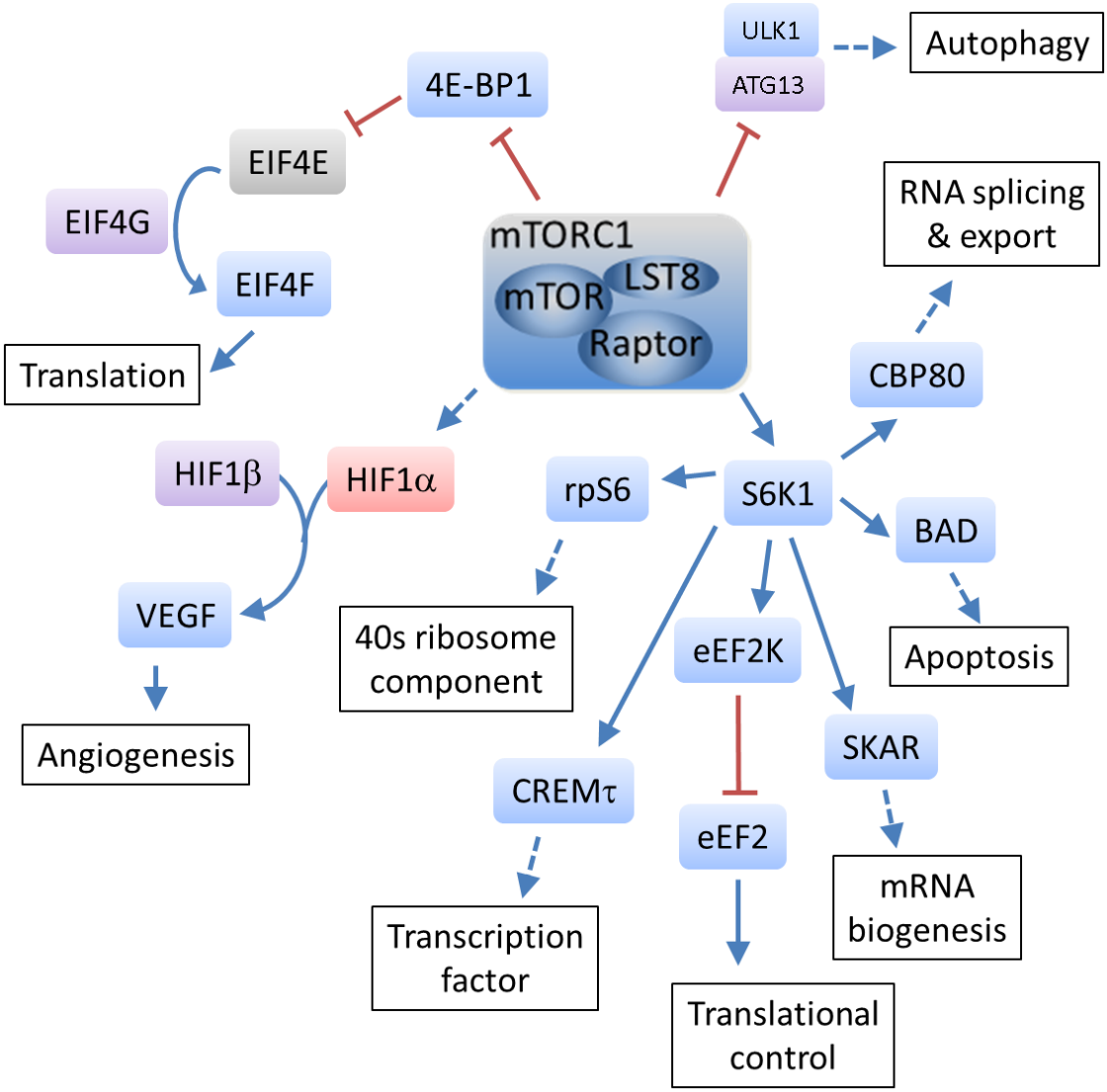

Figure 1.1: Signalling pathways and outcomes downstream of mTORC1. mTORC1 increases translation through inhibition of 4E-BP1, and increases angiogenesis through HIF1α-mediated VEGF expression. mTORC1 increases activation of S6K1 which targets many downstream pathways, including translational control and mRNA biogenesis. ULK1 is inhibited by mTORC1, reducing induction of autophagy.

1.1.2 mTORC2

As well as forming mTORC1, the mTOR catalytic subunit forms another kinase complex termed mTORC2. mTORC2 is composed of a rapamycin-insensitive companion of mTOR (RICTOR), protein observed with RICTOR-1 (PROTOR-1), stress-activated protein kinase-interacting protein 1 (mSIN1) and mLST8. As with mTORC1, mTORC2 is activated in response to growth factor stimulation, resulting in association with the ribosome. mTORC2 controls regulation of the actin cytoskeleton and has an involvement in cell survival (Dazert and Hall, 2011). Phosphorylation of Akt by mTORC2 is essential for downstream mTORC1 activation. Both mTORC1 and mTORC2 are positioned within the PI3K/Akt signalling pathway, where mTORC2 lies upstream of Akt and mTORC1 lies downstream of Akt and the Tuberous Sclerosis Complex 1 (TSC1) and TSC2 proteins.

1.1.3 TSC1 and TSC2

The tuberous sclerosis complex (TSC) is formed of the TSC1 and -2 tumour suppressor protein products of *TSC1* and *TSC2* (hamartin and tuberin, respectively). TSC1 and TSC2 form a GTPase activating protein (GAP) complex in addition to TBC1D7. Recently characterised by Dibble *et al.,* (2012), TBC1D7 primarily binds to TSC1, which prevents its degradation, before stabilising the TSC1/TSC2 heterodimer (Dibble *et al.*, 2012). TSC1/TSC2/TBC1D7 (hereafter referred to as TSC1/2) is the main effective inhibitor of mTORC1.

In mammalian cells, growth factor stimulation of the MAPK and PI3K pathways converge to inhibit TSC1/2 through extracellular signal-related kinase (ERK) and Akt-mediated phosphorylation, allowing downstream activation of mTORC1 by $Rheb^{GTP}$. Insufficient mitogenic stimulus, low energy levels or hypoxia stimulate AMP-activated protein kinase (AMPK) to activate TSC1/2 which has GAP activity towards Rheb, converting Rheb to an inactive, GDP-bound form and therefore preventing activation of mTORC1 (Fig 1.2). Consequently, loss-of-function mutations in either of the *TSC1* or *TSC2* genes causes overactive mTORC1 signalling and resultant tumour formation (Tee *et al.*, 2005). Additionally, knockdown of TBC1D7 resulted in mitogen-independent mTORC1 signalling which was not additive upon knockdown of TSC1 or TSC2, indicating the important role of TBC1D7 in the TSC1/2 complex. However, no mutations in TBC1D7 have been found in TSC patients (Dibble *et al.*, 2012).

Overactive mTORC1 signalling shares common features with hallmarks of cancer, such as advanced cell growth, differentiation and angiogenesis, as well as increasing adipogenesis and cellular metabolism. Unsurprisingly, *TSC1* and *TSC2* are both tumour suppressor genes and thus inactivating mutations are found in some sporadic cancers. *TSC1* mutations have been identified in approximately 54 % of bladder cancers (Guo *et al.*, 2013) and 4 % of clear cell renal carcinomas (Kucejova *et al.*, 2011). *TSC2* mutations were detected in 29 % of hepatocellular carcinomas (Huynh *et al.*, 2015), 3 % of urothelial carcinomas (Sjodahl *et al.*, 2011), and 57 % of pancreatic cancers (Kataoka *et al.*, 2005).

1.2 Tuberous sclerosis complex (TSC)

1.2.1 Overview of TSC

TSC is an autosomal dominant condition characterised by benign multi-organ tumours (hamartomas) including; subependymal giant cell astrocytomas (SEGAs), angiomyolipomas (AMLs), and specialised lung AMLs termed lymphangioleiomyomatosis (LAM). Affecting approximately 1.5 million people worldwide, TSC is typically diagnosed through detection of a mutation in either *TSC1* (20-30%) or *TSC2* (70-80%), alongside medical history and clinical signs. There is a tendency for *TSC2* mutations to be phenotypically more severe (Franz and Weiss, 2012). In approximately 20 % of individuals with symptoms of TSC, no mutation is identified.

1.2.2 Symptoms of TSC

Although not the most problematic, the most common symptom of TSC is the formation of facial angiofibromas and other skin tumours. The latest therapies involve a combination of topical creams, electrosurgery, laser treatment and skin resurfacing (Bae-Harboe and Geronemus, 2013, Koenig *et al.*, 2012, Weiss and Geronemus, 2010). Central nervous system abnormalities are the leading cause of death in TSC patients. Subependymal nodules (SENs) occur in 80% of TSC patients. SENs can develop into SEGAs in 5-15% of patients, typically during childhood or adolescence (Franz *et al.*, 2010). Although slow growing, SEGAs can cause potentially fatal obstruction and hydrocephalus. Additionally, up to 90 % of TSC patients can suffer from neuro-

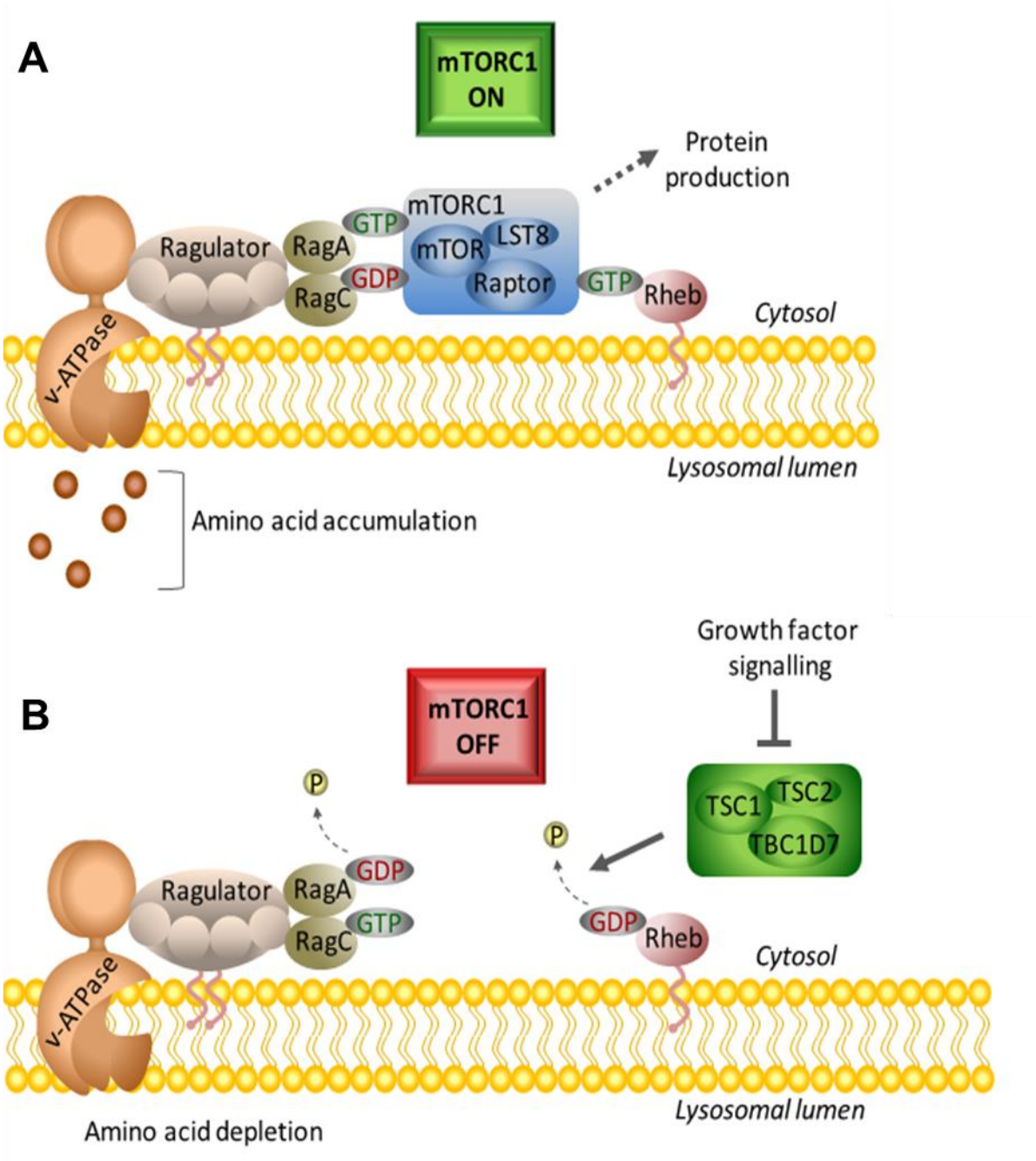

Figure 1.2: Regulation of mTORC1. A) Under nutrient and amino acid-sufficient conditions, mTORC1 is activated. Accumulation of amino acids within the lysosome causes a conformational change within the v-ATPase, allowing binding of the ragulator complex which, along with RagA/C, recruits and tethers mTORC1 to the lysosome. Further phosphorylation of mTORC1 by GTP-bound Rheb is required before activation. B) mTORC1 is inactivated when dissociated from the lysosome surface, e.g. by amino acid depletion, or when TSC inactivates Rheb. Growth factor signalling prevents activation of TSC, allowing mTORC1 activation.

cognitive defects including epilepsy, cognitive and behavioural disorders. Renal AMLs are the second leading cause of mortality in TSC, affecting approximately 75% of patients (Franz and Weiss, 2012). Composed of blood vessels, myocyte-like and adipocyte-like cells, AMLs are typically frequent in both kidneys (bilateral) and are at risk of haemorrhage when greater than 4cm in diameter. Treatment is limited to surgery through embolisation, ablation or excision in severe cases (Franz and Weiss, 2012). A severe kidney phenotype is seen in patients with the contiguous gene deletion syndrome resulting from deletions of both the *TSC2* and *PKD1* genes.

1.2.3 Lymphangioleiomyomatosis (LAM)

Predominately in premenopausal females (30-40%), LAM is defined by the appearance of smooth muscle-like cells and cysts which infiltrate lung structures, causing dyspnea and pneumothorax (Franz *et al.*, 2010). Although the cause of LAM is still unknown, it is thought to derive from AMLs which migrate to the lungs. LAM is currently untreatable and ultimately results in death from respiratory failure. LAM-associated smooth muscle cells are positive for estrogen and progesterone receptors, and lesions express vascular endothelial growth factor (VEGF)-C and -D involved in angiogenesis. Recent research found LAM nodules contain fibroblast-like cells with functional TSC2, which may contribute to development of LAM pathology by generation of a supportive microenvironment (Clements *et al.*, 2015).

1.3 Rapamycin

1.3.1 Mechanism of rapamycin

Rapamycin was isolated from *Streptomyces hygroscopicus* from a soil sample collected from Easter Island. Rapamycin was found to be a poor antibiotic but exhibited anti-proliferative and immonosuppressant activity and is currently used as an immunosuppressive treatment. Sirolimus and Everolimus are the present names for licenced rapamycin-based therapies. Rapalogues selectively inhibit mTORC1 allosterically through the formation of a ternary complex with FKBP12 (Choi *et al.*, 1996). Association of RAPTOR with mTOR weakens, inactivating downstream P70 S6 kinase 1 (S6K1) and 4E-BP1 signalling (Kohrman, 2012). Current research suggests that binding of the rapamycin-FKBP12 drug/protein complex to the FKBP12/rapamycin

binding domain of mTOR effectively reduces the accessibility of the mTOR catalytic cleft almost to the extent of capping it (Yang *et al.*, 2013).

1.3.2 Rapamycin analogues (rapalogues)

Everolimus (RAD001, an analogue of rapamycin) was recently approved for the treatment of AMLs and SEGAs and is the first choice of treatment in the NHS. Rapalogues, including everolimus, as single agents are currently in clinical trials for all aspects of TSC described above (clinicaltrials.gov NCT00790400 [LAM], NCT01730209 [Neuropsychological deficit and autism], NCT00411619 [SEGAs], NCT01853423 [Angiofibroma]). In cancer, everolimus is used for treatment of renal cell carcinoma, advanced breast cancer, pancreatic cancer and astrocytoma and a Phase II clinical trial for everolimus for treatment of cancers specifically with *TSC1* or *TSC2* mutation has recently begun (clinicaltrials.gov NCT02201212). Rapalogues are being trialled in combination with conventional therapies or small molecule inhibitors in a wide range of cancers: there are currently 281 open studies with an additional 358 having already been completed (clinicaltrials.gov).

In some TSC patients, LAM tumours and SEGAs regressed but regrowth occurred after treatment cessation (Bissler *et al.*, 2013, Franz *et al.*, 2006). Some rare tumour legions within renal cell carcinoma appear resistant to rapamycin treatment and can even be present amongst other, rapamycin sensitive legions within the same kidney. Furthermore, prolonged treatment of some rapamycin-sensitive tumours still retain rapamycin-insensitive cells, which contribute to tumour recurrence (Jozwiak *et al.*, 2006). Clinical therapies using rapalogues indicate that inhibition of mTORC1 is cytostatic rather than cytotoxic, and requires continuous treatment to prevent regrowth. This highlights the importance of new drug therapies that selectively kill tumour cells rather than repress growth. One potential new line of therapy is to target existing cell stress pathways within tumour cells that lack functional TSC1/2. TSC1/2-deficient cells have a high endoplasmic reticulum (ER) stress burden and a defective response to ER stress, which can be targeted to induce cell death (Siroky *et al.*, 2012, Ozcan *et al.*, 2008). This study investigated the use of a clinically relevant ER stress-inducing agent, nelfinavir (Viracept, Roche), which is minimally toxic in humans. Nelfinavir will be discussed further in chapter 3.

1.4 The ER

The ER was discovered by a group of electron microscopists led by Keith R. Porter in the 1940's and was named for its lacy, net-like structure and location within the cell (Porter, 1953). It was later classified further into either rough (RER) or smooth (SER) membranes, which are visually and functionally distinct. RER is defined by membrane-bound ribosomes and is concerned with synthesis, folding, and post-translational modification of proteins. The absence of ribosomes defines SER, where sterols and lipids are synthesised. The SER is also involved in macromolecule delivery chiefly through vesicle budding and fusion, and direct contact with other organelles (Voeltz *et al.*, 2002). The ratio and extent of RER to SER is highly dependent on cell type e.g. specialised cells such as adrenal cells secreting steroids require a large amount of SER (Shibata *et al.*, 2006). Both RER and SER share a continuous membrane but are spatially separated within the cell, where RER is primarily found localised to the nucleus and SER is located more distally.

Impaired ER homeostasis causes ER stress. Quality control allows only correctly folded proteins to be exported to the golgi, whereas incomplete or misfolded proteins are retained within the ER for completion or to be targeted for degradation. Defects in any of the transport, sorting or folding stages can result in retention of protein within the ER and this is associated with a number of ER storage diseases including cystic fibrosis, albinism, and osteogenesis imperfecta. ER storage diseases cover a wide clinical spectrum due to the large range of mutations, which can occur in any cell type (Rutishauser and Spiess, 2002). ATP-dependent chaperone proteins assist in protein folding and are upregulated by stress conditions to facilitate clearance of protein aggregates. Failure to pass quality control results in one of two ER-associated degradation (ERAD) pathways, an ubiquitin/proteasome pathway and an autophagic/lysosomal pathway. Insufficient amelioration of ER stress results in cell death (Healy *et al.*, 2009).

1.5 ER stress

1.5.1 Overview of ER stress

In addition to excessive amounts of unfolded proteins, nutrient deprivation, dysfunction of calcium regulation, mutational load and oxidative stress or hypoxia can cause ER stress. The effects of ER stress are not localised to the ER alone but are spread to interacting organelles and throughout the cell as the required functional protein products are not produced. The initial ER stress response is prosurvival – to reduce misfolded protein load and restore cellular homeostasis. However, cumulative unresolved ER insult results in a switch to programmed cell death to minimise the chances of damage to surrounding cells through necrosis, and also to prevent passing any accumulated genetic defects to daughter cells. The pro-survival arm of ER stress has the following functions: to increase protein folding capacity, to decrease protein synthesis on transcriptional and translational levels, and to upregulate misfolded protein clearance through ERAD pathways.

Molecular chaperones, including foldases, heat shock proteins (HSPs), and lectins (calnexin, calreticulin and EDEM), are upregulated in response to ER stress in order to enhance protein folding and expand the ER itself to increase protein turnover. Under normal conditions, these molecular chaperones fold proteins into their final structures and undergo post-translational modifications, but during stress primarily help to refold misfolded proteins or to reduce aggregation. Generally, misfolded proteins are recognised by molecular chaperones through exposed hydrophobic regions which would normally be hidden in the native state (Schroder and Kaufman, 2005).

A series of signalling pathways function to inhibit protein synthesis and promote protein clearance: upon accumulation of misfolded proteins, glucose-regulated protein of molecular mass 78 (GRP78, or BiP) binds to unfolded proteins, allowing activation of protein kinase-like ER kinase (PERK), inositol-requiring enzyme-1α (IRE1α) and activating transcription factor-6 (ATF6). PERK, IRE1α, and ATF6 recognise ER stress and initiate compensatory responses (Fig 1.3).

1.5.2 BiP

BiP is a HSP70 class molecular chaperone with a *C*-terminal binding domain and an *N*-terminal ATPase. Identified alongside GRP94 in the mid 1970s, this group of proteins

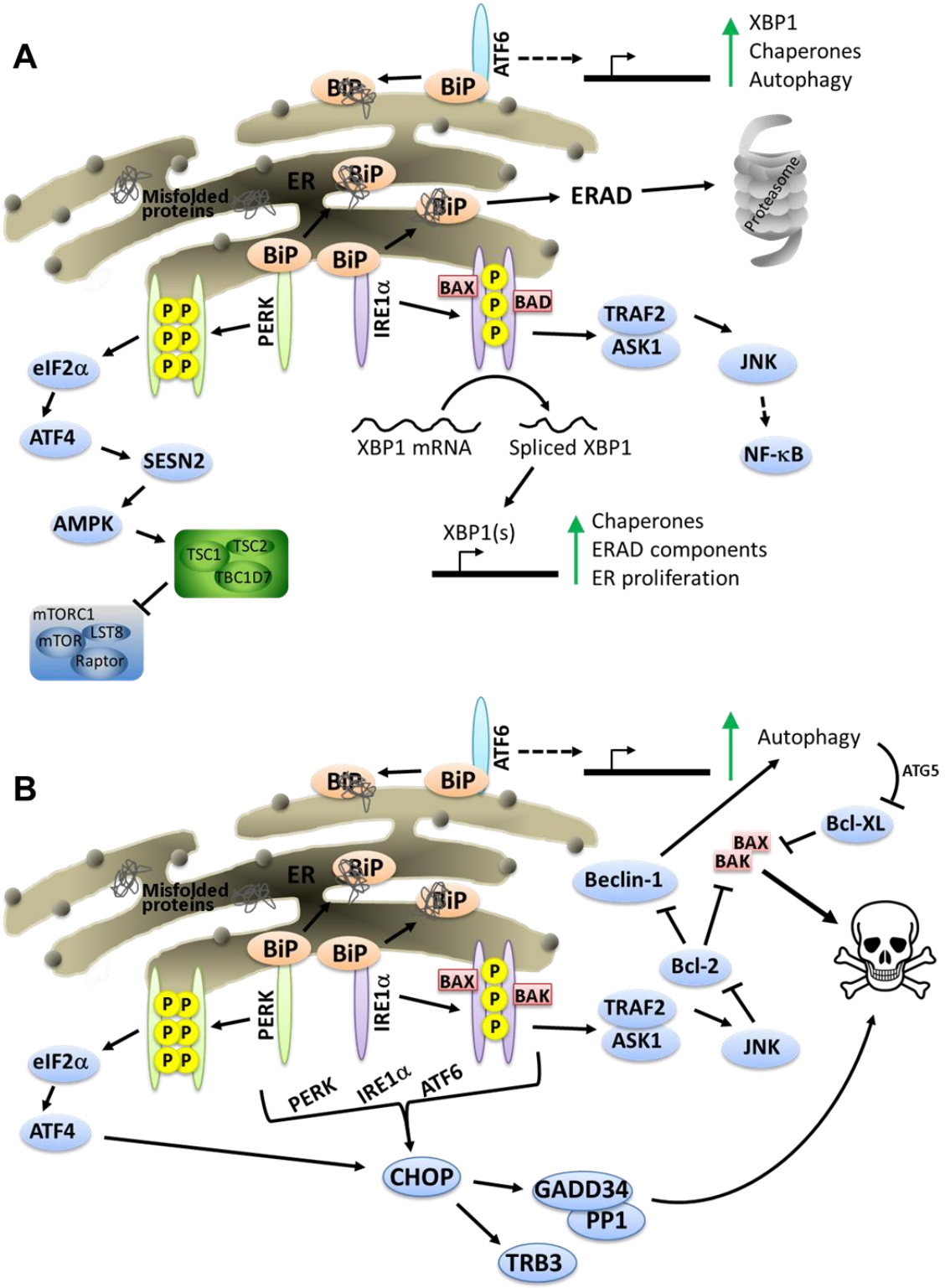

Figure 1.3: ER stress signalling. ER stress triggers 3 main signalling arms through PERK, IRE1α, and ATF6. A) The initial ER stress response is pro-survival, upregulating autophagic and proteasomal degradation pathways, reducing mTORC1-mediated protein synthesis, and increasing NF-κB. B) Prolonged or excessive ER stress switches to a pro-death response, principally mediated by CHOP and GADD34-induced apoptosis.

were named after their induction following depletion of glucose (Lee, 1987). BiP was later so termed after another group found it to be associated with the ER and that it bound Ig heavy chains (Haas and Wabl, 1983). Multiple studies investigating the role of BiP helped to elucidate its role in ER stress (Gething and Sambrook, 1992), with BiP being the initiator of the unfolded protein response (UPR) upon unfolded protein accumulation in the ER.

1.5.3 PERK

PERK is a transmembrane protein that is ubiquitously expressed, but found in high levels in secretory tissues. Monomers of PERK are sequestered by BiP until BiP dissociates during ER stress. This results in dimer/oligomerisation of PERK and trans-autophosphorylation. Once activated, the *C*-terminal domain of PERK phosphorylates eukaryotic initiation factor 2α (eIF2α), inhibiting global protein synthesis by blocking translation initiation. Due to the lower efficiency of translation initiation as a consequence of eIF2α phosphorylation, ribosomes are more prone to skip start codons, which allows them to bypass earlier reading frames and translate specific proteins such as ATF4 (Schroder and Kaufman, 2005). ER stress-response genes such as BiP contain internal ribosomal entry sequences which allow continued protein production even when eIF2α is phosphorylated. Additionally, PERK phosphorylates nuclear factor (erythroid-derived 2)-like 2 (Nrf2), resulting in nuclear localisation and transcription of Nrf2 targets: antioxidant response element (ARE) genes. These genes reduce reactive oxygen species (ROS) within the cell which can accumulate during ER stress.

1.5.4 ATF4

The translation of ATF4 is induced upon eIF2α phosphorylation. ATF4 governs the exact switch point of ER stress between pro-survival and pro-death. In the pro-survival phase, ATF4 migrates to the nucleus and upregulates homocysteine-induced ER protein (HERP) which is essential for ERAD, molecular chaperones, and ATF3 which has roles in downstream metabolic signalling. It also increases levels of proteins required for autophagy and, perhaps most crucially, activates sestrin 2 (SESN2) which induces AMPK-mediated activation of the TSC1/2 complex and inhibition of protein synthesis through mTORC1 (Brüning *et al.*, 2013). If ER stress is prolonged or excessive, ATF4 switches to a pro-death response by upregulation of C/EBP homologous protein

(CHOP) transcription. CHOP promotes transcription of growth arrest and DNA damage protein 34 (GADD34), a protein phosphatase 1 (PP1) binding protein that promotes dephosphorylation of eIF2α. Consequently, GADD34-PP1 reverses the inhibition of protein translation to generate an apoptotic signal through translation of pro-apoptotic proteins (Sano and Reed, 2013). This process appears to be regulated by ATF4-CHOP-mediated promotion of Tribbles 3 (TRB3), a pro-apoptotic protein which negatively regulates ATF4 (Ohoka *et al.*, 2005). Furthermore, GADD34-PP1 can bind to and dephosphorylate the TSC1/2 complex to inhibit mTORC1 during glucose deprivation (Watanabe *et al.*, 2007).

1.5.5 ATF6

Under normal conditions, ATF6 is sequestered by BiP and calreticulin. ATF6 has α– and β–isoforms, both activated by the same mechanism during ER stress. ER stress causes BiP to preferentially bind to misfolded protein, and underglycosylation interferes with calreticulin-binding to newly synthesised ATF6 (Schroder and Kaufman, 2005). Once released, ATF6 dissociates from the luminal domain of the ER and is transported to the golgi. Here, the membrane anchor of ATF6 is cleaved allowing translocation to the nucleus where the transcription factor binds to promotors of ER stress response genes, upregulating production of molecular chaperones and proteins involved in ERAD. In addition, ATF6 activates transcription of pro-survival X box-binding protein 1 (XBP1) (Jager *et al.*, 2012).

1.5.6 IRE1α

IRE1α is an ER transmembrane protein similar to PERK in structure and also found in monomeric form bound to BiP under normal conditions. Released during ER stress, IRE1α forms homodimers and trans-autophosphorylates itself to activate its endonuclease domain. The RNase activity of the actiated IRE1α endonuclease splices mRNA of XBP1, which can be used as an early marker of ER stress (Brüning, 2011). Spliced XBP1 (XBP1s) is pro-survival and upregulates molecular chaperones, ERAD components and ER expansion. It is regulated by the unspliced form, which targets XBP1s for degradation by the proteasome (Yoshida *et al.*, 2006). IRE1α signalling is primarily pro-survival (Lin *et al.*, 2007), but can also be pro-apoptotic through binding to tumour necrosis factor (TNF) associated factor 2 (TRAF2) and downstream C-Jun N-terminal kinase (JNK)-mediated upregulation of pro-apoptotic proteins such as Bim,

and down-regulation of anti-apoptotic proteins such as B cell lymphoma 2 (Bcl-2) (Zhu *et al.*, 2014).

1.6 The UPR

ER stress signalling is an essential part of the induction of the UPR (Frand *et al.*, 2000, Aebi *et al.*, 2010, Ma and Hendershot, 2004). The UPR is a series of events that serve to reduce ER stress and restore ER homeostasis through relief of misfolded protein burden. This is done by multiple means; existing mRNAs are degraded, transcription/translation of new mRNA is inhibited, protein folding is facilitated and mis-folded proteins are eliminated. Protein degradation is carried out through autophagy and via the proteasome, which are discussed further in chapters 4 and 5, respectively.

1.7 General Aims

mTORC1 overactivation is a common feature of a broad spectrum of cancer types since it can be caused by a number of upstream mutations within mitogenic signalling pathways, including: pathological increases in growth factors, growth factor receptor activating mutations, oncogenic mutations within the MAPK pathway, oncogenic mutations or loss-of-function tumour suppressor mutations in the PI3K pathway. Additionally, overactivation of mTORC1 can also be caused by any direct impairment in TSC1/2. mTORC1 overactivation causes ER stress which can be exploited in order to kill tumour cells. The main aims of this study were:

1. To utilise specific *in vitro* models of mTORC1 overactivation to assess sensitivity to ER stress-induction

2. To identify repositionable drugs and novel drug combinations which cause selective cell death in mTORC1-overactive cells

3. To investigate the mechanisms of said drugs in order to refine and direct future treatment strategies

Chapter 2. General methods and materials

2.1 Cell culture and reagents

2.1.1 Cell lines

Tsc2+/+ *p53*−/− and *Tsc2*−/− *p53*−/− mouse embryonic fibroblasts (MEFs) were kindly provided by David J. Kwiatkowski (Harvard University, Boston, USA). *Tsc2*−/− ELT3 (Eker rat leiomyoma-derived cells) and control ELT3-*Tsc2* cells in which *Tsc2* is re-expressed were kindly provided by Cheryl Walker (M.D. Anderson Cancer Center, Houston, USA). *TSC2-/-* human angiomyolipoma cells (AMLs) were kindly provided by Elizabeth Henske (Harvard Medical School, Boston, USA). Human lung carcinoma (NCI-H460) cells were purchased from ATCC.

2.1.2 Cell culture and reagents

All cell lines were cultured in Dulbecco's Modified Eagle's Medium (DMEM) supplimented with 10% fetal bovine serum (FBS), 100 U/ml penicillin and 100 µg/ml streptomycin (Life Technologies Ltd., Paisley, UK) with the exception of AML cells which were cultured in DMEM supplimented with 15% FBS. Cells were incubated in T75 cell culture flasks at 37 °C, 5% (v/v) CO_2. Cells were passaged once every 48 h using 3 x 1ml washes with Trypsin EDTA (0.25 %) followed by incubation at 37 °C over 5 min. Cells were then resuspended in culture medium and re-seeded into a T75 flask for continued culture. Surplus cells were used to setup experimentation at a set seeding density, as appropriate.

2.1.3 Drugs

Nelfinavir mesylate hydrate, ritonavir, lopinavir, chloroquine di-phosphate salt, mefloquine hydrochloride, bafilomycin-A1, 3-methyladenine (3-MA), N-acetyl-cysteine (NAC), digoxin, MG132, celecoxib, JSH23, etoposide and thapsigargin were purchased from Sigma–Aldrich Company Ltd. (Dorset, UK). Bortezomib, 17AAG and Z-IETD-FMK were purchased from Millipore (Hertforshire, UK). Ku0063794 was purchased from ChemQuest (Cheshire, UK).

All drugs were dissolved in 100 % dimethyl sulfoxide (DMSO) to stock solutions and stored at -20 °C, with the exception of chloroquine which was dissolved in fresh culture

medium to 100mM stock and further diluted to the required concentration in culture medium, and 3-MA which was dissolved in dH_20 to 100mM. Drug(s) or DMSO vehicle control was added to culture medium for treatment at a final DMSO concentration of <0.5% (v/v). Drug stock solutions and final concentrations are shown in Table 1.

2.2 mRNA extraction and reverse transcription

Cells were seeded on 6 cm^2 plates (TPP Helena Biosciences, Newcastle, UK) and allowed to adhere overnight. After treatment, cells were washed in phosphate buffered saline (PBS, Sigma) and lysed in RNAprotect reagent (Qiagen, West Sussex, UK). Cells were removed from the plate surface by scraping and stored at -80 °C before mRNA extraction.

2.2.1 mRNA extraction

RNA was extracted using the RNeasy Plus mini kit and homogenised using Qiashredders (Qiagen). Briefly, samples were thawed and centrifuged (5,000 g, 5 min) to form a loose pellet. Supernatant was discarded before resuspending in buffer RLT supplimented with 10 % β-mercaptoethanol (600 µl/sample) and transfering to a Qiashredder spin column. Following centrifugation (full speed, 2 min) flow-through was transferred to a gDNA spin column with collection tube and again centrifuged (8,000 g, 30 sec). An equal volume of 70 % ethanol was added to the flow-through and transferred to an RNeasy spin column with collection tube. Samples were centrifuged (8,000 g, 15 sec) and flow-through was discarded before addition of 700 µl buffer RW1 and another centrifugation (8,000 g, 15 sec). Flow-through was discarded before addition of 500 µl buffer RPE and centrifugation (8,000g, 15 sec). This step was repeated with a longer centrifugation of 2 min. The spin column was then placed into a fresh collection tube and 50 µl RNase-free water was added directly to the column membrane and left to incubate at room temperature for 5 min. Samples were centrifuged (8,000 g, 1 min) before assessment of RNA concentration and purity by measurement of absorbance (260 nm and 280 nm) on a Nanodrop spectrophotometer (Thermo Scientific, Hemel Hempsted, UK).

Table 2.1: Drug stock solutions and final concentrations. * standard dose, other concentrations as indicated.

DRUG	SOLUTION	STOCK CONCENTRATION (mM)	FINAL CONCENTRATION (µM)
Nelfinavir	DMSO	30	20*
Ritonavir	DMSO	40	20*
Lopinavir	DMSO	40	20*
Chloroquine	Culture Media	100	20*
Mefloquine	DMSO	50	10*
Rapamycin	DMSO	0.1	0.1
Ku0063794	DMSO	1	1
Etoposide	DMSO	100	100
3-Methyl Adenine	dH_20	100	5
N-Acetyl Cysteine	DMSO	500	20
Thapsigargin	DMSO	10	1
Bafilomycin-A1	DMSO	2.5	2.5
Digoxin	DMSO	10	5
MG132	DMSO	10	1
Celecoxib	DMSO	500	50
Bortezomib	DMSO	0.1	0.05
17AAG	DMSO	1	1
JSH23	DMSO	10	10
Z-IETD-FMK	DMSO	5	10

2.2.2 Reverse transcription

1 µg total RNA per sample was transcribed to cDNA using Quantitect reverse transcription kit (Qiagen) in a thermal cycler (Applied Biosystems, California, USA) and subjected to a gDNA wipeout stage. Briefly, 1 µg total RNA per sample was calculated and diluted to a volume of µl with RNase-free water before addition of 2 µl gDNA wipeout reagent. Samples were incubated at a volume of 14 µl at 42 °C for 2 min. Reverse transcription master mix was composed of 1 µl primer mix, 1 µl Quantiscript reverse transcriptase (RT) and 4 µl RT 5x buffer per sample. 6 µl of master mix was added to each sample. Samples were incubated at a final volume of 20 µl at 42 °C for 30 min, followed by 95 °C for 3 min. Following reverse transcription, samples were stored at -80 °C until further use.

2.3 Detection of endoplasmic reticulum stress

2.3.1 Q-PCR

Quantitative PCR (Q-PCR) reactions were conducted in 96 well plates (Thermo Fisher Scientific, Leicestershire, UK) using 25 ng DNA per reaction, appropriate primer sets and SYBR Green PCR Master mix (Qiagen). Quantitect β-actin, C/EBP Homologous Protein (CHOP), HSP70, and ER degradation enhancer mannosidase-like 1 (EDEM1) primers were purchased from Qiagen. Q-PCR was performed using an Applied Biosystems 7500 real-time cycler as follows: initial denaturation step (95 °C, 15 min); 40 cycles of denaturation (94 °C, 15 s); annealing step (55 °C, 30 s); extension step (72 °C, 30 s). The amplification products were quantified during the extension step in the 40th cycle. Relative quantification was performed using the comparative CT method (ddCT) with β-actin as the reference gene and DMSO vehicle-treated *Tsc2*+/+ MEFs as the calibrator. Melting curve analysis was performed to verify specificity of the Q-PCR products.

2.3.2 XBP1 splicing

XBP1 primers [Forward: 5'-AAA CAG AGT AGC AGC TCA GAC TGC-3', Reverse: 5'-TCC TTC TGG GTA GAC CTC TGG GA-3'] were synthesised through MWG Operon-Eurofin (Ebersberg, Germany).

Per sample, XBP1 master mix was composed of the following: 10 µl 5x Phusion GC buffer, 1 µl dNTPs, 2.5 µl 5 % DMSO, 34 µl sterile dH_20, 0.5 µl Phusion DNA polymerase, 0.5 µl forward XBP1 primer 10 pM, 0.5 µl reverse XBP1 primer 10 pM. Per sample, β-actin master mix was composed of the following: 10 µl 5x Phusion GC buffer, 1 µl dNTPs, 32.5 µl sterile dH_20, 0.5 µl Phusion DNA polymerase (all from New England Biolabs), 5 µl β-actin primer (Qiagen). PCR was performed using an Applied Biosystems GeneAmp 9700 PCR system as follows: initial denaturation step (98 °C, 3 min); 31 cycles of denaturation (9 °C, 30 s); annealing step (60 °C, 30 s); extension step (72 °C, 1 min).

XBP1 products were run on 3 % (w/v) agarose gels, 1x TAE (pH 8.0) using 10 % GelRed nucleic acid stain (Cambridge Bioscience, Cambridge, UK). DNA samples were prepared for loading by the addition of 5 µl 5x orange G loading buffer. 25 µl of XBP1 samples and 5 µl β-actin samples were loaded per well alongside 1Kb plus ladder (Life Technologies). PCR products of XBP1 were 480 bp, unspliced, and 454 bp, spliced. Gels were run at 100 volts over 1 h (actin) or up to 3 h (XBP1).

2.3.3 Gel extraction

XBP1 products were isolated from gels to confirm splicing by restriction digest with PST1, which digests unspliced XBP1 mRNA into 2 further products of 312 bp and 298 bp. The PST1 site is lost in spliced XBP1 so the product remains 454 bp.

Following the XBP1 assay, unspliced and spliced XBP1 products were extracted from the agarose gel using QIAquick Gel Extraction Kit (Qiagen) following the manufacturer's protocol. Briefly, extracted gel was weighed to calculate the amount of buffer QG (6 volumes/100 mg gel) for dissolving the gel, before incubation at 50 °C with agitation over 10 mins. When fully dissolved, an equal amount of isopropanol was added and the solution was centrifuged in a QIAquick spin column (13,000 rpm, 1 min) and flow-through was discarded. 500 µl buffer QG was added to the spin column before centrifugation (13,000 rpm, 1 min) and discard of flow-through. 750 µl buffer PE was added to the spin column, centrifuged (13,000 rpm, 1 min), and flow-through discarded. The spin column was then dry-centrifuged (13,000 rpm, 1 min) before placing in a fresh collection tube and adding 50 µl sterile dH_2O which was left at room

temperature for 5 min. After a final centrifugation (13,000 rpm, 1 min), samples were stored at -80 °C until use.

2.3.4 PST1 digest

Per sample, 45 µl XBP1 gel extract was mixed with 0.5 µl 100x BSA and 5 µl NE buffer 3 before adding either 1 µl PST1 restriction enzyme (all from New England Biolabs), or no further reagents for negative controls. Samples were incubated at 37 °C for 1.5 h. After addition of 5 µl 5x orange G loading dye, 25 µl sample was run on 3% (w/v) agarose gels, 1× TAE (pH 8.0) using 10 % GelRed nucleic acid stain to distinguish uncut and PST1 cut bands of 312 bp and 289 bp alongside a 1Kb ladder. Gels were run at 100 volts for up to 3 h.

2.4 Antibodies and western blotting

2.4.1 Western blotting

Whole lysates were collected from treated cells by first washing in PBS and lysing in radio immunoprecipitation assay (RIPA) buffer (Sigma-Aldrich) supplemented with protease inhibitors (Complete Mini protease inhibitor cocktail, Roche Diagnostics Ltd., Burgess Hill, UK) and dithiothreitol (DTT) on ice. Cells were removed from plates by scraping after 5 min in RIPA solution. All supernatants, washes and cells were collected into 15 ml (Thermo Fisher Scientific) and centrifuged (1,500 rpm, 10 min). Supernatants were discarded and cells were resuspended in 0.5 ml RIPA solution before transfer into 1.5 ml eppendorf tubes and storage at -80 °C until further use.

Samples were subjected to sonication (high: 3 x 20 sec on, 15 sec off) before centrifugation at 13,000 rpm for 8 min. Supernatants were transferred to fresh eppendorf tubes and sample protein concentrations were optimised using Bradford assay (Sigma-Aldrich). 4 x NuPAGE loading buffer (Life Technologies) supplemented with 25 mM DTT was added to samples before storage at -20 °C.

Following boiling at 70°C for 10 min, 25 µl protein samples per well were loaded into NuPAGE 4-12 % Bis-Tris protein gels (Life Technologies) alongside a protein ladder (Geneflow LTD, Stafforshire, UK) for separation using SDS-PAGE. Proteins were then transfered onto activated polyvinylidine difluoride (PVDF) membranes (Millipore) using the Novex system (Life Technologies). Membranes were blocked in 5% (w/v) milk

powder dissolved in tris-buffered saline (TBS) before probing with primary antibody (see Table 2 for concentration - diluted in TBS-T, supplimented with 2 % BSA) overnight. Primary antibodies were then removed and membranes were washed 3 times in 1 x TBS-T for 10 min at room temperature with agitation. Following washing, membranes were incubated at room temperature with horse radish peroxidase (HRP)-conjugated secondary antibody (1:10,000 in TBS-T, New England Biolabs) over 1 h. Membranes were then washed (TBS-T, 3 x 10 min) before detection with enhanced chemiluminescent (ECL) solution (GE Healthcare) to visualise protein bands using Hyperfilm (Fujifilm).

2.4.2 Antibodies

A full list of antibodies is shown in Table 2.

2.5 Late cell death assay

Following treatment, cells were removed from plates using trypsin. All washes and cells were collected in 15 ml falcon tubes (Thermo Fisher Scientific) before centrifugation at 900 rpm for 10 min to form a loose pellet of cells without affecting viability. Supernatant was discarded and cells were resuspended in 0.5 ml culture medium and transferred to 5ml Falcon round bottom tubes (Thermo Fisher Scientific). Cell viability was assessed using 3 µM DRAQ7 (Biostatus, Leicestershire, UK) non-cell permeable DNA stain incubated with cell suspensions at 37°C over 10 min. DRAQ7 fluorescence was detected using flow cytometry and excitation at 488 nm in log mode at wavelengths greater than 695 nm (far red). Flow cytometry using a FACS Calibur flow cytometer (Beckton Dickinson, Cowley, UK) and Cell Quest Pro software (Beckton Dickinson Immunocytometry Systems) was used for data acquisition. Unstained cells were analysed for autofluorescence (using FL3-H plots). Correlated signals were collected for 10,000 events. Collected data was gated to exclude debris (using SSC/FSC plots) from the final analysis.

2.6 Time lapse microscopy analysis

Tsc2+/+ or *Tsc2*-/- MEFs were seeded into 6-well tissue culture plates and allowed to adhere over 24 h before treatment with either DMSO control, 20 µM nelfinavir or co-treatment with 20 µM nelfinavir and 20 µM chloroquine. Following initial treatment,

Table 2.2: Table of primary antibodies and suppliers. * New England Biolabs are the UK distributer for Cell Signalling Technology antibodies. Primary antibodies were used at a concentration of 0.1 µg/ml.

ANTIBODY	SUPPLIER
ACC	New England Biolabs (Hertfordshire, UK)
Phospho-ACC (Ser79)	New England Biolabs
AMPKα	New England Biolabs
Phospho-AMPKα (Thr172)	New England Biolabs
ATF4	Santa Cruz Biotechnology (Heidelberg, Germany)
Phospho-ATM (S1981)	New England Biolabs
β-actin	New England Biolabs
BiP	New England Biolabs
Phospho-Beclin1 (S30)	Dr James Murray (Trinity College, Dublin, UK)
Caspase 3	New England Biolabs
Cleaved caspase 8	New England Biolabs
CHOP	Santa Cruz Biotechnology
CHOP	New England Biolabs
Phospho-4E-BP1 (Thr36/45)	New England Biolabs
Phospho-eIF2α (S51)	New England Biolabs
ERK	Prof. John Blenis (Harvard University, Boston, USA)
Phospho-ERK (Thr202/Tyr204)	New England Biolabs
GADD34	Proteintech (Manchester, UK)
Phospho-H2AX (S139)	New England Biolabs
TSC2	New England Biolabs
IRE1α	New England Biolabs
LC3	Novus (Cambridge, UK)
PARP	New England Biolabs
Phospho-Raptor (S859)	Prof. Diane Fingar, (University of Michegan Medical School, Michegan, USA)
Phospho-RelA (S536)	New England Biolabs
rpS6	New England Biolabs
Phospho-rpS6 (Ser235/236)	New England Biolabs
S6K1	New England Biolabs
Phospho-S6K1 (Thr389)	New England Biolabs
SQSTM1	PROGEN Biotecknik (Heidelberg, Germany)
Ubiquitin	Enzo Life Sciences (Exeter, UK)

plates were immediately installed into the time-lapse instrument comprising of an Axiovert 100 microscope (Carl Zeiss, Welwyn Garden City, UK) fitted with an incubator and CO_2 regulator (37°C, 5% CO_2). Images were captures with an ORCA-ER CCD camera (Hamamatsu, Reading, UK) and illumination was regulated by a shuttered transmission lamp. An X and Y stage with Z-focus was used to set multi-field acquisition. Images were taken in 15 min intervals over 48 h, with 3 fields per well. Sequence capture was controlled by MetaMorph software (Molecular Devices, California, USA).

2.7 Microscopy

Images of live cells were taken at x 40 or x 100 magnification using phase contrast on an EVOS XL Core microscope (Fisher).

2.8 Statistical analysis

Experiments were carried out a minimum of 3 times wherever possible. The arithmetic mean was used to measure the central tendency of data. The dispersion of values around the mean was expressed as the standard deviation (SD) in analysis of raw data, i.e. mean ± SD. The significance of difference was tested using Miscosoft Excel and R statistical analysis software (R Core Team, 2013 [Available at: http://www.R-project.org/]). Statistical tests included Student's t-test for initial assessment of significance, followed by ANOVA for confirmation of significance accounting for multiple variables. General linear model with gamma distribution and comparisons was used for analysis of the larger data sets generated by flow cytometry to effectively summarise significant outcomes. The level of statistical significance was set at $P<0.05$.

2.9 General buffers and solutions

<u>1 x Phosphate-buffered saline (PBS)</u>

200 ml ddH_2O, 1 x PBS tablets (Sigma): 10 mM phosphate buffer, 2.7 mM potassium chloride and 0.137 M NaCl, pH 7.4

<u>10 x Tris-buffered saline (TBS)</u>

500 ml ddH_2O, 12.1 g Tris (Sigma), 40 g NaCl (Sigma), pH 7.6

1 x TBS-tween (TBS-T)

450 ml ddH_2O, 50 ml 10 x TBS, 0.5 ml 0.1 % (w/v) Tween-20 (Sigma)

10 x Tris–Acetate–EDTA (TAE)

1 L ddH_2O, 1.14 ml glacial acetic acid (Sigma), 4.84 g Tris (Sigma), 1 ml 0.5 M EDTA

1 x running buffer for SDS PAGE

380 ml ddH_2O, 20 ml 20x NuPAGE MES SDS running buffer (Life Technologies)

10 x transfer buffer

1L ddH_2O, 144.07 g Glycine (Sigma), 30.285 g Tris (Sigma), 2 g sodium docecyl sulfate (Sigma)

Western blot transfer buffer

400 ml ddH_2O, 50 ml methanol (Thermo Fisher Scientific), 50 ml 10 x transfer buffer

5 % Milk block

20 ml 1 x TBS, 0.5% (w/v) skimmed milk (Marvel)

RIPA buffer (Sigma)

150 mM NaCl, 1.0% (v/v) IGEPAL® CA-630, 0.5% (w/v) sodium deoxycholate, 0.1% (w/v) SDS, and 50 mM Tris, pH 8.0.

Chapter 3. Detection of nelfinavir-induced ER stress and cell death

3.1 Background

3.1.1 Nelfinavir

As a first generation human immunodeficiency virus (HIV) protease inhibitor (PI), nelfinavir has been used extensively in the treatment of HIV for over a decade but is now rarely used for antiretroviral therapy (ART) due to continuing development of new drugs. Nelfinavir was derived from saquinavir, designed to inhibit cleavage of viral precursor polyproteins, and approved by the Food and Drug Administration (FDA) for HIV treatment in 1997. Nelfinavir was the first non-peptidomimetic PI and contains a novel 2-methyl-3-hydroxybenzamide group. It was the first PI approved for paediatric treatment of HIV (Wlodawer, 2002). Modern day ART combines a PI (of which there are 10 approved forms including nelfinavir) with reverse transcriptase inhibitors. ART reduces mortality, infection, and AIDS-related cancers such as Kaposi sarcoma (Sgadari *et al.*, 2003). For treatment of HIV, nelfinavir was given orally to achieve mean plasma concentrations of 2.2 ± 1.25 μg/ml which efficiently inhibited the retroviral proteinase, but this low dose is insufficient to induce ER stress in cancer cells. For this, 8-15 μg/ml is required. The amount of 250 μg tablets required to achieve this dose is high, but a 625 μg bolus is also available (Brüning, 2011). Nelfinavir is well absorbed and metabolised primarily through the liver within 3.5 – 5 h (Pai and Nahata, 1999).

Kaposi sarcoma (KS) is an acquired immune deficiency syndrome (AIDS)-related cancer caused by opportunistic infection of human herpesvirus 8 (HHV8), as HIV-infected persons are immunosuppressed. 1997 saw a flurry of research publications showing HIV-infected patients with KS treated with PIs showed regression and reduction of the cancerous regions (Blum *et al.*, 1997, Conant *et al.*, 1997, Murphy *et al.*, 1997). This prompted further research into the effects of PIs other than on the HIV protease which found the regression of KS legions linked to reduction of both angiogenesis and invasion though VEGF-A and matrix-metalloprotease-2 (MMP2) inhibition in multiple human xenograft KS models (Barillari *et al.*, 2003) and primary KS cells (Grosso *et al.*, 2003).

3.1.2 PIs in preclinical research

Sequential studies have shown that nelfinavir displays anticancer activity through induction of ER stress in preclinical cell and xenograft models. Gills *et al.,* (2007) tested a panel of 6 PIs in 60 cancer cell lines derived from 9 tumour types and found nelfinavir, ritonavir and saquinavir to be effective at inducting cell death with nelfinavir being the most effective (mean 50% growth inhibition). They demonstrated that nelfinavir caused both caspase-dependent and –independent cell death, which was mediated through ER stress, and went on to further validate this finding *in vivo* (Gills *et al.*, 2007). More recently, Taura *et al.,* (2013) investigated a range of 9 PIs in 3 human cancer cell lines, 2 non-malignant cell lines and primary peripheral blood mononucleocytes (PBMCs). They found lopinavir, a second generation PI, to be most effective at induction of ER stress (as detected by CHOP expression), following 24 h of 40 µM treatment. However, lopinavir appeared equally effective at ER stress-induction throughout all cell types, whereas nelfinavir showed some selectivity. Additionally, the study investigated darunavir, a more recent second generation PI with very high specificity and binding affinity (Taura *et al.*, 2013). These properties result in lower side effects in HIV patients, possibly because it is a poor inducer of ER stress and therefore might not be as promising for repositioning for the treatment of cancer. Kraus *et al.,* (2014) again examined all 9 approved PIs, this time in the context of leukaemia. They used acute myeloid leukaemia cell lines and primary cells as well as primary acute lymphocytic leukaemia cells, and primary PBMCs. Results showed saquinavir, ritonavir, nelfinavir and lopinavir induced similar levels of ER stress (Kraus *et al.*, 2014). Ritonavir proved to be an effective and selective inducer of cell death in primary cultures at 40 µM over 48 h, but in this study, ritonavir was not directly compared alongside the other PIs. A summary of the PIs and other drugs used in this study is presented in table 3.

3.1.3 Nelfinavir inhibits Akt

The PI3K-Akt mitogenic signalling pathway acts to increase mTORC1 activity through Akt which directly inhibits the TSC complex whilst also inhibiting activatory phosphorylation of AMPK. In the context of cancer, this action to increase mTORC1 signalling could result from any upstream oncogenic mutation (e.g. PI3K), tumour suppressor dysfunction (e.g. phosphatase and tensin homologue (PTEN)), or increased

Table 2.3: Mechanisms of drugs relevant to the present study. Adapted from Brüning and Jückstock (2015) and Gantt *et al.* (2013).

DRUG	ACTION	CLINICAL USE	CANCER TRIALS (clinicaltrials.gov)	MAIN TOXICITIES
Nelfinavir (Viracept)	ER stress-inducer ROS generator HSP90 inhibitor Akt inhibitor Proteasome inhibitor Apoptosis inducer Autophagy effector	Previously used as HIV-PI	37 trials in multiple solid cancers and leukaemias	Gastro-intestinal effects, defective lipid metabolism, insulin resistance (long-term)
Ritonavir (Norvir)	CYP3A4 inhibitor Akt inhibitor ER stress-inducer MMP inhibitor NF-κB inhibitor Proteasome inhibitor	Used in combination with lopinavir as HIV-PI	5 trials in breast cancer & glioma. Multiple trials in AIDS-related sarcoma	Gastro-intestinal effects
Lopinavir (Kaletra)	Akt inhibitor Apoptosis inducer Proteasome inhibitor	Used in combination with ritonavir as HIV-PI	2 trials in glioma and Hodgkin lymphoma. 2 in AIDS-related sarcoma	Gastro-intestinal effects
Chloroquine (Resochin)	Autophagy inhibitor	Prophylaxis and treatment of malaria, arthritis	16 trials in lung, breast, pancreatic cancers, glioblastoma, MM, metastatic melanoma	Gastro-intestinal effects, renal & cardiac toxicity
Mefloquine (Lariam)	Unknown	Prophylaxis and treatment of malaria	1 in glioblastoma	Neurological and neuropsychological effects, cardiac toxicity
Bortezomib (Velcade)	Proteasome inhibitor	MM, mantle cell lymphoma	720 trials in multiple solid cancers and leukaemias	Neuropathy, muscle weakness, neutropenia

mitogenic stimulus from malfunctional or upregulated growth factor receptors (e.g. epidermal growth factor receptor (EGFR)). Since all these potential and common situations result in upregulation of Akt, an Akt inhibitor would be a useful anti-cancer agent. Although several PIs appear to inhibit Akt to a certain degree, nelfinavir is the most potent of its class (Gills *et al.*, 2007, Yang *et al.*, 2006). The mechanism may be through nelfinavir-mediated inhibition of the proteasome, resulting in ER stress and induction of the UPR, leading to downstream Akt inhibition (Gupta *et al.*, 2007). However, nelfinavir-mediated Akt inhibition appears to be dependent on cell type, dosage and treatment length and does not consistently correlate with induction of ER stress (Kraus *et al.*, 2013, Gills *et al.*, 2007). It is important to note that inhibition of Akt signalling is not always associated with antitumour activity and there have been studies published showing nelfinavir activates Akt (Shim *et al.*, 2012, Jiang *et al.*, 2007).

3.1.4 Relating to angiogenesis

Increased Akt signalling upregulates angiogenesis through mTORC1-mediated elevation of hypoxia-inducible factor (HIF) 1α and downstream VEGF-A expression. Angiogenesis allows solid tumours to grow beyond 2-4 mm in size and also facilitates metastasis. Drug inhibition of angiogenesis is useful for limiting tumour growth but also has serious side effects including reduced maintenance of vasculature leading to bleeding and poor wound healing. PIs have been shown to decrease angiogenic signalling, likely through Akt inhibition. In particular, nelfinavir decreased HIF-1α and VEGF-A expression both under normoxic and hypoxic conditions, in both *in vitro* and *in vivo* assays of glioblastoma model systems, which sensitised tumour xenografts to radiotherapy (Pore *et al.*, 2006b, Pore *et al.*, 2006a).

3.1.5 PIs relating to apoptosis

PIs have been shown to induce cell death in multiple cancer cell lines. Although the precise mechanism varies, and one single mechanism may not be responsible, ER stress and other pathways have been implicated. It is known that nelfinavir inhibits the proteasome in multiple cell types (Gantt *et al.*, 2013), which in turn may reduce degradation of the inhibitory IκB protein, therefore preventing activation of the powerful pro-survival complex, Nuclear Factor-κ B (NF-κB). Indeed, ritonavir repressed NF-κB levels in *in vitro* and *in vivo* models of AIDS-related lymphoma (Dewan *et al.*, 2009). Conversely, long-term incubation with PIs led to activation of NF-κB due to

degradation of IκB through the lysosome (an alternative degradation pathway) in a lung cancer cell line (Lee *et al.*, 2013). Further research into the use of PIs to induce ER stress combined with a NF-κB inhibitor may show therapeutic value.

3.1.6 Nelfinavir inhibits the cell cycle

One recent paper using castration-resistant prostate cancer cells showed single treatment with nelfinavir inhibited cell proliferation through inhibition of site-2 proteases, resulting in downstream interference of regulated intramembrane proteolysis which is essential for ATF6-mediated induction of the UPR (Guan *et al.*, 2015). Another study using human cervical cancer cells found nelfinavir inhibited the cell cycle at G1, concurrent with many other studies, but also induced apoptosis which was potentially mediated through increased mitochondrial ROS production (Xiang *et al.*, 2015).

3.1.7 Mechanisms of nelfinavir-induced ER stress

Multiple studies have shown that nelfinavir induces ER stress in a wide range of *in vitro* and *in vivo* models. The exact mechanism of nelfinavir has not been determined and appears to vary with cell type, but speculation includes theories affecting proteolytic processing of newly synthesised proteins or their degradation (Brüning, 2011). Furthermore, it is difficult to implicate a single mechanism since nelfinavir acts on multiple targets and has hundreds of predicted off-target kinase binding partners, the most dominant of these are within the PI3K signalling pathway, including Akt (Xie *et al.*, 2011). This is primarily through the ability of nelfinavir to inhibit HSP90 (Shim *et al.*, 2012). HSPs were discovered in 1962 in chromosomes of drosophila salivary glands following thermal shock (Ritossa, 1962), though it is now known their expression is increased within cells during stress, regardless of the stimulus. The general role of HSPs is to promote protein folding and restore misfolded proteins (Hartl *et al.*, 2011). In addition to this role, HSP90 preferentially interacts with transcription factors and regulatory kinases which become stabilised and functional by HSP90 binding. During low levels of ER stress, HSP90 associates with and stabilises IRE1a and PERK, which promote a pro-survival response (Marcu *et al.*, 2002). Shim *et al.,* (2012) proposed nelfinavir binds to HSP90 at the C-terminal domain, in a way distinct to other HSP90 inhibitors, and causes a conformational change. Therefore, inhibition of HSP90 by

nelfinavir causes increased misfolded proteins within the ER and may also reduce the pro-survival IRE1α response.

Nelfinavir was shown to definitively cause ER stress through upregulation of eIF2α and BiP, which accumulated in swollen ER vacuoles in ovarian cancer cells (Brüning *et al.*, 2009). Downstream of BiP, nelfinavir-induced ER stress signalling was found to upregulate ATF4 which targeted SESN2 (Brüning *et al.*, 2013), which subsequently phsophorylated AMPK and activated TSC2 to inhibit mTORC1 (Budanov and Karin, 2008).

3.1.8 PIs in clinical trials

To date, nelfinavir has been included in 27 clinical trials for cancer treatment, most commonly in combination with chemo- or radiotherapy. Of the 9 currently recruiting, the focus is on cancers with particularly poor outcome including pancreatic cancer and multiple myeloma.

A phase I trial to determine maximum tolerated dose of nelfinavir in adults with solid tumours was recently completed and concluded a dose of 3125 mg twice daily, 2.5 fold typical HIV doses, was tolerated. Neutropenia was observed at high doses which was reversible with drug discontinuation. Most commonly observed adverse effects were diarrhea, anemia, lymphopenia, fatigue and hypoalbuminemia (Blumenthal *et al.*, 2014). No dose limiting toxicities were observed in dose escalation trials using oral treatments up to 4250 mg twice daily in liposarcoma patients but pharmacokinetic data suggests only minimal plasma drug concentration increases in doses above 1875 mg twice daily, with treatments of 4500 mg twice daily inducing self-clearance (Gantt *et al.*, 2013, Pan *et al.*, 2012).

Only 1 study was undertaken using ritonavir and lopinavir for non AIDS-related cancer, which failed to meet the primary objective of progression-free survival after 6 months and was consequently terminated (clinicaltrials.gov NCT01095094).

3.2 Aims of Chapter 3

A wide range of cancers exhibit increased basal ER stress as a consequence of mTORC1 overactivation. A targeted strategy to exploit mTORC1 overactivation and associated ER stress without causing genotoxicity is required. HIV protease inhibitors have shown

potential for induction of ER stress in multiple cancer types and are a good candidate for drug repositioning. The main aims of this chapter were:

1. To establish reliable detection methods for ER stress and cell death

2. To evaluate the ability of nelfinavir to induce ER stress in a specific model of mTORC1 overactivation

3. To investigate the potential mechanisms of nelfinavir-induced ER stress

4. To establish effective drug combinations with nelfinavir

5. To identify whether ritonavir or lopinavir are more effective at induction of cell death than nelfinavir

3.3 Results

3.3.1 *Tsc2*-/- MEFs have increased basal ER stress

The induction of ER stress by nelfinavir was initially assessed using a range of doses at a short timepoint. 1 μM thapsigargin, a known ER stress-inducer, was used as a positive control. CHOP protein was used as a readout of ER stress following 6 h of treatment (Fig 3.1A). However, this produced an unreliable result with unclean CHOP protein bands and degradation of β-actin in *Tsc2*-/- cells at the highest dose of nelfinavir. A standard dose of 20 μM nelfinavir was chosen for further assessment. To establish more reliable antibodies for early detection of ER stress, nelfinavir-treated cells were probed for BiP and IRE1α (Fig 3.1B). Following 3 h treatment, little change in protein levels was detectable between treated and untreated cells. Despite this, there are clear differences in basal ER stress levels between cell lines with BiP and IRE1α proteins both being basally increased in *Tsc2*-/- compared to the *Tsc2*+/+ MEFs.

3.3.2 Nelfinavir induces ER stress

Since changes in ER stress-associated protein levels were undetectable in nelfinavir-treated cells at 3 h of treatment, mRNA was examined. PCR was used to assess XBP1 splicing, with spliced XBP1 indicating ER stress (Fig 3.2A). Untreated cells show increased basal levels of spliced XBP1 in *Tsc2-/-* MEFs, consistent with increased basal ER stress proteins observed in Figure 3.1B. Thapsigargin clearly induced complete XBP1 splicing in both *Tsc2*-/- and *Tsc2*+/+ MEFs. Interestingly, nelfinavir treatment showed a differential effect between MEF cell lines, with a clear increase in spliced XBP1 in *Tsc2*-/- compared to *Tsc2*+/+ MEFs. The XBP1 products were confirmed by gel extraction and PST1 digest, where unspliced XBP1 was digested into 2 further fragments of 312bp and 289bp by PST1 but spliced XBP1 was resistant to PST1 digestion (Appendix I).

To confirm ER stress induction at the mRNA level and establish reliable primers, a panel of ER stress markers were measured by Q-PCR (Appendix II). The most consistent of these was found to be CHOP (Fig 3.2B). Although significantly different between cell lines (P=0.0022), CHOP mRNA was increased in both *Tsc2*-/- and *Tsc2*+/+ to a similar level compared to untreated cells (5.7 and 5.4 fold increase, respectively).

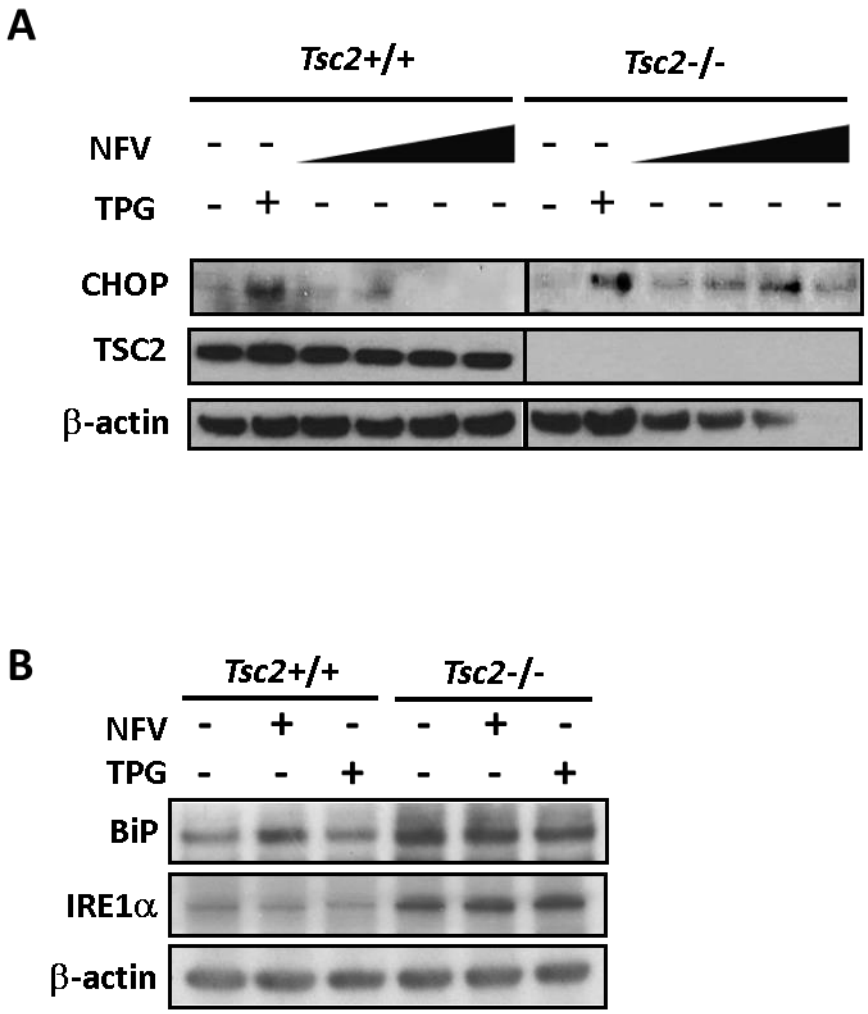

Figure 3.1: Establishment of reliable antibodies for detection of ER stress-associated proteins. A) *Tsc2*+/+ and *Tsc2*-/- MEFs were treated with either DMSO vehicle alone, 10 μM, 20 μM, 40 μM or 80 μM of nelfinavir (NFV), or 1 μM thapsigargin (TPG) for 6 h. Protein extracts were analysed for CHOP, TSC2 and β-actin. B) MEFs were treated with either DMSO vehicle alone, 20 μM NFV, or 1 μM TPG for 3 h. Protein extracts were analysed for BiP, IRE1α and β-actin.

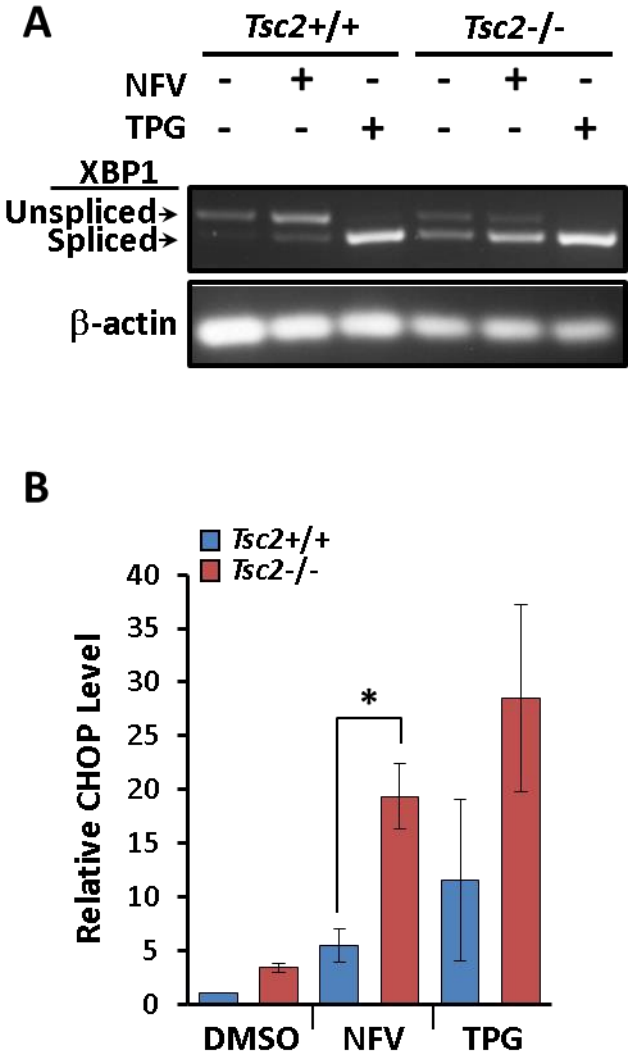

Figure 3.2: Establishment of reliable mRNA markers and techniques for early detection of ER stress. *Tsc2*+/+ and *Tsc2*-/- MEFs were treated with either DMSO vehicle alone, 20 μM nelfinavir (NFV), or 1 μM thapsigargin (TPG) for 3 h. A) PCR products for XBP1 mRNA were resolved on agarose gels (unspliced 480 bp upper band, spliced 454 bp lower band). β-actin is shown as a control. B) CHOP mRNA was analysed and standardised against β-actin. n=3, *P< 0.05.

3.3.3 Nelfinavir affects multiple cellular pathways including mTORC1 and autophagy signalling

Further analysis explored the effect of nelfinavir treatment on mTORC1 and autophagy signalling through examination of phosphorylated ribosomal protein S6 (rpS6), microtubule-associated proteins 1A/1B light chain 3 (LC3-I/-II) and sequestosome 1 (SQSTM1 or P62) protein levels (Fig 3.3). As expected, *Tsc2*-/- MEFs express basally elevated levels of phosphorylated rpS6 due to increased mTORC1 signalling compared to *Tsc2*+/+ MEFs. *Tsc2*+/+ MEFs showed inhibition of rpS6 phosphorylation following nelfinavir treatment but this was not observed in the *Tsc2*-/- MEFs. In contrast, thapsigargin reduced rpS6 phosphorylation in *Tsc2*-/- but not the *Tsc2*+/+ MEFs. This could be explained by an increase in autophagy flux, as indicated by increased conversion of LC3-I to LC3-II and reduced SQSTM1 protein, a negative marker of autophagy. Similarly, nelfinavir also increased LC3-II and reduced SQSTM1 levels in *Tsc2*-/- MEFs, yet the phosphorylated rpS6 levels were not reduced. There was no observable effect on LC3-II and SQSTM1 levels in *Tsc2*+/+ MEFs following nelfinavir treatment.

A wider investigation of the effect of nelfinavir on cellular signalling was undertaken by assessing phosphorylated levels of RelA (the p65 subunit of the pro-survival NF-κB complex), ERK (a major component of the Ras/Raf mitogenic pathway and a part of a negative feedback loop for mTORC1 signalling), AMPK (a key activator of TSC1/2 and a downstream target of ATF4), and acetyl co-A carboxylase (ACC, a downstream target of AMPK, Fig 3.4). Phosphorylation of RelA was basally higher in the *Tsc2*-/- MEFs and was enhanced with nelfinavir treatment. In contrast, thapsigargin reduced phosphorylated RelA in *Tsc2*-/- MEFs. Phosphorylated ERK was slightly reduced by nelfinavir treatment in *Tsc2*+/+ MEFs but this was not replicated in the *Tsc2*-/- MEFs. Contrastingly, thapsigargin had no effect on phosphorylated levels of ERK in *Tsc2*+/+ MEFs but slightly increased the levels within the *Tsc2*-/- MEFs. Thapsigargin had no effect on phosphorylated AMPK or ACC but nelfinavir treatment increased phosphorylation of both AMPK and ACC in both cell lines.

3.3.4 Nelfinavir does not cause cell death as a single agent

After discovering that short treatment length had rapid effects on cellular signalling pathways including ER stress and autophagy, a longer treatment was investigated to

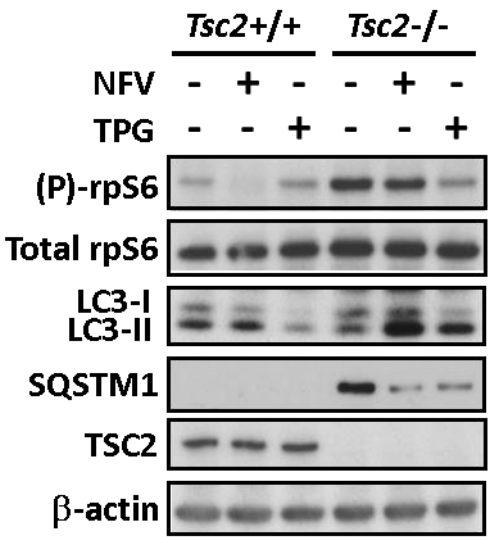

Figure 3.3: Assessment of the effect of nelfinavir on mTORC1 signalling and autophagy flux. *Tsc2*+/+ and *Tsc2*-/- MEFs were treated with either DMSO vehicle alone, 20 μM nelfinavir (NFV), or 1 μM thapsigargin (TPG) for 3 h. Protein extracts were analysed for phosphorylated and total rpS6, LC3-I and –II, SQSTM1, TSC2 and β-actin.

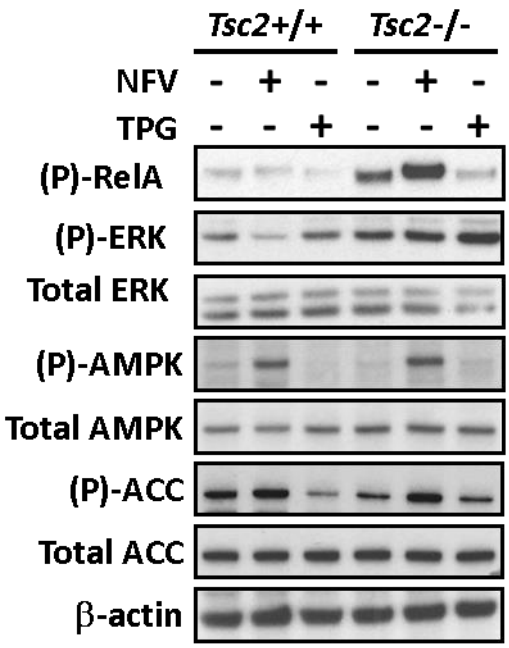

Figure 3.4: Assessment of the effect of nelfinavir on cellular signalling. *Tsc2*+/+ and *Tsc2*-/- MEFs were treated with either DMSO vehicle alone, 20 μM nelfinavir (NFV), or 1 μM thapsigargin (TPG) for 3 h. Protein extracts were analysed for phosphorylated RelA, phosphorylated and total ERK, phosphorylated and total AMPK, phosphorylated and total ACC, and β-actin.

assess the ability of nelfinavir to induce cell death. Initially, cell morphology was examined following 24 h nelfinavir treatment (Fig 3.5). In DMSO vehicle control treated cells, both *Tsc2*+/+ and *Tsc2*-/- MEFs are fully confluent and well adhered to the plate. After treatment with nelfinavir, both cell lines are far less confluent. The *Tsc2*+/+ MEFs are mostly triangular in shape with pseudopodia and appear to be larger or perhaps more flat due to greater adherence than the *Tsc2*-/- MEFs, which are mostly more spindle-like in shape. These images do not exhibit hallmarks of apoptosis, nor can any non-adherent (likely dead) cells be seen.

To accurately quantify cell death, flow cytometry was employed using the non-permeable DNA stain, DRAQ7. Cells were checked and adjusted for auto-fluorescence for flow cytometric analysis using Cell Quest Pro software (Fig 3.6A), and gated to exclude cell debris for data analysis using FlowJo software (Fig 3.6B). Gated cells were divided into viable (below line) and non-viable (above line) populations based on DRAQ7 fluorescence, using dot and contour plots for guidance (Fig 3.6C).

3.3.5 Nelfinavir causes cell death when combined with inhibitors of survival pathways

Flow cytometry was used to assess whether combination of nelfinavir with a panel of drugs affecting ER stress, autophagy or survival pathways would cause selective cell death in *Tsc2*-/- MEFs (Fig 3.7A). Viable (below line) and non-viable (above line) cells were gated according to log DRAQ7 fluorescence. As a single agent, nelfinavir did not induce cell death compared to untreated cells in either cell line (*Tsc2*+/+ MEFs: 11 % to 8 %,++ *Tsc2*-/- MEF: 15.1 % to 6.9 %. A greater than 20% increase in cell death in *Tsc2*-/- MEFs was observed when nelfinavir was combined with chloroquine, JSH23, or MG132 compared to nelfinavir treatment alone (6.9 % to 31.1 %, 78.3 % and 99.6 %, respectively). The same treatments also increased cell death in *Tsc2*+/+ MEFs compared to nelfinavir treatment alone (8 % to 19.7 %, 34.1 % and 99.6 %, respectively). Whilst nelfinavir modestly enhanced *Tsc2-/-* MEF cell death seen with celecoxib (8.7 % to 18 %) and 17AAG (15.1 % to 21.8 %), cell death did not appear to be selective between cell lines (*Tsc2*+/+ MEF nelfinavir-celecoxib: 15 %, nelfinavir-17AAG: 19.9 %). Flow cytometry results were supported by microscopy to assess cell density (Fig 3.7B).

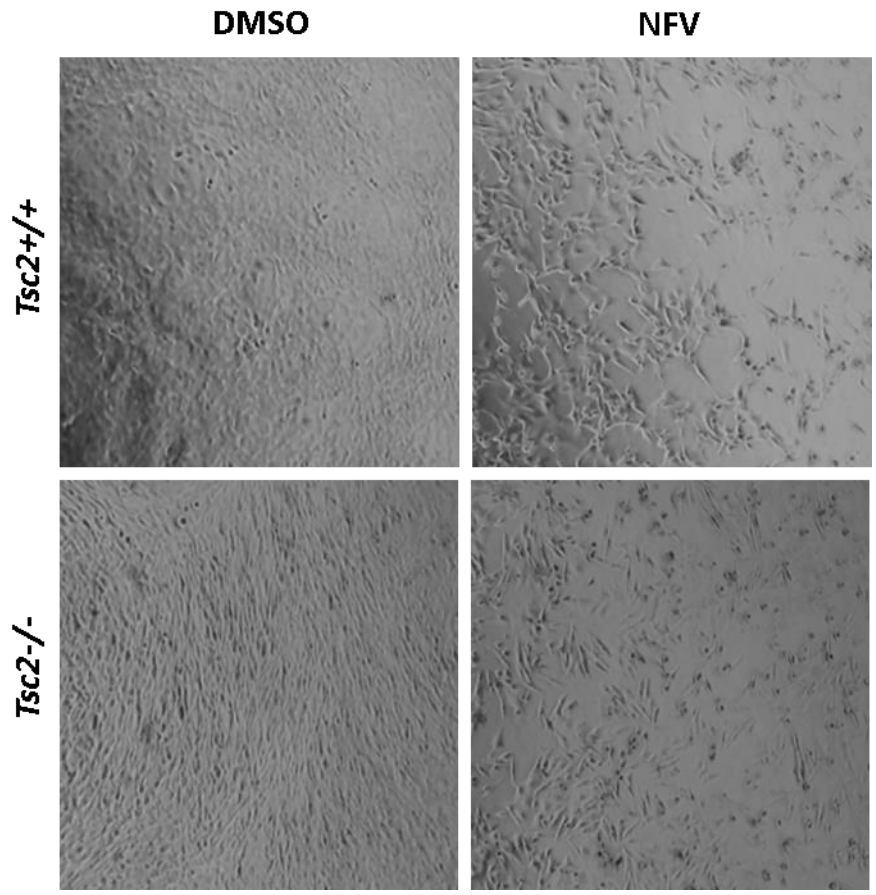

Figure 3.5: Nelfinavir affects cell density and morphology. *Tsc2*+/+ and *Tsc2*-/- MEFs were treated with either DMSO vehicle alone, 20 µM nelfinavir (NFV), or 1 µM thapsigargin (TPG) for 24 h. Images were taken at x 40 magnification using phase contrast.

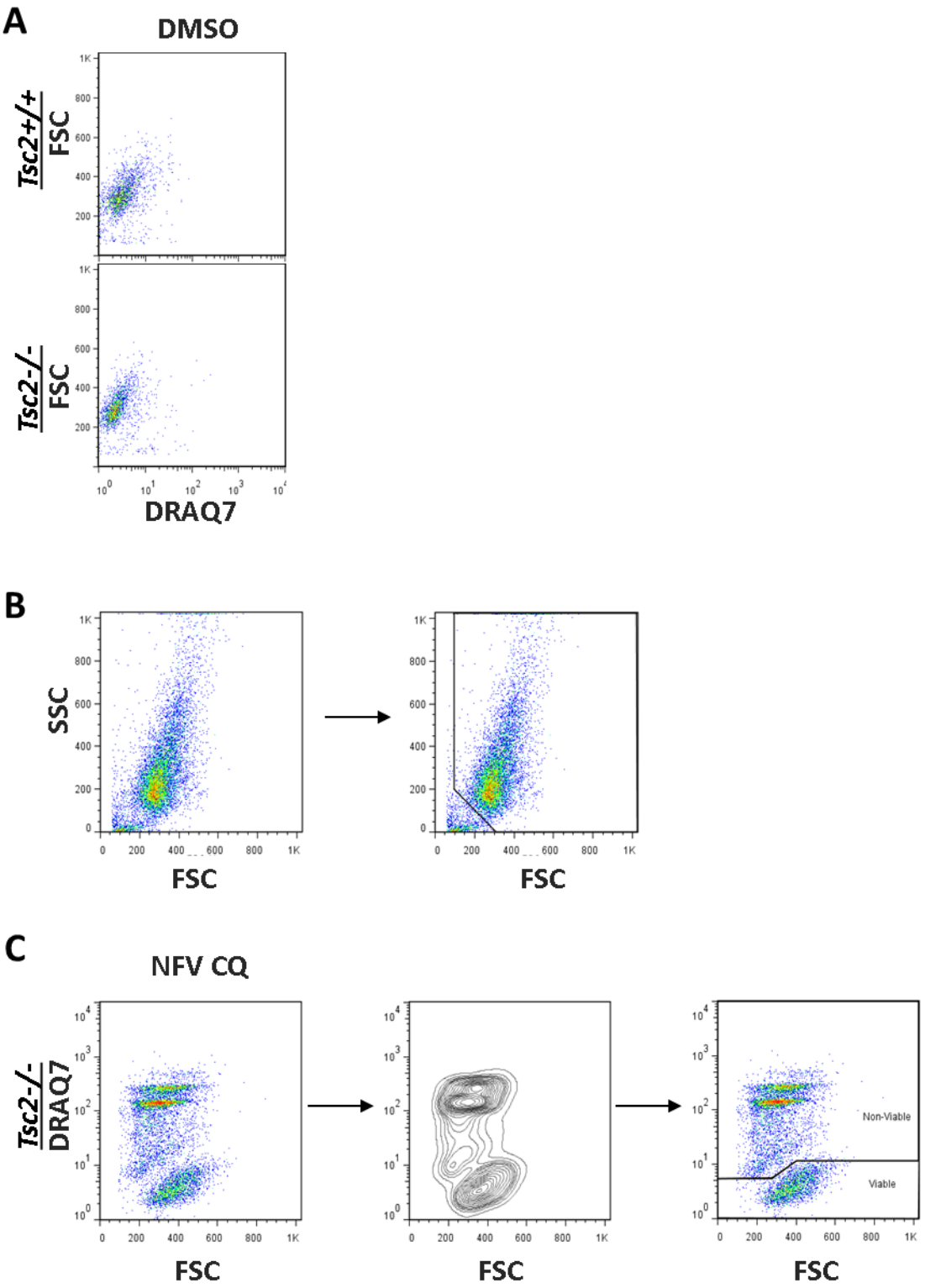

Figure 3.6: Establishment of autofluorescent parameters and gating for DRAQ7 flow cytometry. For quantification of cell death, *Tsc2*+/+ and *Tsc2*-/- MEFs were subjected to flow cytometry analysis and A) unstained cells were checked for autofluorescence, and B) gated to remove debris based on side scatter/forward scatter. C) Non-viable and viable cell gating was based populations of DRAQ7 stained and unstained cells, as determined by dot and contour plots: DRAQ7 exclusion (below line) represents the viable cell population, whilst positive DRAQ7 staining (above line) indicates cell death.

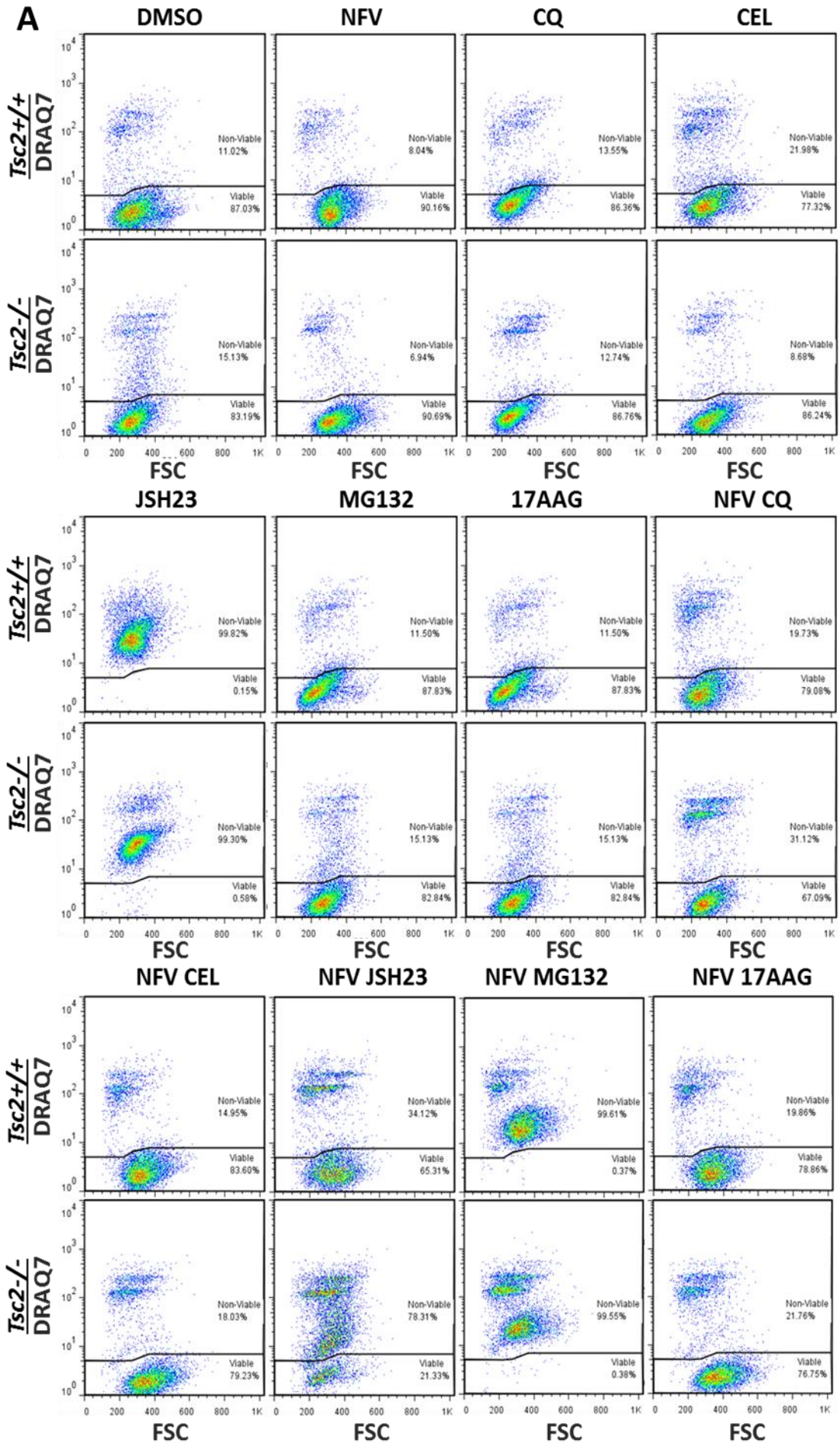
A
DMSO
NFV
CQ
CEL
Tsc2+/+ DRAQ7
Tsc2-/- DRAQ7
Non-Viable 11.02%
Viable 87.03%
Non-Viable 8.04%
Viable 90.16%
Non-Viable 13.55%
Viable 86.36%
Non-Viable 21.98%
Viable 77.32%
Non-Viable 15.13%
Viable 83.19%
Non-Viable 6.94%
Viable 90.69%
Non-Viable 12.74%
Viable 86.76%
Non-Viable 8.68%
Viable 86.24%
FSC
JSH23
MG132
17AAG
NFV CQ
Non-Viable 99.82%
Viable 0.15%
Non-Viable 11.50%
Viable 87.83%
Non-Viable 11.50%
Viable 87.83%
Non-Viable 19.73%
Viable 79.08%
Non-Viable 99.30%
Viable 0.58%
Non-Viable 15.13%
Viable 82.84%
Non-Viable 15.13%
Viable 82.84%
Non-Viable 31.12%
Viable 67.09%
NFV CEL
NFV JSH23
NFV MG132
NFV 17AAG
Non-Viable 14.95%
Viable 83.60%
Non-Viable 34.12%
Viable 65.31%
Non-Viable 99.61%
Viable 0.37%
Non-Viable 19.86%
Viable 78.86%
Non-Viable 18.03%
Viable 79.23%
Non-Viable 78.31%
Viable 21.33%
Non-Viable 99.55%
Viable 0.38%
Non-Viable 21.76%
Viable 76.75%

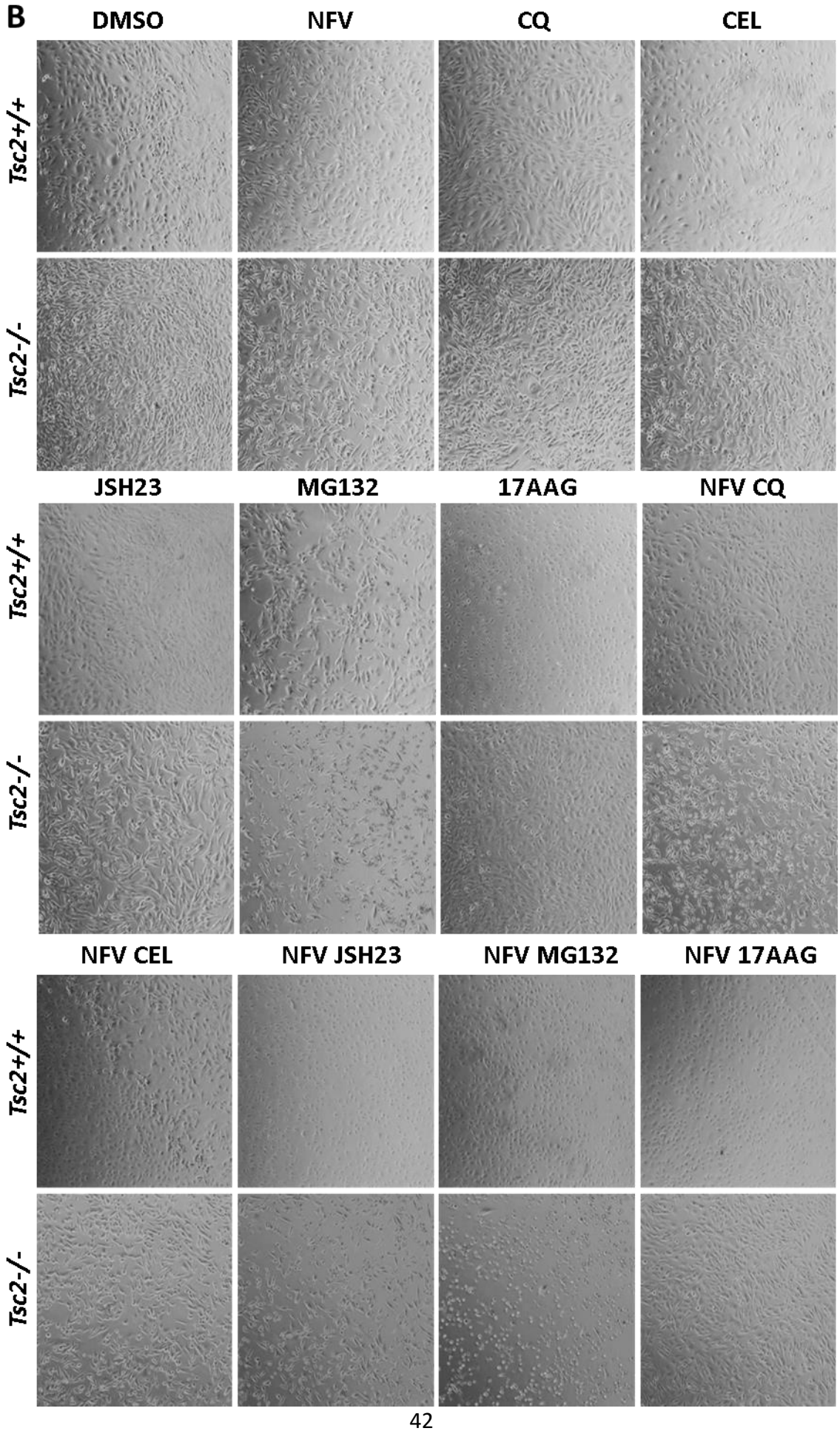
B
DMSO
NFV
CQ
CEL
Tsc2+/+
Tsc2-/-
JSH23
MG132
17AAG
NFV CQ
Tsc2+/+
Tsc2-/-
NFV CEL
NFV JSH23
NFV MG132
NFV 17AAG
Tsc2+/+
Tsc2-/-

Figure 3.7: Nelfinavir is effective at cell death induction in combination with multiple drug inhibitors of cell survival pathways. *Tsc2*+/+ and *Tsc2*-/- MEFs were treated with either DMSO vehicle alone, 20 µM nelfinavir (NFV), 20 µM chloroquine (CQ), 50 µM celecoxib (CEL), 10 µM JSH23, 1 µM MG132, 1 µM 17AAG, or a combination with NFV as shown for 24 h. A) Flow cytometry analysis with DRAQ7 staining. B) Images were taken at x 40 magnification using phase contrast.

3.3.6 Nelfinavir analogues do not exhibit selective cytotoxicity

Lopinavir and ritonavir-induced cell death was examined by visual assessment of cell density following 24 h treatment (Appendix III A) and flow cytometric analysis using DRAQ7 staining (Appendix III B), where neither ritonavir or lopinvir treatment increased the levels of cell death in the *Tsc2*-/- MEFs. Since these results are similar to those observed with nelfinavir single treatment, which was enhanced when combined with chloroquine, lopinavir and ritonavir were combined with chloroquine and cell death was assessed. Both combined lopinavir and chloroquine, and ritonavir and chloroquine greatly increased cell death as assessed by flow cytometry, but similar levels of cell death (~30%) were observed in both *Tsc2*+/+ and *Tsc2*-/- MEFs (Appendix IV A). Assessment of protein markers of apoptosis, caspase 3 and poly-ADP ribose polymerase (PARP, where cleaved products indicate apoptosis) showed no cleavage of either PARP or caspase 3 regardless of treatment or cell type (Appendix IV B).

3.4 Discussion

3.4.1 Nelfinavir induces ER stress

A dose of 20 µM nelfinavir was chosen along with a time point of 3 h for early assessment of ER stress. Initial western blots probing for CHOP protein at 6 h treatment using an antibody purchased from Santa Cruz Biotechnology were unreliable (Fig 3.1A). This is most likely due to the fact that CHOP is difficult to detect at early time points (Brüning, 2011). As an important downstream mediator of ER stress and pro-apoptotic signalling, it was imperative that an alternative assay for assessment of CHOP be found. Since increases in protein levels are subsequent to upregulation of mRNA, it was decided to analyse mRNA for ER stress markers through Q-PCR. 3 ER stress markers were tested in a single initial Q-PCR experiment: CHOP, HSP70, and EDEM1 (Appendix II). Both HSP70 and EDEM1 proteins assist with protein folding and are upregulated during ER stress. EDEM1 mRNA levels were very low and did not show effective differences between *Tsc2*+/+ and *Tsc2*-/- MEFs after treatment. Both HSP70 and CHOP mRNA levels gave similar results in that mRNA was increased following both thapsigargin and nelfinavir treatments, more so in *Tsc2*-/- MEFs. Consequently, it was decided that levels of CHOP mRNA would be used for early assessment of ER stress (Fig 3.2B).

Kang *et al.,* (2011) discuss a 'truncated' ER stress response in *Tsc1*-/- and *Tsc2*-/- MEFs and state that induction of CHOP and XBP1 by 4 h treatment with ER stress inducers (thapsigargin, tunicamycin and MG132) was blunted compared to control cells. This comparatively reduced expression of CHOP in *Tsc1*-/- MEFs and was shown at the level of both protein and mRNA. This is in contrast with results from the present study whereby *Tsc2*-/- MEFs were clearly shown to have basally elevated levels of ER stress at the level of both protein and mRNA which was elevated following 3 h treatment with either thapsigargin or nelfinavir (Fig 3.1-3.2). These results are supported in the literature (Ozcan *et al.*, 2008).

3.4.2 Nelfinavir affects multiple cellular pathways including mTORC1 and autophagy signalling

Tsc2-/- MEFs were observed to express basally higher levels of phosphorylated rpS6 than *Tsc2*+/+ MEFs, as expected due to overactive mTORC1 signalling. This supports

previous findings (Kang *et al.*, 2011). Nelfinavir decreased phosphorylation of rpS6 in *Tsc2*+/+ MEFs but not in *Tsc2*-/- MEFs (Fig 3.3). This indicates a TSC2-dependent mechanism of mTORC1 inhibition and is likely initiated through ER stress signalling. This is confirmed by previous findings (Budanov and Karin, 2008). Basal expression of SQSTM1 (a negative indicator of autophagy) was elevated in *Tsc2*-/- MEFs compared to *Tsc2*+/+ MEFs, again expected due to overactive mTORC1 signalling. Treatment with either nelfinavir or thapsigargin reduced expression of SQSTM1 and increased LC3-II. This indicates nelfinavir increases autophagy induction, but may also block autophagy at later stages and this effect appears to be specific to *Tsc2*-/- MEFs. Nelfinavir-induced autophagy likely occurs through ER stress signalling.

Figure 3.4 shows phosphorylayion of RelA is basally elevated in *Tsc2*-/- MEFs, indicating active NF-κB in these cells, which is increased by nelfinavir treatment but reduced with thapsigargin treatment. Since NF-κB is a major pro-survival transcription factor within the cell, nelfinavir-induced NF-κB is likely part of pro-survival ER stress signalling. The lack of phophorylated RelA in *Tsc2*+/+ MEFs, regardless of treatment, may indicate the requirement of cells to reach a certain threshold of ER stress before NF-κB activation. *Tsc2*+/+ MEFs show reduced phosphorylation of ERK with nelfinavir treatment which is not seen in *Tsc2*-/- MEFs. S6K1 is known to negatively feedback to the insulin receptor and therefore impact MAPK signalling, hence it is unlikely that ERK phosphorylation seen here reflects this feedback and is more likely to indicate an unknown effect of nelfinavir treatment which has previously been suggested to be related to pro-survival signalling (Kraus *et al.*, 2013). Nelfinavir elevated phosphorylated levels of AMPK and its downstream target, ACC. This is likely part of ER stress signalling and may indicate how nelfinavir reduces levels of phosphorylated rpS6 in *Tsc2*+/+ MEFs: Nelfinavir-induced ER stress signalling phosphorylates AMPK to activate TSC1/2 and inhibit mTORC1. This explains why rpS6 phosphorylation is not reduced in *Tsc2*-/- MEFs and indicates this action of nelfinavir is TSC2-dependent.

3.4.3 Nelfinavir does not cause cell death as a single agent

Figure 3.5 shows decreased cell density of both MEF cell lines following nelfinavir treatment, likely due to the known cytostatic effect of nelfinavir (Brüning *et al.*, 2009). Visually, cells appear healthy and this is confirmed by flow cytometry for detection of cell death (Fig 3.7). It is possible to surmise that although nelfinavir induces ER stress,

the dose or length of treatment with nelfinavir is insufficient to cause cell death in this case. Furthermore, the effects of nelfinavir on cellular signalling observed in figures 3.3 and 3.4 suggest nelfinavir may induce pro-survival ER stress signalling.

3.4.4 Nelfinavir causes cell death when combined with inhibitors of survival pathways

A recent drug screen identified nelfinavir as one of several FDA approved compounds to selectively inhibit proliferation in *TSC2*-/- AML cells (Medvetz *et al.*, 2015). However, since nelfinavir appears to be more cytostatic than cytotoxic, it may be more efficacious to combine it with other drugs - the theory being combining nelfinavir with other drugs to push ER stress beyond a tolerated threshold selectively in *TSC2*-/- cells and trigger a cell death response. As this chapter showed, *Tsc2*+/+ MEFs had a lower basal level of ER stress which allows them to tolerate treatment with an ER stress inducer, nelfinavir, to a greater extent than the *Tsc2*-/- MEFs. However, ER stress induction with nelfinavir was not sufficient to cause cell death alone. Therefore, nelfinavir was combined with other drug inhibitors which target compensatory pathways for ER stress. Through this initial drug screen, selective cell death of *Tsc2*- cells was observed when nelfinavir was combined with either an autophagy inhibitor (CQ), a proteasome inhibitor (MG132), or a NF-κB inhibitor (JSH23).

Chloroquine was used as an autophagy inhibitor. In a similar principle to combining nelfinavir with a proteasome inhibitor, pushing ER stress with nelfinavir and inhibiting compensatory autophagy with chloroquine should result in cell death, particularly in cells with higher basal levels of stress. Although single treatment with either nelfinavir or chloroquine had little effect on cell death, combination of the two produced an increase in cell death, more so in *Tsc2*-/- MEFs. Combined treatment with nelfinavir and chloroquine is discussed further in section 4.

MG132 is a potent and specific inhibitor of the 26S proteasome. Inhibition of the proteasome prevents degradation of type I and some type II proteins, which can result in their dysregulation. As already mentioned, one example of this is IκB and NF-κB. Inhibition of the proteasome also enhances ER stress as accumulated protein degradation must rely more heavily on autophagy, which degrades some type II and type III proteins. Combined treatment with nelfinavir and MG132 had a deadly effect

on both *Tsc2*+/+ and *Tsc2*-/- MEFs. It was decided to pursue this further with the FDA approved proteasome inhibitor, bortezomib, which is the subject of chapter 3.

JSH23 is an inhibitor of the p65 subunit of NF-κB which prevents its localisation to the nucleus and therefore transcriptional activity (Shin *et al.*, 2004). NF-κB has a strong pro-survival role and is linked to many signalling pathways including those involved in cell proliferation and cycle, migration, apoptosis and the inflammatory response. Unsurprisingly, it is frequently upregulated in multiple cancer types and is linked to treatment resistance (Piva *et al.*, 2006). NF-κB is upregulated through both PERK and IRE1α arms of ER stress by inhibition of IκB, preventing NF-κB sequestration degradation by the proteasome. As a single agent, JSH23 was highly cytotoxic to both cell lines at the concentration used for preliminary investigation (Fig 3.7). Interestingly, combination of JSH23 with nelfinavir had a protective effect, particularly in *Tsc2*+/+ MEFs, which resulted in far greater cell death in *Tsc2*-/- MEFs. Although this effect was clearly worth researching further, there are currently no clinically approved NF-κB drug inhibitors. Instead, proteasome inhibitors are typically used to inhibit degradation of IκB, preventing NF-κB activation.

Celecoxib is a cycoloxegenase 2 (COX2) inhibitor and non-steroidal anti-inflammatory treatment for arthritis and ankylosing spondylitis (McCormack, 2011). COX2 has been found to promote mitogenic signalling through RAS/RAF and PI3K pathways, and also cell cycle progression through C-MYC and upregulation of cyclin proteins, as well as angiogenesis through VEGF-A. Increased COX2 during ER stress elevated levels of BiP protein and triggered downstream apoptosis in mouse lungs exposed to hyperoxia and IFN-γ. Apoptosis was through CHOP-mediated activation of caspase-3 which was rescued through COX2 inhibition with celecoxib (Choo-Wing *et al.*, 2013). Additionally, the COX 2 inhibitor niflumic acid was successfully used in combination with a PPARγ inhibitor to induce cell death in multiple lung cancer cell lines, which was significantly attenuated by CHOP siRNA knockdown. Activation of CHOP was found to be essential for caspase-8-mediated apoptosis in this context (Kim *et al.*, 2011). If COX2 is indeed involved in activation of the ER stress response, then celecoxib should suppress induction of compensatory UPR signalling. This may prevent activation of autophagic and proteasomal degradation pathways and allow toxic accumulation of misfolded protein, possibly resulting in necrotic cell death long term rather than apoptosis as a

result of the UPR in a more timely manner. The present study combined nelfinavir with celecoxib (Fig 3.7), but no differential effect between cell lines or substantial increase in cell death was observed. It seems likely that the effects on ER stress of the two drugs overlap at some point in the signalling pathway or else cancel each other out. In any case, this initial examination did not suggest the combination of nelfinavir and celecoxib was worth continuing.

17AAG (Tanespimycin) is a HSP90 inhibitor and derivative of the antibiotic geldanamycin. In the present study, 17AAG had little effect on *Tsc2*+/+ or *Tsc2*-/- MEFs, which was subtly increased by combination with nelfinavir (Fig 3.7). These results suggest that nelfinavir could be acting in part through HSP90 inhibition. As combination of nelfinavir with an HSP90 inhibitor did not increase cell death to any greater extent than single treatment alone, this combination was not pursued any further.

3.4.5 Nelfinavir analogues do not exhibit selective cytotoxicity

The nelfinavir analogues ritonavir and lopinavir were compared alongside nelfinavir to determine which analogue might be more effective for future study. As shown in appendix III A and B, ritonavir or lopinavir did not cause cell death as single agents in either *Tsc2*-/- or *Tsc2*+/+ MEFs, similar to nelfinavir. Lopinavir and ritonavir were combined to replicate the drug, 'Kaletra', which shows improved efficacy in HIV treatment. This combination also failed to induce cell death. Increased cell death was seen in *Tsc2*-/- MEFs when nelfinavir was combined with chloroquine, so a combination of chloroquine with either ritonavir or lopinavir was assessed (Appendix IV). Flow cytometry analysis of cell death showed combination of either ritonavir or lopinavir with chloroquine increased cell death, but this increase was seen in both *Tsc2*+/+ and *Tsc2*-/- MEFs to similar levels (Appendix IV A). This contrasts the selective cell death seen in *Tsc2*-/- MEFs with combined nelfinavir and chloroquine treatment. Cleavage of apoptosis indicating proteins caspase 3 and PARP was not detected with ritonavir or lopinavir when combined with chloroquine, suggesting cell death was not mediated by apoptosis (Appendix IV B). Differences in treatment effects between PIs may be due to structural differences between nelfinavir, lopinavir and ritonavir. Nelfinavir contains a unique *cis*- decahydroisoquinoline-2-carboxamide moiety not

present in ritonavir or lopinavir (Appendix V). The only other PI containing this moiety is saquinavir, from which nelfinavir was derived.

3.4.6 Summary of chapter 3

In this chapter, nelfinavir was shown to effectively induce ER stress at a concentration of 20 µM, which was detected at the level of both mRNA and protein. Although nelfinavir did not cause cell death as a single agent, it effectively induced selective cell death in *Tsc2*-/- MEFs when combined with chloroquine-mediated inhibition of autophagy, or inhibition of the proteasome with MG132. Combination of nelfinavir analogues ritonavir or lopinavir with chloroquine failed to replicate the selective cell death observed with nelfinavir and chloroquine.

Chapter 4. Investigation of combination treatment with nelfinavir and chloroquine

4.1 Background

4.1.1 Autophagy

Autophagy serves to recycle cellular components through catabolic degradation, generating energy and components for biosynthetic reactions (Puissant et al., 2010). Autophagy can function as a main survival pathway in normal and abnormal cells (Glick et al., 2010). Autophagy is a finely balanced system, where tipping the balance one way or another can mean the difference between survival and death (Notte et al., 2011). Regulation of autophagy occurs through ULK1/2 kinases which form an active complex with ATG13 and FIP200. In energy and nutrient-sufficient conditions, mTORC1 inhibits ULK1 through direct phosphorylation at Ser757. When energy levels are low, AMPK inhibits mTORC1 through activatory phosphorylation of TSC1/2 and inhibitory phosphorylation of RAPTOR, and continues to activate ULK1 through phosphorylation at Ser317 and Ser777 (Sengupta 2010, Kim 2011).

There are three known processes of autophagy; chaperone-mediated autophagy (CMA), microautophagy and macroautophagy. The first observation of the self-eating phenomenon was observed in 1963 by Christian de Duve (deDuve, 1963), whose subsequent researched to the detection of both macro- and microautophagy (deDuve & Wattiaux, 1966). CMA was discovered much later in 1981 by Nicola Neff *et al.* (Neff *et al.,* 1981). All forms of autophagy ultimately serve to shuttle macromolecules into lysosomes where they are digested in order for the components to be recycled by the cell. Although there are many forms of autophagy, this study will mainly focus on macroautophagy.

The most well documented form of autophagy is macroautophagy whereby cytoplasm, proteins and organelles are internalised within double-membrane vesicles termed autophagosomes. Macroautophagy is activated within the first few hours of starvation, increasing activity until around 6 hours before slowly declining (Cuervo, 2010).

CMA differs from other forms of autophagy by the involvement of a translocation protein complex which eliminates the need for membrane deformity, fusion, or vesicular transport. However, this only allows delivery of single, soluble proteins which must be unfolded before entry into the lysosome. CMA is highly selective, directed by heat shock cognate 70 (HSC70) which binds to and transports specific proteins directly to the lysosome. Activation of CMA occurs initially between 6-8 hours of starvation, becoming increasingly active up until 24 hours where it can remain active for 3 days or more. The high selectivity of CMA following macroautophagy may prevent degradation of structures essential for survival whilst still obtaining the required amino acids. CMA also functions to remove oxidized, mis-folded and truncated proteins. Interestingly, reduction in CMA has been implicated in aging due to degradation of the substrate receptor, lysosome-associated membrane protein type 2A (LAMP-2A). Blockage or malfunction of CMA has also been discovered in neurodegeneration, metabolic disorders, kidney pathologies, and is suspected to underlie some immunoreactive and autoimmune disorders (Cuervo, 2010).

Microautophagy is concerned with maintenance of organelle size, membrane homeostasis and survival and is induced in conditions of nitrogen starvation (also by rapamycin treatment). In microautophagy, lysosomes directly engulf malfunctioning or damaged organelles (Li et al., 2012).

Salinomycin, an inducer of ER stress, has been shown to selectively kill breast cancer stem cells *in vivo* (Gupta *et al* 2009), and a range of other transformed cells. Li *et al* (2013) combined salinomycin with chloroquine in a range of non-small cell lung cancer cell (NSCLC) lines and found increased apoptosis compared to salinomycin treatment alone. However, salinomycin is currently only approved for use in veterinary practice, whereas nelfinavir is immediately available for repositioning.

4.1.2 Autophagy as part of the UPR

Autophagy is increased as part of the UPR following ER stress-induction. The aim of autophagy in this context is to help clear larger misfolded proteins, and other proteins which the proteasome cannot degrade, in order to reduce ER stress burden and to normalise cellular stress levels. This pro-survival arm of autophagy is often utilised by

cancer cells and has been shown to contribute to resistance to drug resistance (White and DiPaola, 2009).

One main mechanism by how the UPR increases autophagy flux is via inhibition of mTORC1, which directly represses autophagy through ULK1 phosphorylation and inhibition. All 3 arms of the UPR are able to inhibit mTORC1 though various signalling pathways: The PERK/eIF2α/ATF4 arm was found to be essential for stress-induced autophagy and induces translation (through ATF4) and transcription (through CHOP) of many principal autophagy inducer and regulator proteins, including Beclin1, ATG5/7, LC3-II and SQSTM1 (B'Chir *et al.*, 2013). ATF4 and CHOP also upregulate GADD34 and TRB3 expression which sequentially inhibits mTORC1 through promotion of TSC1/2, and inhibition of Akt, respectively (Uddin *et al.*, 2011, Schleicher *et al.*, 2010). The IRE1α/TRAF2 arm similarly increases CHOP and downstream TRB3 activity and promotes JNK suppression of Bcl-2-mediated Beclin1 inhibition. XBP1 splicing is promoted by both IRE1α and ATF6 arms of the UPR and increases transcription of autophagy components. Further to the UPR, ER stress-induced calcium increase triggers calcium/calmodulin-dependent kinase kinase-β (CAMKKβ) which mediates reduced mTORC1 signalling through AMPK activation. This is regulated by ER-localised Bcl-2 (Hoyer-Hansen and Jaattela, 2007).

Autophagy inhibition using drug antagonists would contribute to ER stress, particularly in combination with ER stress-inducers. In a panel of cancer cell lines, nelfinavir was combined with the autophagy inhibitor 3-methyladenine (3-MA) and this combination of drugs increased nelfinavir-induced cell death (Gills *et al.*, 2007). Cell death in triple-negative breast cancer cell lines was found to be synergistically enhanced when nelfinavir or celecoxib, another ER stress-inducer, was combined with chloroquine (Thomas *et al.*, 2012). Similarly, castration-resistant prostate cancer cells treated with nelfinavir showed an additive increase in apoptosis when combined with hydroxychloroquine (Guan *et al.*, 2012). In primary cells from chronic lymphocytic leukaemia patients, treatment with nelfinavir induced ER stress but not cell death. When nelfinavir was combined with chloroquine treatment, significant cytotoxicity was achieved (Mahoney *et al.*, 2013).

4.1.3 Chloroquine

The first successful treatment of malaria was performed in the 18th century using bark from cinchona trees containing the active ingredient, quinine. Quinine was used to control malaria until the 1940's when chloroquine was developed, which produced fewer side effects. Chloroquine synthesis stemmed from research by the Ehrlich group (1891) showing malaria could be cured using the synthetic dye, methylene blue. Multiple analogues were developed until the production of resochin in 1934, which was originally thought to be unsuitable for clinical use due to toxicity. Over a decade later, resochin was re-examined and found to be safe. It was then rebranded as chloroquine and marketed in 1947 for the prophylactic treatment of malaria, for which it is still used today (Solomon and Lee, 2009).

There are several consequences of chloroquine treatment which may contribute to its observed anticancer effects. Prepared as a diphosphate salt, chloroquine is diprotic. This allows unprotonated forms to travel freely across cell and organelle membranes, but protonated forms become trapped. Chloroquine is highly lysosomotropic and its accumulation in the lysosome results in inhibition of lipases, resulting in downstream dysregulation of neoglycolipid metabolism affecting multiple cellular signalling pathways.

There has been speculation from early physiochemical studies that chloroquine can cause double strand DNA damage through intercalation. Indeed, it is an effective antibiotic as it binds to prokaryotic topoisomerases, but binding to human homologues is approximately 100 – 1,000 x less efficacious and therefore should not cause DNA damage at normal achievable doses (Mitscher, 2005). However, since doses used in cancer treatment are expected to be higher than those used for malaria and due to potential unknown drug interactions in combination treatments, this aspect of chloroquine should not be ignored, particularly when used in combination with other DNA-damaging agents.

Chloroquine has been reported to interfere with phospholipase C, MAPK, Akt, and cell cycle signalling (Solomon and Lee, 2009). Chloroquine can induce apoptosis, necrosis and inhibit macrophage activity, but the main use for chloroquine in cancer therapy is to inhibit autophagy and sensitise cancer cells to drug treatment. Cancer cells typically

have an upregulated autophagic flux due to their increased cellular stress by their nature. Chloroquine was first noticed to affect autophagy in 1967 (Fedorko, 1967), but it wasn't until the 1980's that chloroquine was recognised as an autophagy inhibitor through prevention of autophagosomal fusion with lysosomes (Trout *et al.*, 1981, Kovacs and Seglen, 1982).

Chloroquine is currently in 15 clinical trials for cancer treatment, but only 1 as a single drug agent (clinicaltrials.gov NCT02333890).

3.1.4 Mefloquine

Mefloquine is a synthetic analogue of quinine which is highly effective against chloroquine-resistant strains of malaria but it is associated with adverse neurological or psychiatric symptoms, particularly in females (Shin *et al.*, 2012). It is currently in a single phase I clinical trial in combination with temozolomide, memantine, and/or metformin in post radio- and chemotherapy treated patients with glioblastoma (clinicaltrials.gov NCT01430351). Mefloquine has previously been shown to disrupt calcium signalling, ER stress through BiP and CHOP, and interfere with the P-glycoprotein (Pgp) membrane ATP pump/transporter, enabling it to cross the blood/brain barrier. This ability to cross the blood/brain barrier is why it has previously been investigated for treatment of neuroblastoma and is used for malarial infection of the nervous system. There are conflicting reports on the ability of mefloquine to induce or inhibit autophagy, it seemingly being dependent on cell type, nutrient status, dose and length of treatment (Sharma *et al.*, 2012, Shin *et al.*, 2012, Golden *et al.*, 2015). Mefloquine has been shown to be more potent than chloroquine in killing a range of glioblastoma cells lines, regardless of *p53* status (Geng *et al.*, 2010) and in a treatment-resistant human fibroblast carcinoma cell line where the effect of mefloquine was shown to be mediated through inhibition of Pgp, sensitising cells to the anti-mitotic effects of vinblastine (Kim *et al.*, 2013). Two further studies using mefloquine for treatment of prostate cancer *in vitro* and *in vivo* showed mefloquine induced non-apoptotic cell death which was mediated through ROS and downstream mitotic signalling (Yan *et al.*, 2013a, Yan *et al.*, 2013b).

4.2 Aims of Chapter 4

Combination therapy of ER stress-induction and autophagy inhibition has been shown to be effective at killing a range of cancer cells. This study theorised that induction of ER stress with nelfinavir and concurrent inhibition of autophagy with chloroquine would lead to accumulation of misfolded proteins and terminal levels of stress specifically within mTORC1 overactive cells. The main aims of this chapter were:

1. To determine whether chloroquine enhances nelfinavir-induced ER stress

2. To investigate whether nelfinavir affects chloroquine-mediated autophagy inhibition

3. To assess whether combination of nelfinavir and chloroquine is an effective and selective inducer of cell death in a panel of mTORC1-overactive cells

4. To identify the mechanism of nelfinavir-chloroquine-mediated cell death

5. To evaluate whether mefloquine is a more effective mediator of cell death than chloroquine in combination with nelfinavir

4.3 Results

4.3.1 Chloroquine enhances nelfinavir-induced ER stress

Autophagy is a survival mechanism employed by cells to alleviate ER stress. Chloroquine was used to determine whether autophagy inhibition would enhance the effects of nelfinavir treatment in mTORC1-overactive cells, as suggested by the drug screen in chapter 1 (Figure 3.7). To establish the best dose of chloroquine for co-treatment with nelfinavir, a western blot was performed to detect the ER stress markers, CHOP and IRE1α (Fig 4.1A). Both proteins were best elevated in *Tsc2*-/- MEFs at a dose of 20 µM chloroquine with the established dose of 20 µM nelfinavir after 6 h of treatment. At this dose in *Tsc2*+/+ MEFs, CHOP and IRE1α were also elevated but this is likely to be partially as a result of unequal protein loading, as indicated by elevated levels of β-actin. PCR to detect spliced XBP1 clearly shows increased spliced XBP1 (lower band) in cells co-treated with nelfinavir and chloroquine compared to treatment with either agent alone (Fig 4.1B). This is evident in both cell lines, but more so in *Tsc2*-/- MEFs, likely due to already basally increased levels of ER stress. This is supported by Q-PCR of CHOP mRNA levels (Fig 4.1C) which showed significantly increased CHOP with co-treatment compared to treatment with either nelfinavir or chloroquine alone (P=0.003, P=0.0009, respectively). CHOP mRNA was significantly increased in *Tsc2*-/- MEFs compared to *Tsc2*+/+ MEFs following co-treatment with nelfinavir and chloroquine (P=0.0012).

4.3.2 Chloroquine blocks the autophagy flux

Western blot was used to examine mTORC1 and autophagy signalling in *Tsc2*+/+ and *Tsc2*-/- MEFs (Figure 4.2). Analysis of phosphorylated rpS6 and S6K1 proteins, both markers of mTORC1 signalling, showed nelfinavir treatment, either singly or in co-treatment with chloroquine, greatly reduced phosphorylation of both proteins in *Tsc2*+/+ but not in *Tsc2*-/- MEFs. This supports data previously seen in chapter 1 (Figure 3.3). There is a modest reduction in phosphorylation of S6K1 in Tsc2-/- MEFs with nelfinavir and chloroquine co-treatment but this is not replicated by rpS6 protein. As expected, LC3-II and SQSTM1 accumulation was seen in all chloroquine treatments regardless of co-treatment with nelfinavir, consistent with a block in late stage autophagy.

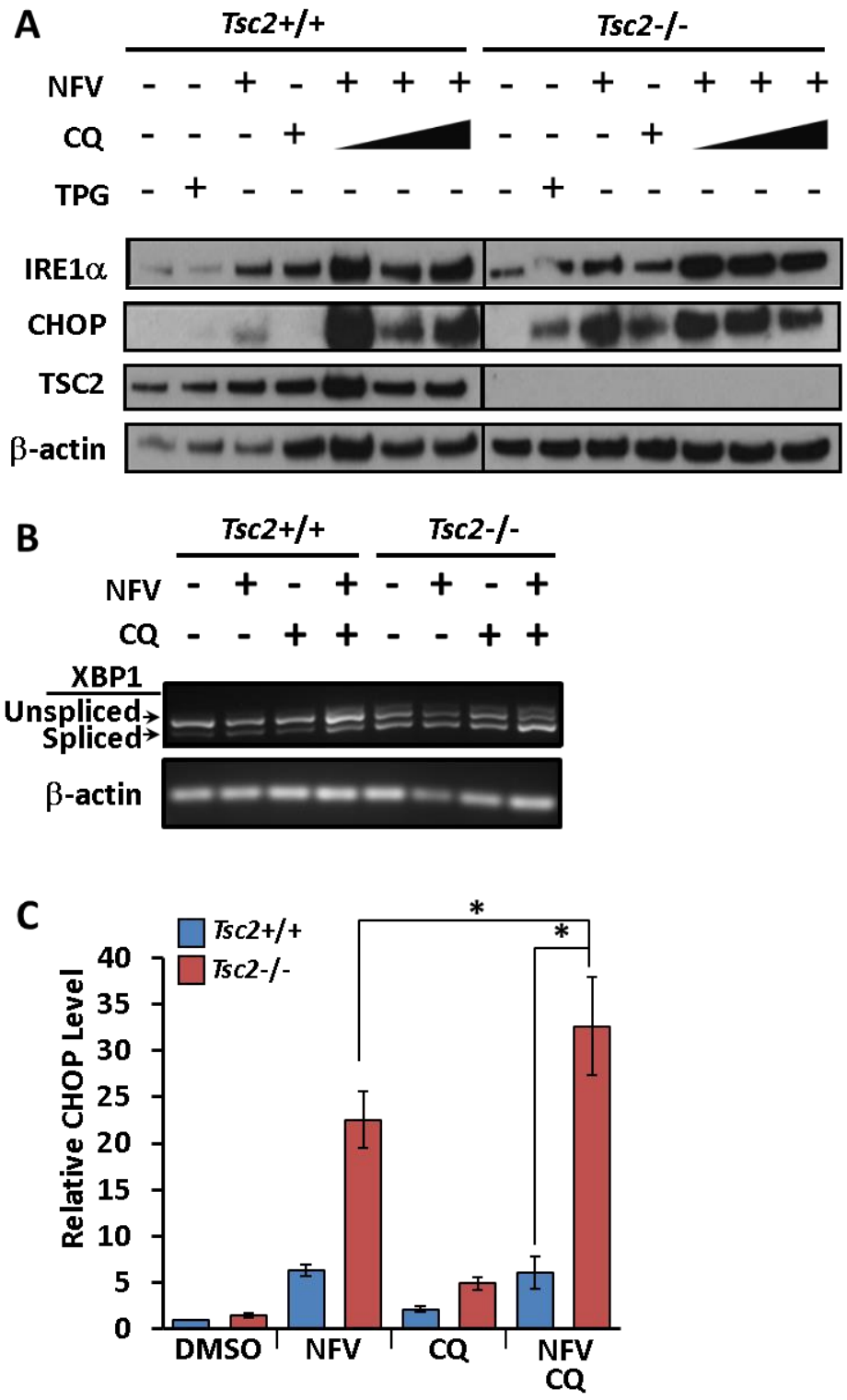

Figure 4.1: Chloroquine enhances nelfinavir-induced ER stress. A) *Tsc2*+/+ and *Tsc2*-/- MEFs were treated with either DMSO vehicle alone, 1 µM thapsigargin (TPG), 20 µM nelfinavir (NFV), 20 µM chloroquine (CQ) or a combination of NFV and 5 µM, 20 µM or 50 µM CQ for 6 h. Protein extracts were analysed for CHOP, IRE1α, TSC2 and β-actin. B and C) *Tsc2*+/+ and *Tsc2*-/- MEFs were treated with either DMSO vehicle alone, 20 µM nelfinavir (NFV), 20 µM chloroquine (CQ) or a combination of NFV and 20 µM CQ for 3 h. B) PCR products for XBP1 mRNA were resolved on agarose gels (unspliced 480 bp [upper band], spliced 454 bp [lower band]). β-actin is shown as a control. C) CHOP mRNA was analysed and standardised against β-actin. n=3, *P< 0.05.

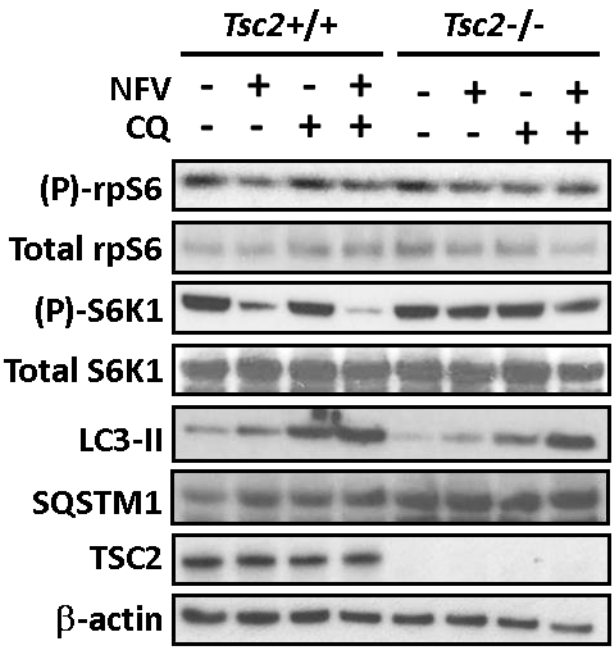

Figure 4.2: Chloroquine arrests the autophagy flux which is enhanced by nelfinavir. *Tsc2*+/+ and *Tsc2*-/- MEFs were treated with either DMSO vehicle alone, 20 μM nelfinavir (NFV), 20 μM chloroquine (CQ) or a combination of NFV and 20 μM CQ for 3 h. Protein extracts were analysed for phosphorylated and total rpS6, phosphorylated and total S6K1, LC3-II, SQSTM1, TSC2 and β-actin.

4.3.3 *Tsc2*-/- MEFs are more motile than *Tsc2*+/+ MEFs

Figure 4.3 shows stills from time lapse analysis of *Tsc2*+/+ and *Tsc2*-/- MEFs with and without treatment over 48 h. Cells were plated at a low density to allow for continuous analysis of movement over the duration of the experiment. Data analysis of movement in micrometers in shown per 15 minute interval (Appendix VI A) and cumulatively (Appendix VI B) over the initial 0-6 h of the experiment to assess cell behaviour around the 3 h treatment timepoint used to assess ER stress. DMSO vehicle control (untreated) *Tsc2*-/- MEFs were significantly more motile than *Tsc2*+/+ MEFs (P=<0.001). Both single treatment with nelfinavir and co-treatment with nelfinavir and chloroquine significantly reduced motility in both *Tsc2*-/- cells (P=<0.001) and in *Tsc2*+/+ MEFs (P=<0.01), but *Tsc2*-/- MEFs were significantly less motile than *Tsc2*+/+ MEFs following nelfinavir-chloroquine co-treatment (P=<0.001). Cumulatively, *Tsc2*-/- MEFs travelled an average distance of 198.3 µm which was reduced to 117.8 µm with nelfinavir treatment, and to 50 µm following nelfinavir-chloroquine co-treatment – a 75 % reduction. *Tsc2*+/+ MEFs travelled an average distance of 165.7 µm which was reduced to 108.3 µm with nelfinavir treatment, and to 132.1 µm following nelfinavir-chloroquine co-treatment – a 20 % reduction.

4.3.4 Nelfinavir and chloroquine co-treatment causes significant and selective cell death in multiple *in vitro* models with overactive mTORC1

Flow cytometry with DRAQ7 staining was used to investigate whether co-treatment with neflinavir and chloroquine caused cell death in *Tsc2*-/- MEFs (Fig 4.4). As previously shown in chapter 1 (Fig 3.7A), neither nelfinavir nor chloroquine was particularly effective at induction of cell death as single agents (Fig 4.4A). However, combined nelfinavir and chloroquine induced significant and selective cell death in *Tsc2*-/- MEFs compared to *Tsc2*+/+ MEFs after 24 h (9 % vs 49 %, P=<0.001, Fig 4.4B). Figure 4.4C shows morphological changes apparent in *Tsc2*+/+ MEFs and *Tsc2*-/- MEFs with and without treatment with nelfinavir and chloroquine after 24 h.

To test whether the effects of nelfinavir and chloroquine co-treatment could be replicated in another model of overactive mTORC1 signalling, the p53-positive Eker rat leiomyoma cells which are *Tsc2*-null (ELT3-V3), and a rescued cell line with *Tsc2* added back (ELT3-T3) were used. Initial assessment of mTORC1 and autophagy signalling

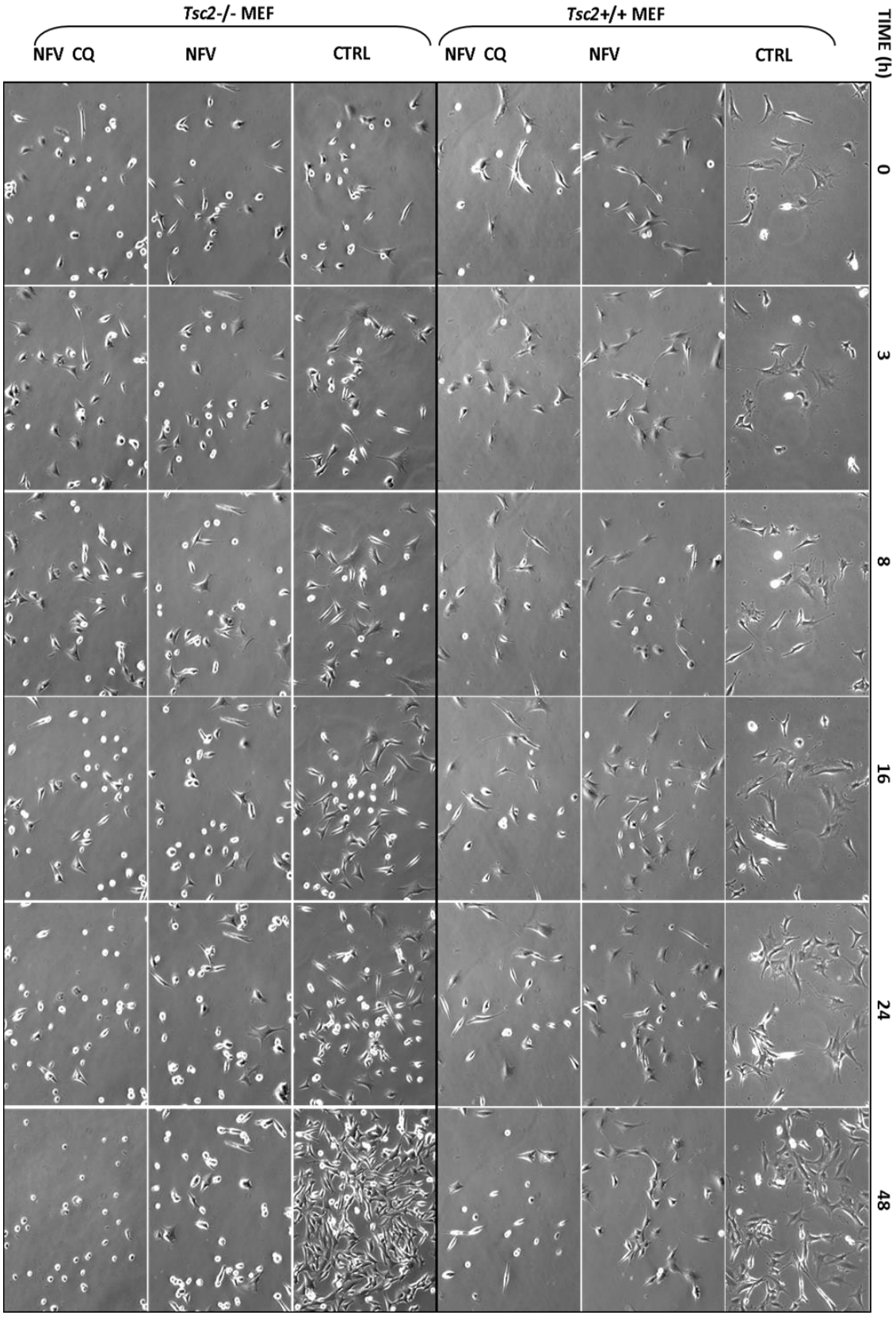

Figure 4.3: Combination of nelfinavir and chloroquine causes selective cell death in *Tsc2*-/- MEFs at 24 h of treatment. *Tsc2*+/+ and *Tsc2*-/- MEFs were plated at low density and allowed to adhere for 24 h before treatment with either DMSO vehicle alone, 20 µM nelfinavir (NFV), or a combination of NFV and 20 µM CQ and assessment over 48 h using time lapse microscopy. Images shown are representative of 3 technical replicates.

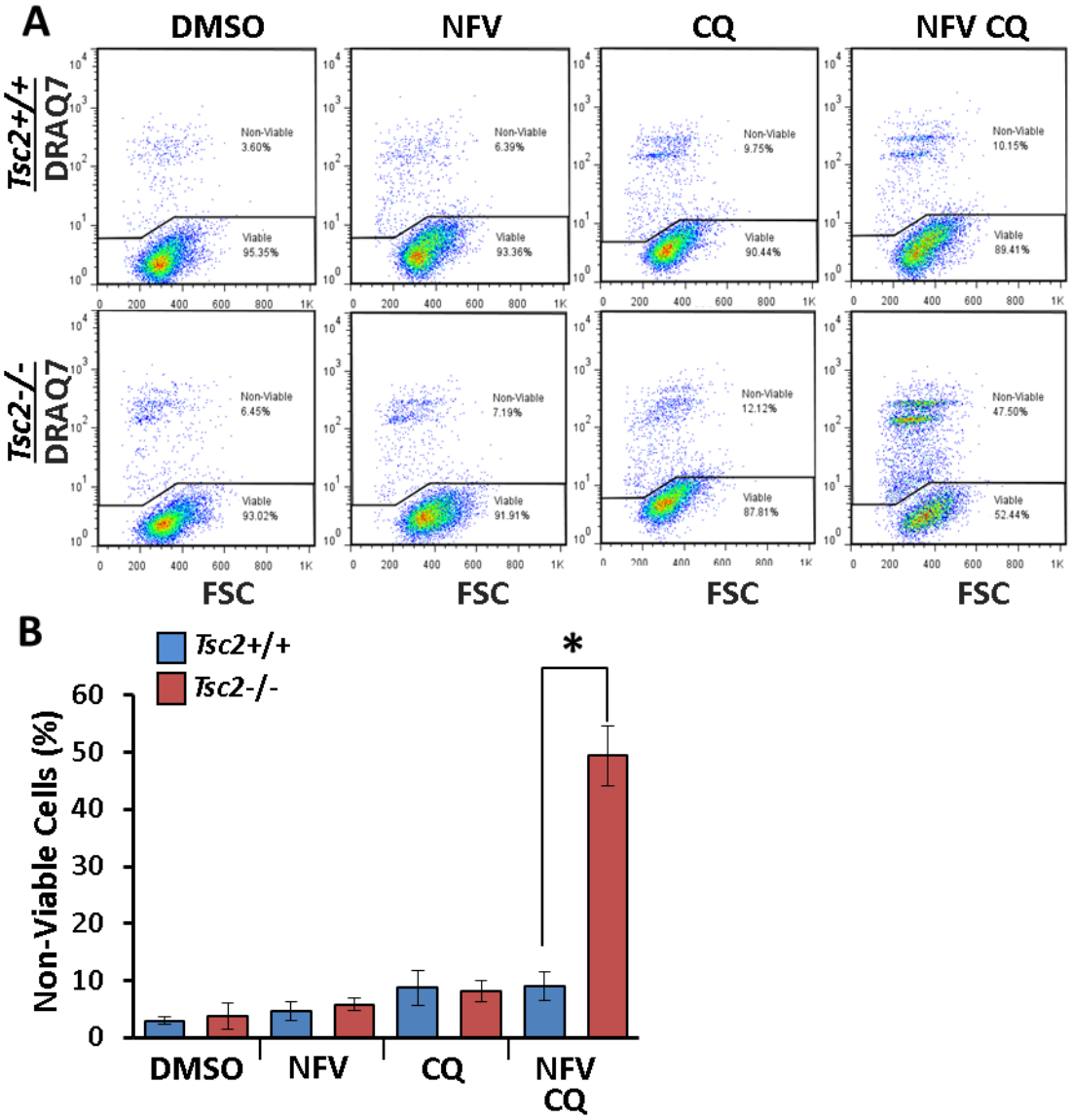
A
DMSO
NFV
CQ
NFV CQ
Tsc2+/+ DRAQ7
Tsc2-/- DRAQ7
Non-Viable 3.60%
Viable 95.35%
Non-Viable 6.39%
Viable 93.36%
Non-Viable 9.75%
Viable 90.44%
Non-Viable 10.15%
Viable 89.41%
Non-Viable 6.45%
Viable 93.02%
Non-Viable 7.19%
Viable 91.91%
Non-Viable 12.12%
Viable 87.81%
Non-Viable 47.50%
Viable 52.44%
FSC
B
Tsc2+/+
Tsc2-/-
*
Non-Viable Cells (%)
0
10
20
30
40
50
60
DMSO
NFV
CQ
NFV CQ

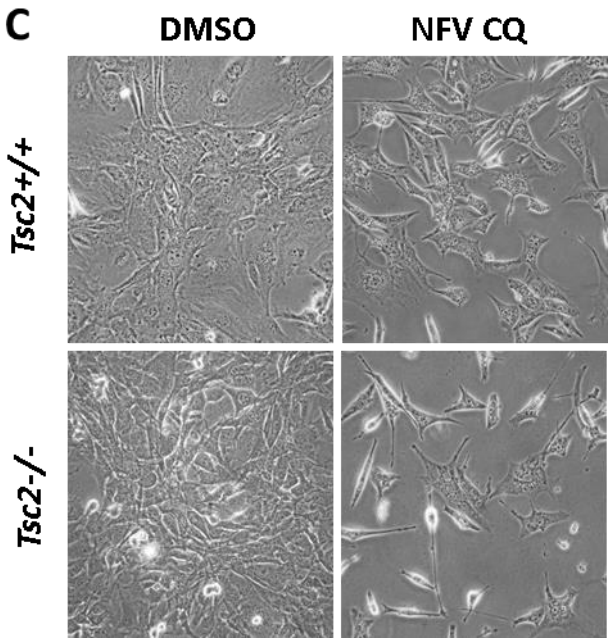

Figure 4.4: Combination of nelfinavir and chloroquine causes selective and significant cell death in *Tsc2*-/- MEFs. *Tsc2*+/+ and *Tsc2*-/- MEFs were treated with either DMSO vehicle alone, 20 µM nelfinavir (NFV), 20 µM chloroquine (CQ), or a combination of NFV and CQ for 24 h. A) For quantification of cell death, cells were subjected to flow cytometry analysis with DRAQ7 staining. The number of DRAQ7-stained cells are graphed in B. n=3, *P<0.05. C) Phase contrast images at x 100 magnification.

following short drug treatment replicated results seen in MEFs (Fig 4.5A) in that co-treatment produced a modest reduction in phosphorylation of S6K1 was seen ELT3-V3 cells, and LC3-II was elevated where cells were treated with chloroquine. Interestingly, SQSTM1 is reduced in ELT3-V3 cells treated with nelfinavir and chloroquine, despite elevated LC3-II. This could be interpreted as an increase in autophagy induction but flux is still blocked at later stages by chloroquine. Cell death was assessed by flow cytometry with DRAQ7 staining following 24 h treatment (Fig 4.5B). Although there was a trend for cell death to be increased following co-treatment with nelfinavir and chloroquine in ELT3-V3 cells compared to ELT3-T3 cells, there was no significant effect and percentage levels of cell death were insubstantial compared to MEFs (Fig 4.5C). As the time lapse data in MEFs showed nelfinavir and chloroquine continued to induce cell death for at least 48 h (Fig 4.3), the treatment length was increased to 48 h for ELT3 cells (Fig 4.6A/B). At this time point, significant and selective cell death was observed in ELT3-V3 cells compared to ELT3-T3 cells with nelfinavir and chloroquine co-treatment (37.8% vs 10.5%, P=<0.001). This was significantly increased compared to either nelfinavir or chloroquine single treatment in ELT3-V3 cells (5.6 %, P=<0.001, and 12.7 %, P=0.003, respectively).

To further test the general ability of nelfinavir and chloroquine to induce cell death in mTORC1-overactive models, a human *TSC2*-null AML cell line was used (Fig 4.7). Short term co-treatment with nelfinavir and chloroquine modestly reduced phosphorylation of rpS6 and increased levels of LC3-II (Fig 4.7A). In Figure 3.6B/C, 24 h treatment showed increased cell death with nelfinavir and chloroquine which was significantly different to untreated cells (10.1 % vs 25.3 %, P=0.001) and to single treatment with nelfinavir (14.4 %, P=0.015), but not to single treatment with chloroquine (17.6 %, P=0.083).

To test whether nelfinavir and chloroquine treatment was effective in a human cancer cell line with overactive mTORC1 signalling, the lung cancer cell line NCI-H460 was used (Fig 4.8). This cell line has intact TSC1/2 and has over active mTORC through KRas oncogenic mutation. Rapamycin was used in conjunction with drug treatments to reduce mTORC1 signalling and replicate a ‘rescued’ version of the cells for comparison purposes. Flow cytometry with DRAQ7 staining was used to assess cell death following 48 h nelfinavir and chloroquine treatment in the presence or absence of rapamycin

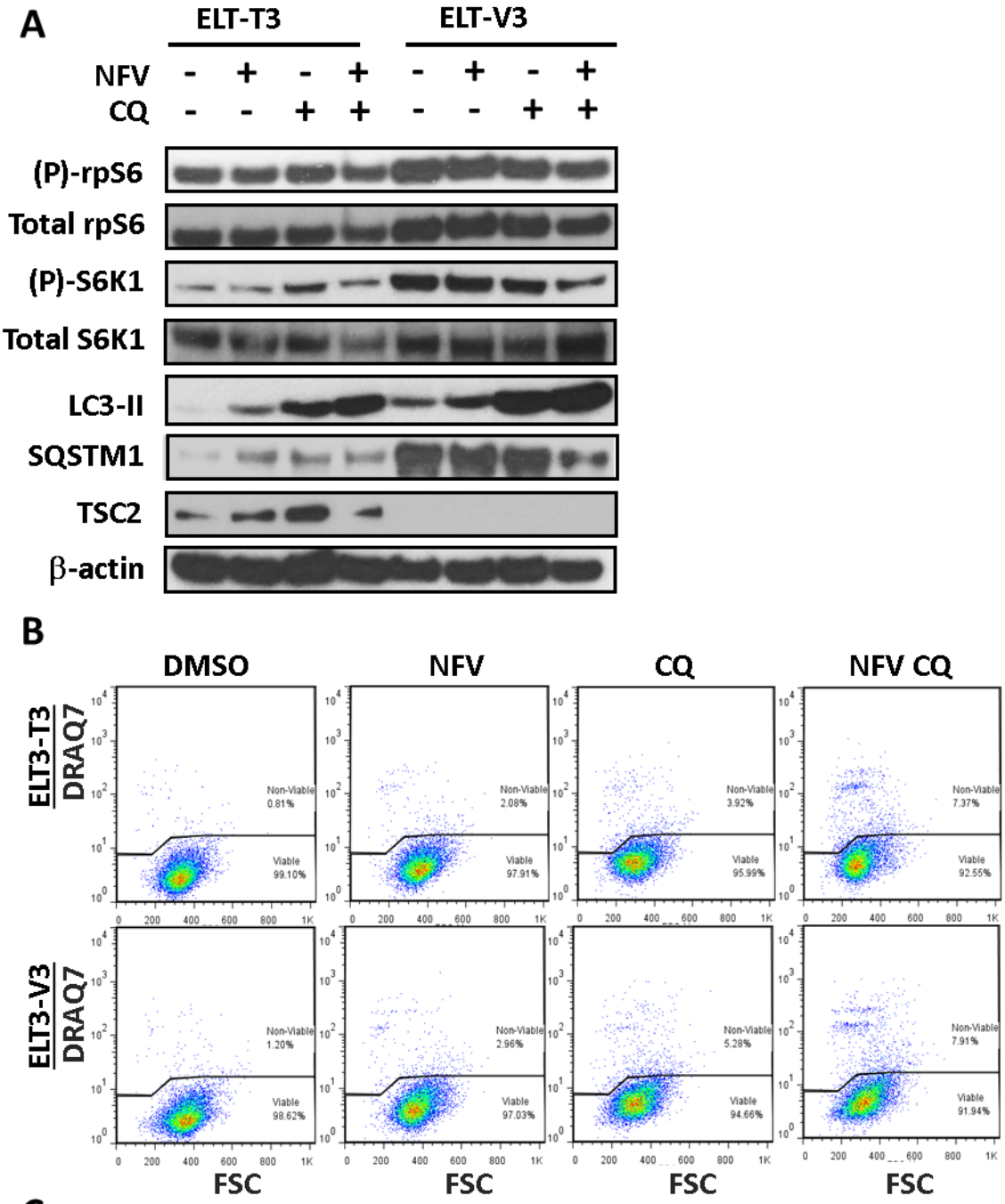
A
ELT-T3
ELT-V3
NFV
CQ
(P)-rpS6
Total rpS6
(P)-S6K1
Total S6K1
LC3-II
SQSTM1
TSC2
β-actin
B
DMSO
NFV
CQ
NFV CQ
ELT3-T3
DRAQ7
ELT3-V3
DRAQ7
Non-Viable 0.81%
Viable 99.10%
Non-Viable 2.08%
Viable 97.91%
Non-Viable 3.92%
Viable 95.99%
Non-Viable 7.37%
Viable 92.55%
Non-Viable 1.20%
Viable 98.62%
Non-Viable 2.96%
Viable 97.03%
Non-Viable 5.28%
Viable 94.66%
Non-Viable 7.91%
Viable 91.94%
FSC
C
Non-Viable Cells (%)
ELT3-T3
ELT3-V3
DMSO
NFV
CQ
NFV CQ

Figure 4.5: 24 h combination of nelfinavir and chloroquine is insufficient to kill ELT3-V3 cells at 24 h of treatment. ELT3-T3 and ELT-V3 cells were treated with either DMSO vehicle alone, 20 μM nelfinavir (NFV), 20 μM chloroquine (CQ), or a combination of NFV and CQ for A) 3 h; protein extracts were analysed for phosphorylated and total rpS6, phosphorylated and total S6K1, LC3-II, SQSTM1, TSC2 and β-actin, or B) 24 h; cells were subjected to flow cytometry analysis with DRAQ7 staining. The number of DRAQ7-stained cells are graphed in C. n=3, *P<0.05.

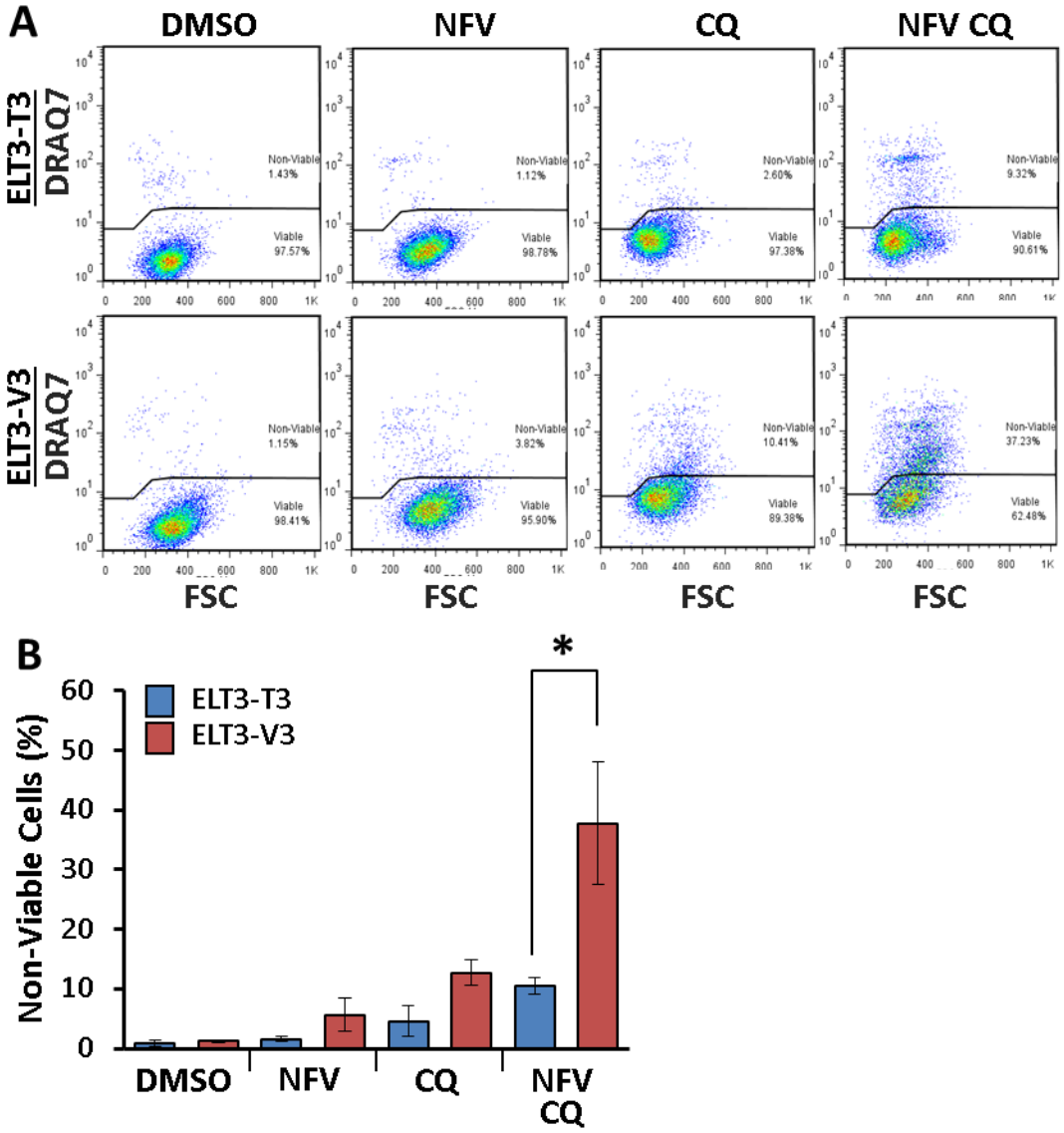

Figure 4.6: Combination of nelfinavir and chloroquine causes selective and significant cell death in ELT3-V3 cells at 48 h of treatment. ELT3-T3 and ELT-V3 cells were treated with either DMSO vehicle alone, 20 µM nelfinavir (NFV), 20 µM chloroquine (CQ), or a combination of NFV and CQ for 48 h. A) Cells were subjected to flow cytometry analysis with DRAQ7 staining. The number of DRAQ7-stained cells are graphed in B. n=3, *P<0.05.

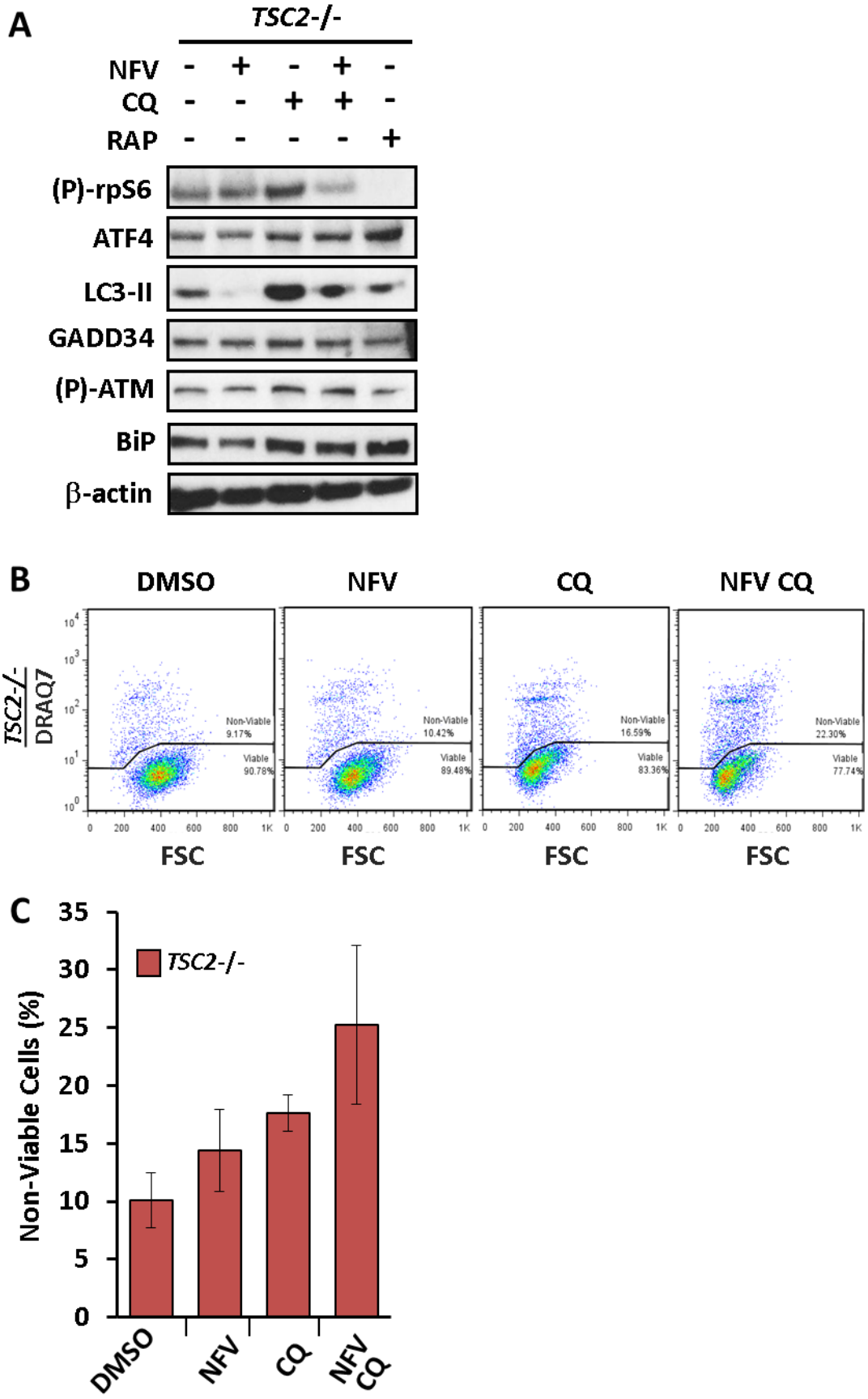
A
TSC2-/-
NFV - + - + -
CQ - - + + -
RAP - - - - +
(P)-rpS6
ATF4
LC3-II
GADD34
(P)-ATM
BiP
β-actin
B
DMSO
NFV
CQ
NFV CQ
TSC2-/-
DRAQ7
Non-Viable 9.17%
Viable 90.78%
Non-Viable 10.42%
Viable 89.48%
Non-Viable 16.59%
Viable 83.36%
Non-Viable 22.30%
Viable 77.74%
FSC
C
TSC2-/-
Non-Viable Cells (%)
0
5
10
15
20
25
30
35
DMSO
NFV
CQ
NFV CQ

Figure 4.7: Combination of nelfinavir and chloroquine causes significant cell death in AML cells at 24 h of treatment. *TSC2*-/- AML cells were treated with either DMSO vehicle alone, 20 μM nelfinavir (NFV), 20 μM chloroquine (CQ), or a combination of NFV and CQ for A) 3 h; protein extracts were analysed for phosphorylated rpS6, ATF4, LC3-II, GADD34, phosphorylated ATM, BiP and β-actin. 100 nM Rapamycin was used as a positive control for mTORC1 inhibition. B) Following 24 h of treatment, cells were subjected to flow cytometry analysis with DRAQ7 staining. The number of DRAQ7-stained cells are graphed in C. n=3, *P<0.05.

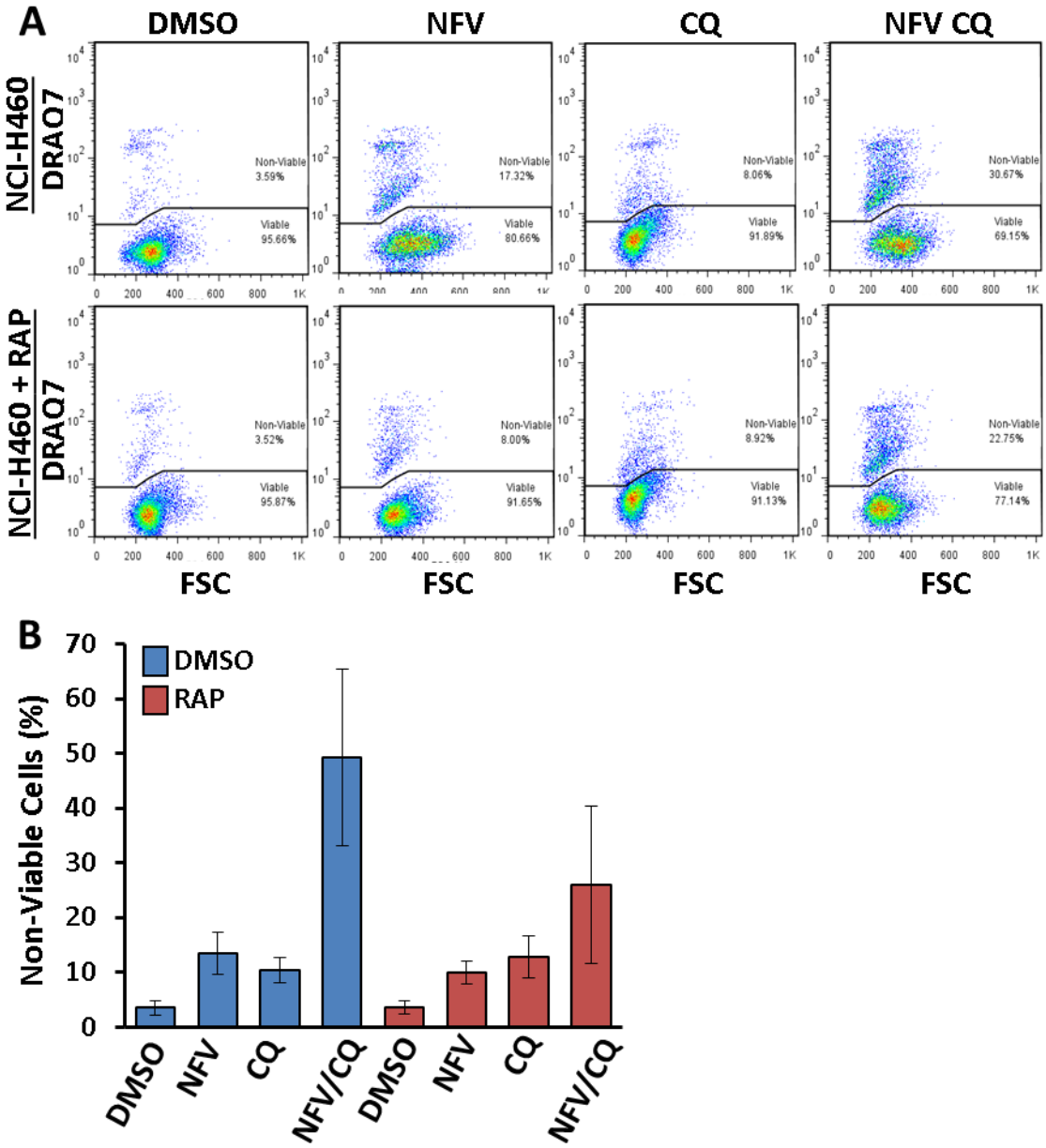
A
DMSO
NFV
CQ
NFV CQ
NCI-H460
DRAQ7
NCI-H460 + RAP
DRAQ7
Non-Viable
3.59%
Viable
95.66%
Non-Viable
17.32%
Viable
80.66%
Non-Viable
8.06%
Viable
91.89%
Non-Viable
30.67%
Viable
69.15%
Non-Viable
3.52%
Viable
95.87%
Non-Viable
8.00%
Viable
91.65%
Non-Viable
8.92%
Viable
91.13%
Non-Viable
22.75%
Viable
77.14%
FSC
FSC
FSC
FSC
B
Non-Viable Cells (%)
DMSO
RAP
0
10
20
30
40
50
60
70
DMSO
NFV
CQ
NFV/CQ
DMSO
NFV
CQ
NFV/CQ

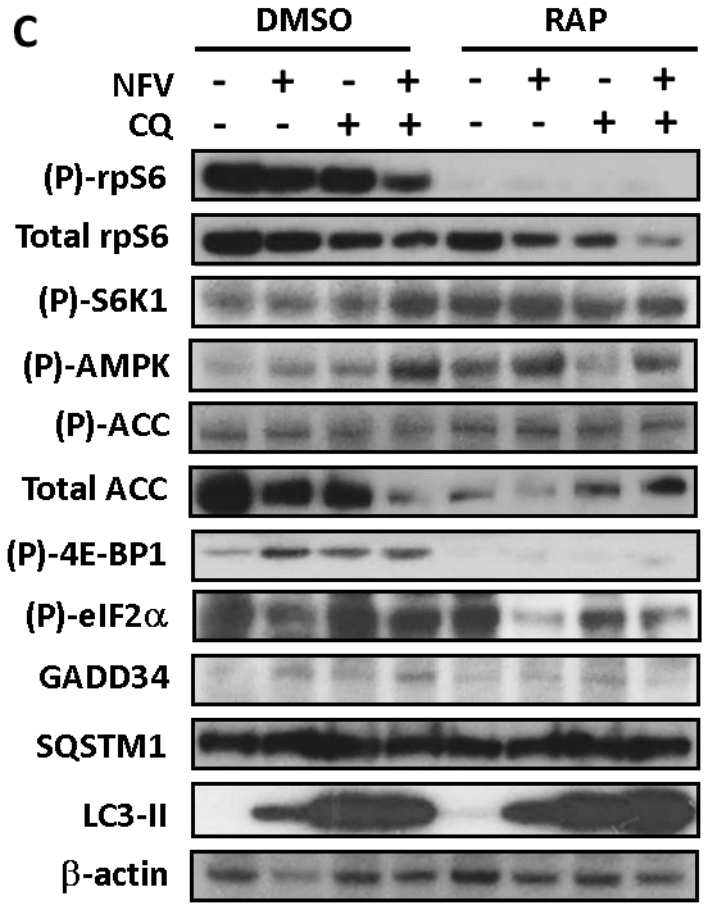

Figure 4.8: Combination of nelfinavir and chloroquine causes significant cell death in NCI-H460 cells at 48 h of treatment. NCI-H460 cells were treated with either DMSO vehicle alone, 20 μM nelfinavir (NFV), 20 μM chloroquine (CQ), or a combination of NFV and CQ for 48 h. 100nM Rapamycin was used to rescue mTORC1 over-activity and compare effectiveness of drug treatments. A) Following 48 h of treatment, cells were subjected to flow cytometry analysis with DRAQ7 staining. The number of DRAQ7-stained cells are graphed in B. C) Protein extracts were analysed for phosphorylated and total rpS6, phosphorylated S6K1, phosphorylated AMPK, phosphorylated and total ACC, phosphorylated 4E-BP1, phosphorylated eiF2α, GADD34, SQSTM1, LC3-II and β-actin. n=3, *P<0.05.

(Fig 4.8A). Figure 4.8A shows combined nelfinavir and chloroquine treatment induced significant cell death compared to untreated cells (49.2 % vs 3.6 %, P=<0.001) which was distinct from single treatment with either nelfinavir or chloroquine alone (13.4 %, P=<0.001, and 10.5 %, P=<0.001, respectively). This was slightly significantly different to nelfinavir and chloroquine co-treatment with the addition of rapamycin (P=0.035, Fig 4.8B).

A panel of western blots was used to explore the effects of 48 h treatment on cellular signalling in NCI-H460 cells with or without rapamycin (Fig 4.8C). Similar to that observed in *Tsc2*-/- MEFs, ELT3-V3, and AML cells, co-treatment with nelfinavir and chloroquine modestly reduced phosphorylation of rpS6. However, this was not replicated in S6K1. As seen in other cell lines, LC3-II is elevated with chloroquine treatments but also with nelfinavir treatment alone. Of interest, phosphorylation of AMPK is elevated with co-treatment which may link to reduced rpS6 phosphorylation and also the slight increase in GADD34 protein.

4.3.5 Nelfinavir-chloroquine-induced cell death is not caspase-dependent

To discover the mechanism of cell death, a western blot was performed on *Tsc2*+/+ and *Tsc2*-/- MEFs following 24 h treatment with a standard dose of nelfinavir and an escalating dose of chloroquine. Antibodies for detection of whole and cleaved PARP, and whole and cleaved caspase-3 were employed. Appendix VII shows that, even with 50 µM chloroquine combined with 20 µM nelfinavir, no cleaved products of either PARP of caspase-3 can be seen in either cell line. A reduction in whole protein levels can be observed, consistent with what might be expected from co-treatment, but without detection of cleaved protein no real inference can be made.

4.3.6 Nelfinavir-chloroquine-induced cell death is unlikely through DNA damage or ROS induction

To assess whether chloroquine was enhancing nelfinavir through causing DNA damage, a western blot was performed on *Tsc2*+/+ and *Tsc2*-/- MEFs following 24 h treatment for the detection of phosphorylated H2A histone family member X (H2AX), Appendix VIII). H2AX becomes phosphorylated as a reaction following DNA double strand breaks. In the *Tsc2*-/- cells, co-treatment does indeed show a very minimal level of

phosphorylated H2AX, but this is no higher than in untreated cells and does not compare to the large increase shown in thapsigargin treatment. GADD34 was also probed for and, in *Tsc2*-/- MEFs, a small increase can be observed following nelfinavir treatment which is accentuated when combined with chloroquine, to a similar extent to thapsigargin treatment. Together, these results show combined nelfinavir and chloroquine treatment is an effective inducer of ER stress without causing DNA damage.

To investigate whether cell death was autophagy-mediated 'autosis', digoxin was added in combination with nelfinavir and chloroquine over 48 h in an attempt to rescue cell death through Na^+/Ka^+ ATPase inhibition (Appendix IX). Initial observations with this treatment showed no change in percentage of cell death.

Because *Tsc2*-/- cells are known to have defects in mitochondria and increased ROS levels (Parkhitko *et al.*, 2014), the ROS scavenger NAC was employed to assess whether cell death via nelfinavir and chloroquine co-treatment was mediated by ROS. Using flow cytometry and DRAQ7 staining, treated *Tsc2*+/+ and *Tsc2*-/- MEFs were assessed for cell death (Fig 4.9A/B). Addition of NAC to nelfinavir-chloroquine treatment did not rescue cell death in *Tsc2*-/- MEFs (61.2 % vs 36.5 %, P=0.883). Interestingly, NAC increased chloroquine-induced cell death selectively in *Tsc2*-/- MEFs compared to *Tsc2*+/+ MEFs (31.7 % vs 7.5 %, P=<0.001). A brief examination of the effects of NAC in nelfinavir-chloroquine-treated NCI-H460 cells also failed to show rescue of treatment, confirming the results observed in the MEFs (Appendix X).

4.3.7 Mefloquine is an effective inducer of cell death

The chloroquine analogue, mefloquine, was assessed alongside chloroquine in *Tsc2*+/+ and *Tsc2*-/- MEFs (Fig 4.10). A western blot was used to compare the inhibition of autophagy between a standard dose of chloroquine (20 μM) and a low to high dose of mefloquine (2.5, 5, 10, and 20 μM) after 3 h treatment (Fig 4.10A). In *Tsc2*+/+ MEFs, chloroquine strongly induced conversion of LC3-I to LC3-II, which was not replicated by mefloquine at any dose. In *Tsc2*-/- MEFs, only the highest dose of mefloquine compared to chloroquine-induced LC3-II protein levels, but was still not equal. This showed that mefloquine does not induce autophagy to a similar extent to chloroquine. Assessment by flow cytometry and DRAQ7 staining showed mefloquine could induce

cell death in *Tsc2*-/- MEFs at 10 µM (25 %, P=<0.001, Fig 4.10B/C). This was significantly different to *Tsc2*+/+ MEFs (12 %, P=0.004). No significant degree of cell death was seen at lower concentrations of mefloquine.

4.3.8 Nelfinavir-chloroquine-induced cell death is independent of autophagy and is recued by bafilomycin-A1

To confirm chloroquine-mediated autophagy inhibition is the mechanism enhancing nelfinavir, a panel of autophagy inhibitors were employed to replicate the effects of cell death when combined with nelfinavir (Fig 4.11). Bafilomycin-A1 is a well-known inhibitor of late stage autophagy through prevention of autophagosomal-lysosomal fusion. More precisely, this is due to inhibition of the vacuolar type H^+-ATPase on lysosomes which prevents their acidification (Klionsky *et al.*, 2008). 3-MA suppresses autophagy early in the flux through prevention of autophagosome formation by inhibition of class III PI3Ks which stops downstream recruitment of ATG proteins. However, 3-MA has been shown to have contrasting effects on autophagy depending on nutrient conditions (Wu *et al.*, 2010). A western blot to detect disruption of the autophagy flux through LC3-II and SQSTM1 protein levels was employed using 3 h treated samples from *Tsc2*+/+ and *Tsc2*-/- MEFs (Fig 4.11A). In both cell lines, treatment with chloroquine or bafilomycin-A1 caused an increase in LC3-II and SQSTM1 protein levels suggestive of a block in late stage autophagy. However, treatment with either 3-MA or mefloquine did not increase either protein. When autophagy inhibitors were combined with nelfinavir, similar effects were seen apart from combined nelfinavir and 3-MA, which showed increased SQSTM1 protein in both cell lines compared to treatment with either agent alone. Since the effects of chloroquine were previously shown to be prevented when combined with bafilomycin-A1 (Harhaji-Trajkovic *et al.*, 2012, Shacka *et al.*, 2006). Interestingly, bafilomycin-A1 completely rescued the effects of nelfinavir and chloroquine on autophagy in both cell lines (Fig 4.11A). A concurrent experiment to investigate the effects of different autophagy inhibitors on cell death was performed using flow cytometry and DRAQ7 staining following 24 h treatment (Fig 4.11B/C). As single agents, 3-MA and mefloquine were able to cause a small degree in cell death which was increased in *Tsc2*-/- compared to *Tsc2*+/+ MEFs (mean 17 % vs 2.5 %, P=<0.001, and 25.7 % vs 15 %, P=0.087, respectively). Bafilomycin did not cause cell death in either cell line compared

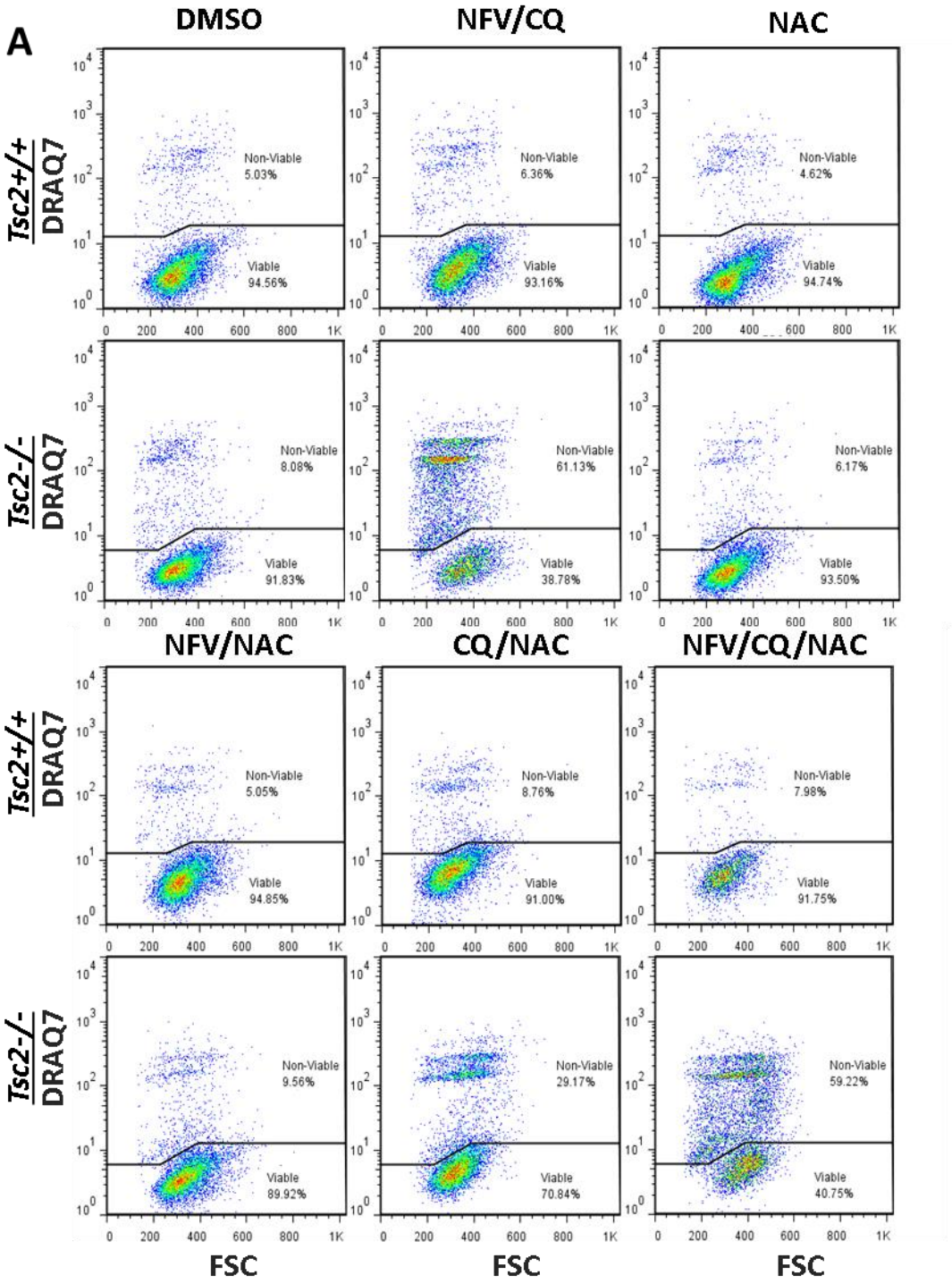
A
DMSO
NFV/CQ
NAC
NFV/NAC
CQ/NAC
NFV/CQ/NAC
Tsc2+/+ DRAQ7
Tsc2-/- DRAQ7
Non-Viable 5.03%
Viable 94.56%
Non-Viable 6.36%
Viable 93.16%
Non-Viable 4.62%
Viable 94.74%
Non-Viable 8.08%
Viable 91.83%
Non-Viable 61.13%
Viable 38.78%
Non-Viable 6.17%
Viable 93.50%
Non-Viable 5.05%
Viable 94.85%
Non-Viable 8.76%
Viable 91.00%
Non-Viable 7.98%
Viable 91.75%
Non-Viable 9.56%
Viable 89.92%
Non-Viable 29.17%
Viable 70.84%
Non-Viable 59.22%
Viable 40.75%
FSC
FSC
FSC

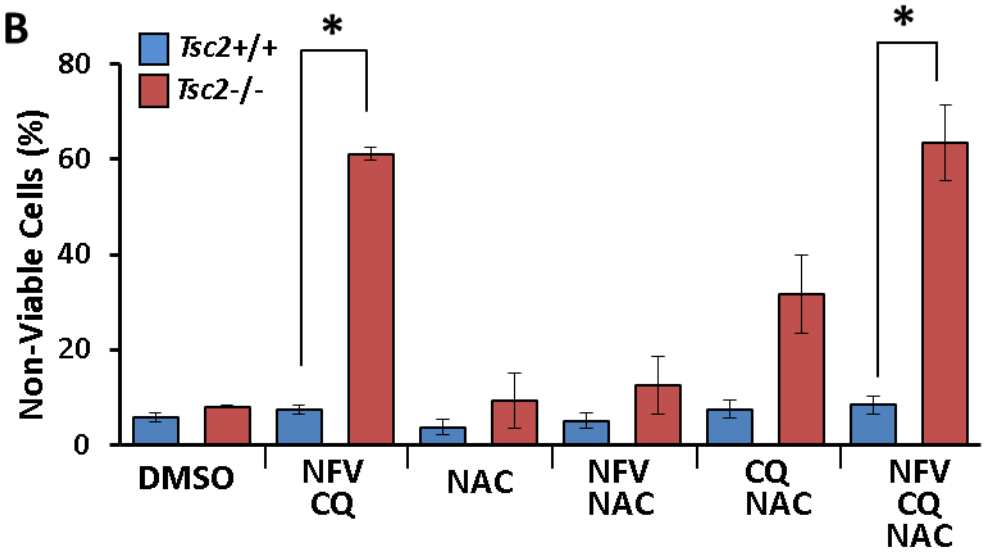

Figure 4.9: Nelfinavir and chloroquine-mediated cell death is unlikely through ROS. *Tsc2*+/+ and *Tsc2*-/- MEFs were treated with either DMSO vehicle alone, 20 µM nelfinavir (NFV), 20 µM chloroquine (CQ), 20 µM N-acetyl-cysteine (NAC) or a combination as shown, for 24 h. A) Cells were subjected to flow cytometry analysis with DRAQ7 staining. The number of DRAQ7-stained cells are graphed in B.

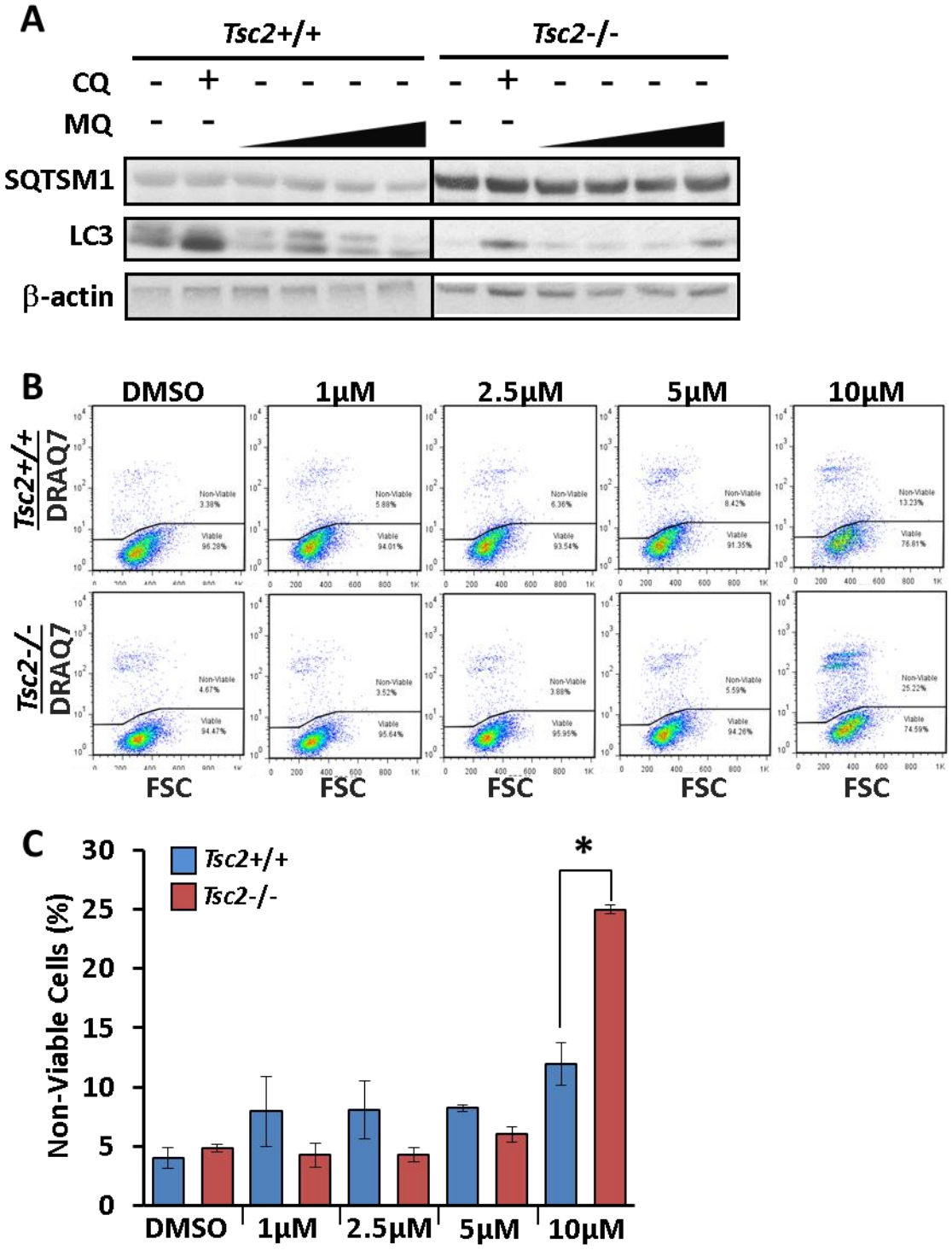

Figure 4.10: Investigation of the chloroquine analogue, mefloquine. *Tsc2*+/+ and *Tsc2*-/- MEFs were treated with either DMSO vehicle alone, 20 μM chloroquine (CQ), or a dose range of mefloquine (MQ) as described. A) Protein lysates were analysed for SQSTM1, LC3-I and –II, and β-actin after 3 h 2.5 μM, 5 μM, 10 μM or 20 μM MQ treatment. B) Cells were subjected to flow cytometry analysis with DRAQ7 staining after 24 h treatment with either 1 μM, 2.5 μM, 5 μM, or 10 μM MQ. The number of DRAQ7-stained cells are graphed in C.

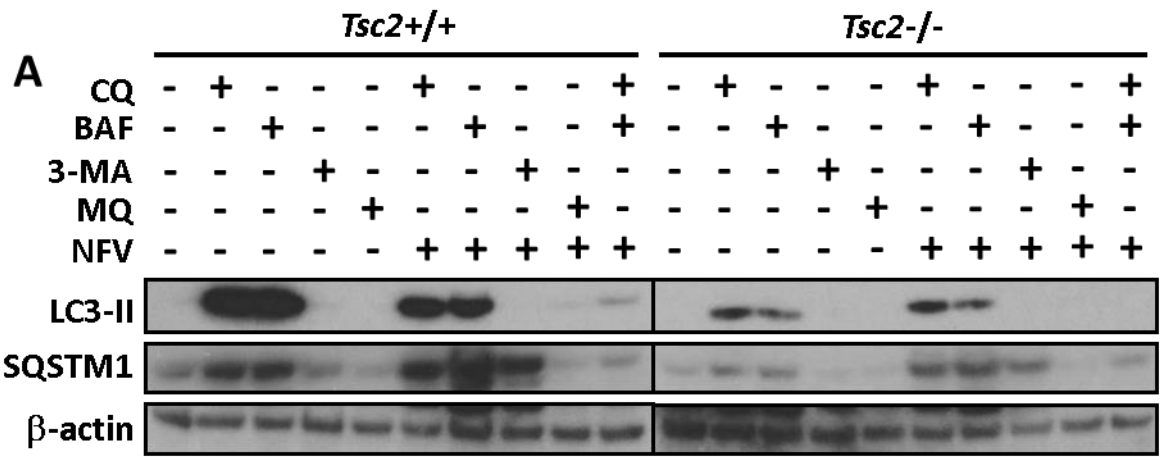
A
Tsc2+/+
Tsc2-/-
CQ
BAF
3-MA
MQ
NFV
LC3-II
SQSTM1
β-actin

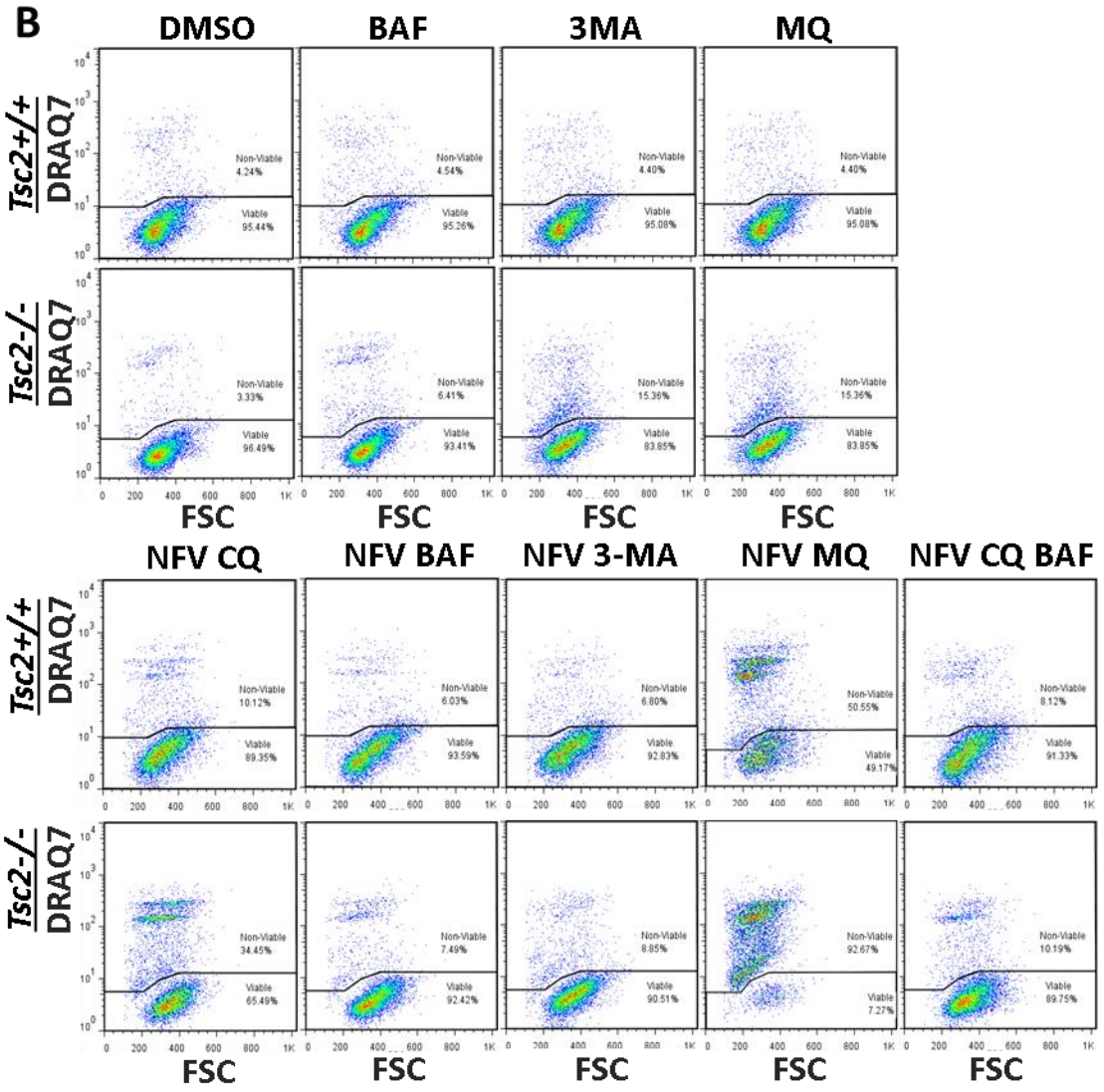
B
DMSO
BAF
3MA
MQ
Tsc2+/+ DRAQ7
Tsc2-/- DRAQ7
FSC
NFV CQ
NFV BAF
NFV 3-MA
NFV MQ
NFV CQ BAF

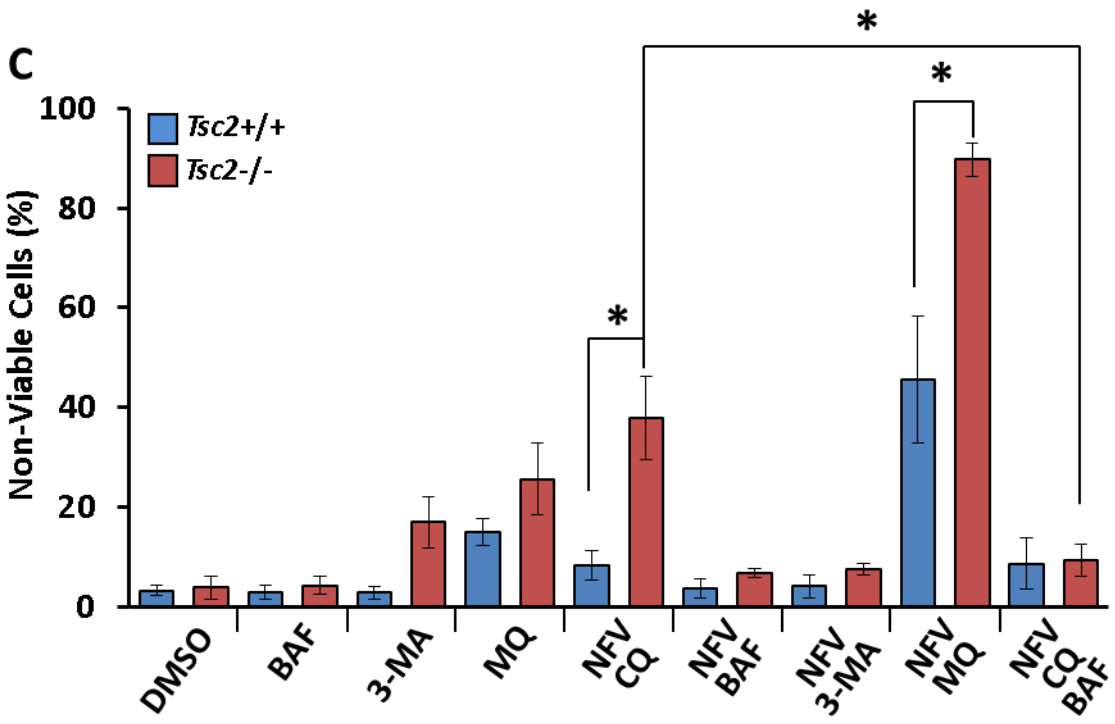

Figure 4.11: Nelfinavir and chloroquine-mediated cell death is independent of autophagy inhibition and is rescued by vacuolar ATPase inhibition with bafilomycin-A1. *Tsc2*+/+ and *Tsc2*-/- MEFs were treated with either DMSO vehicle alone, 20 µM chloroquine (CQ), 2.5 µM bafilomycin-A1 (BAF), 5 µM 3-methyl adenine (3-MA), 10 µM mefloquine (MQ), or a combination with 20 µM nelfinavir (NFV) as shown. A) Following 3 h treatment, protein lysates were analysed for LC3-II, SQSTM1 and β-actin. B) Following 24 h treatment, cells were subject to flow cytometry analysis with DRAQ7 staining. The number of DRAQ7-stained cells are graphed in C.

to untreated cells and this was barely increased when combined with nelfinavir (2.9 % to 3.8 % in *Tsc2*+/+ MEFs and 4.3 % to 6.9 % in *Tsc2*-/- MEFs). When combined with nelfinavir, 3-methyladenine-induced *Tsc2*-/- cell death was reduced from 17 % to 7.6 %. In contrast, combination of nelfinavir with mefloquine greatly enhanced cell death in both cell lines to 46% in *Tsc2*+/+ and 90% in *Tsc2*-/- MEFs (P=0.033) which was significantly increased from single treatment with mefloquine (P=<0.001 in both cell lines). Combination of nelfinavir and chloroquine caused 37.9 % cell death selectively in *Tsc2*-/- MEFs which was rescued to 9.4 %, a similar level as nelfinavir-chloroquine-treated *Tsc2*+/+ MEFs (8.3 %) when combined with bafilomycin-A1 (28.5 % reduction, P=<0.001). Taken together, the results shown in Figure 4.11 infer that inhibition of autophagy is not required for nelfinavir and chloroquine-mediated cell death. This is proven by the fact that mefloquine, shown not to inhibit autophagy at the dose used, caused significant cell death when combined with nelfinavir. Instead, it would appear that cell death is dependent on chloroquine entrapment within the lysosome (or late endosomes where the vacuolar type H^+-ATPase is also known to reside), as proven by rescue with bafilomycin-A1.

4.4 Discussion

4.4.1 Chloroquine enhances nelfinavir-induced ER stress

An alternative antibody was sourced for CHOP (Cell signalling technology) which resulted in improved visualisation of protein bands, rendering any potential issues related to timing of treatment irrelevant. As seen in figure 4.1A, nelfinavir induced increased levels of IRE1α and CHOP protein in both *Tsc2*+/+ and *Tsc2*-/- MEFs which was enhanced by addition of chloroquine. Chloroquine induced ER stress to a similar level to thapsigargin. Increasing the dose of chloroquine in combination with nelfinavir did not appear to enhance IRE1α or CHOP protein in either cell line so a standard dose of 20 μM chloroquine was selected for further treatment. Figure 4.1B shows chloroquine induces XBP1 splicing to a similar level as nelfinavir in both cell lines, but this is enhanced when both drugs are combined, particularly in *Tsc2*-/- MEFs. Similarly, chloroquine enhanced nelfinavir-mediated CHOP mRNA induction (Fig 4.1C). The mechanism of chloroquine-induced ER stress was thought to be through blockade of the autophagy flux. Autophagy inhibition enhances ER stress through multiple mechanisms but in this context the most likely include reduction of protein aggregate breakdown leading to further accumulation within the ER, and reduced feedback inhibition of mTORC1 through ULK1.

4.4.2 Chloroquine blocks the autophagy flux

Chloroquine-mediated inhibition of autophagy was confirmed by western blot showing increased LC3-II protein and SQSTM1 proteins (Fig 4.2). In both *Tsc2*+/+ and *Tsc2*-/- MEFs, nelfinavir enhanced chloroquine-mediated increases in LC3-II, confirming previous results showing nelfinavir affected LC3-II and SQSTM1 levels (Fig 3.3). Chloroquine treatment alone did not appear to have any effect on phosphorylation of rpS6 or S6K1 proteins, but these were both reduced in the presence of nelfinavir in *Tsc2*+/+ MEFs, confirming previous results (Fig 3.3). This suggests chloroquine does not affect mTORC1 signalling and that nelfinavir requires functional TSC2 to reduce activation of mTORC1.

4.4.3 *Tsc2*-/- MEFs are more motile than *Tsc2*+/+ MEFs

Analysis of the time lapse data revealed *Tsc2*-/- MEFs are basally more active cells. Movement is rapid and erratic with cells dividing frequently. They also appear to be

less adherent than *Tsc2*+/+ MEFs with a more refractive appearance (Fig 4.3). This could be due to an elevated metabolic rate due to overactive mTORC1. Appendix VI shows movement analysis from the time lapse data in which treatment with combined nelfinavir and chloroquine greatly reduced cell movement both per 15 minute time interval (Appendix VI A) and cumulatively (Appendix VI B). Treatment with nelfinavir alone was also affective, but not to the same extent as combined treatment. This may be due to the fact that nelfinavir has cytostatic effects and has been shown to arrest the cell cycle at G1 in multiple cell types, including ovarian and cervical cancers, and hepatacellular carcinoma (Brüning *et al.*, 2009, Xiang *et al.*, 2015, Sun *et al.*, 2012). Cytostatic cells are unlikely to be particularly motile. Similarly, the reduction in movement in *Tsc2*-/- MEFs with combination treatment is most likely due to early stages of cell death.

4.4.4 Nelfinavir and chloroquine co-treatment causes significant and selective cell death in multiple *in vitro* models with overactive mTORC1

Although not significant, a trend for increased cell death was observed in ELT3-V3 cells following 24 h nelfinavir-chloroquine treatment (Fig 4.5). In order to cause significant cell death in ELT3-V3 cells, treatment time with nelfinavir and chloroquine was extended to 48 h (Fig 4.6). ELT3-V3 cells are *Tsc2*-null like the *Tsc2*-/- MEFs (Howe *et al.*, 1995), but possibly the most important difference between the cell lines is that the *Tsc2*-/- MEFs required knockdown of P53 in order to prevent early senescence (Zhang *et al.*, 2003). *Tsc2*-/- MEFs were previously found to be hypersensitive to ER stress-inducing treatments, resulting in increased apoptosis (Ozcan *et al.*, 2008), which explains why increased cell death was observed in *Tsc2*-/- MEFs compared to ELT3-V3 cells and also NCI-H460 cells (Fig 4.8), which similarly required an extended treatment time of 48 h. Similar to ELT3-V3 cells, *TSC2*-/- AML cells also showed a limited response to nelfinavir-chloroquine treatment after 24 h (Fig 4.7). Therefore, it may be the P53-null nature of *Tsc2*-/- MEFs which sensitises them to treatment. Mechanistically, this is possibly due P53-mediated activation of sestrins which decreases mTORC1 signalling through activation of AMPK and TSC2 (Budanov and Karin, 2008). More recently, sestrins were found to inhibit mTORC1 independently of AMPK, through interaction with GAP activity towards Rags 2 (GATOR2), which results in failure of Rags to tether

mTORC1 to the lysosome (Parmigiani *et al.*, 2014). However, this mechanism would result in reduction of phosphorylated rpS6 and S6K1 proteins in treated *Tsc2*-null cells, which was not observed in the present study. A reduction of phosphorylated rpS6 and S6K1 proteins was only observed in treated cells with functional TSC2, indicating a TSC2-dependent response.

4.4.5 Nelfinavir-chloroquine-induced cell death is not caspase-dependent

Despite observing differing total amounts of apoptosis markers (Appendix VII), no cleaved products were detected, indicating cell death was unlikely to be apoptotic. Even so, cell death is likely mediated by the UPR, as shown by elevated levels of GADD34 following combined treatment in *Tsc2*-/- MEFs (Appendix VIII). Brief additional investigation was undertaken into the possibility of cell death being mediated through autophagy, so called 'autosis'. Autosis was found to be rescued by treatment with digoxin (Liu *et al.*, 2013). Digoxin is a cardiac glycoside which inhibits the Na+/K+ ATPase and is used in very low doses for treatment of certain heart conditions. Addition of digoxin to nelfinavir and chloroquine treatment did not rescue observed cell death in ELT3-V3 cells and so investigation into autosis was discontinued (Appendix IX).

4.4.6 Nelfinavir-chloroquine-induced cell death is unlikely through DNA damage or ROS induction

To check for treatment-induced DNA double strand breaks, a western blot was performed to assess levels of phosphorylated H2AX (Kuo and Yang, 2008). Appendix VIII shows nelfinavir and chloroquine-induced cell death is cytotoxic rather than genotoxic, as indicated by lack of phosphorylated H2AX compared to thapsigargin treatment. This confirms that chloroquine does not cause DNA damage (Mitscher, 2005) and is not the mechanism of nelfinavir-chloroquine-induced cell death.

Investigation into whether cell death was caused by increases in ROS utilised NAC as an oxygen scavenger in an attempt to rescue cell death. Combined nelfinavir, chloroquine and NAC treatment in *Tsc2*-/- MEFs showed a trend for increased cell death rather than rescue (Fig 4.9), which could indicate the use of ROS in survival pathway signalling. However, brief investigation to confirm the effect of NAC in NCI-H460 cells

showed a small decrease in cell death when NAC was added to nelfinavir-chloroquine treatment (Appendix X). Although unlikely to directly mediate cell death in this context, further research is required to completely rule out ROS as a contributor.

4.4.7 Mefloquine is an effective inducer of cell death

The chloroquine analogue, mefloquine, was investigated to determine which analogue might be more effective for future study. Increasing doses of mefloquine showed little if any effect on autophagy inhibition compared to chloroquine (Fig 4.10A) but mefloquine exhibited induction of cell death in *Tsc2*-/- MEFs, which was approximately two-fold that in *Tsc2*+/+ MEFs (Fig 4.10B/C). The difference in treatment effect between chloroquine and mefloquine could be related to the differing chemical structures (Appendix XI). Mefloquine exists in both (+) and (-) enantiomers, which have differing effects, effectively making it two drugs combined (Ngiam and Go, 1987).

4.4.8 Nelfinavir-chloroquine-induced cell death is independent of autophagy and is recued by bafilomycin-A1

If cell death was not induced through autosis, the question was asked how necessary inhibition of autophagy was for cell death induction. It was assumed that the inhibitory action of chloroquine on the autophagy flux was the catalyst for promotion of nelfinavir-induced death. If that were true, results should be replicated by combining nelfinavir with any autophagy inhibitor. Unexpectedly, no other autophagy inhibitor replicated the cell death observed with combined nelfinavir and chloroquine (Fig 4.11B). Furthermore, cell death was observed when cells were treated with combination of nelfinavir and the chloroquine analogue, mefloquine, which did not inhibit autophagy (Fig 4.11A). Published research is in contention as to whether melfoquine induces or inhibits autophagy, and this seems to be dependent on cell type and fed or starved conditions (Shin *et al.*, 2012, Sharma *et al.*, 2012).

Previous data showed bafilomycin-A1 was able to rescue the cytotoxic effects of combined nutrient deprivation and chloroquine treatment in multiple cancer cell models (Harhaji-Trajkovic *et al.*, 2012). Addition of bafilomyci-A1 to combined nelfinavir and chloroquine treatment in *Tsc2*-/- MEFs completely rescued cell death to levels of *Tsc2*+/+ MEFs (Fig 4.11B/C). Interestingly, this treatment combination also reversed autophagy inhibition despite both chloroquine and bafilomycin-A1 clearly

inhibiting autophagy as single agents (Fig 4.11A). Together, these results indicate that nelfinavir-chloroquine-induced cell death is independent of autophagy. Because bafilomycin-A1 is a v-ATPase inhibitor, its rescue of cell death suggests the requirement of chloroquine entrapment within lysosomal or endosomal compartments is necessary for cytotoxicity.

Research combining nelfinavir and chloroquine or mefloquine in cancer models was published during the course of this PhD. Thomas *et al.,* (2012) found combined nelfinavir and chloroquine treatment was successful in killing a variety of breast cancer cell lines, particularly triple-negative breast cancer, and this effect was replicated in *in vivo* studies (Thomas *et al.*, 2012). However, the mechanism of chloroquine and mefloquine enhancement of nelfinavir-mediated cell death was concluded to be through autophagy inhibition, which was confirmed by Beclin-1 si-RNA knockdown and measurement of colony development in the presence of drug treatment. This result disagrees with the findings in the current study and is not entirely reliable. Cell death would have been better confirmed by generation of ATG5 or ATG7 knockdown cells, treatment with nelfinavir, and measurement of death through assays previously used elsewhere in the published research i.e. MTT assay and ELISA. Indeed, this was the aim of the present research before discovering other drug inhibitors of autophagy failed to induce cell death when combined with nelfinavir. Mahoney *et al.,* (2013) also found combination of nelfinavir and chloroquine induced cell death in primary cell cultures of chronic lymphocytic leukaemia. Their research assumed the increase in cell death when adding chloroquine treatment was due to autophagy inhibition from observation of increased LC3-II and SQSTM1 protein, without testing other autophagy inhibitors or knocking down essential autophagy components. Similarly in medullary thyroid cancer cell lines, nelfinavir was combined with chloroquine and cell death was observed which was attributed to inhibition of autophagy (Kushchayeva *et al.*, 2014). No further tests were carried out to confirm the necessity of autophagy inhibition in cell death induction. The present research suggests chloroquine-mediated autophagy inhibition in mTORC1-overactive cells is not essential for induction of cell death when combined with nelfinavir. Instead, results suggest another property unique to chloroquine and mefloquine is responsible for enhancement of nelfinavir treatment. One such mechanism was proposed by Harhaji-Trajkovic *et al.,* (2012), being that chloroquine

entrapment within lysosomes caused lysosomal accumulation, leading to oxidative stress, mitochondrial depolarization and a mix of apoptotic and necrotic cell death which was not replicated by other inhibitors of autophagy, and could be rescued by co-treatment with bafilomycin-A1 (Harhaji-Trajkovic *et al.*, 2012).

4.4.9 Summary of chapter 4

Combination of nelfinavir and chloroquine effectively induces selective cell death in cells with overactive mTORC1, which is not mediated through apoptosis. Combination of nelfinavir with other autophagy inhibitors failed to replicate cell death observed with nelfinavir-chloroquine, but dramatic cell death was seen with a combination nelfinavir and mefloquine (a chloroquine analogue). Inhibition of the v-ATPase with bafilomycin-A1 completely rescued nelfinavir-chloroquine-induced cell death in *Tsc2*-/- MEFs, indicating the requirement of chloroquine entrapment within the lysosome for cell death induction.

Chapter 5. Investigation of combination treatment with nelfinavir and bortezomib

5.1 Background

5.1.1 The proteasome

The 26S proteasome is a molecular machine consisting of proteolytic core and regulatory subunits with an ATP-dependent protein entry system. The 20S core is composed of a cylindrical stack of 4 heptameric rings with each ring assembled from either α or β subunits, in the order α, β, β, α. 3 of the 7 β subunits are catalytically active with each conferring trypsin, caspase, or chymotrypsin activity (Gu and Enenkel, 2014). The 19S regulatory particle acts as a lid or gateway to regulate entry into the proteasome. The base is composed of 6 ATPase and 4 non-ATPase subunits which receive delivery proteins and recognise ubiquitin chains. ATP binding to the base ATPases opens the 'lid' and allows protein entry for degradation (Bhaumik and Malik, 2008).

The proteasome regulates many critical cellular pathways, aberration in which can eventually lead to oncogenesis. Perhaps the most well studied of these is the mouse double minute 2 homologue (MDM2)-P53 interaction. P53, the 'guardian of the genome' is a critical tumour suppressor in eukaryotic cells. MDM2 has E3 ligase activity and one way it regulates P53 is to target it to the proteasome for degradation by ubiquitination. MDM2 has been reported as overexpressed in as many as 20% of all cancers including osteosarcoma and Hodgkin lymphoma. Overexpression of MDM2 leads to decreased levels of P53 allowing DNA mutation to go unchecked and eventual development of malignant cells (Micel *et al.*, 2013).

5.1.2 Protein degradation by the proteasome

Proteins are targeted to the proteasome by the addition of upwards of 4 chained ubiquitin molecules attached by the sequential actions of E1, E2 and E3 enzymes. Poly-ubiquitin chains interact with the proteasome lid and the protein is unfolded before proteolysis within the central chambers (Bhaumik & Malik, 2008). Once the protein is within the proteasome, ubiquitin molecules are removed from the protein and

recycled by subunits within the base with metalloprotease activity (Gu and Enenkel, 2014).

Proteins are grouped in to three types: type I refers to functional, short-lived proteins which are degraded as part of their regulation e.g. cell cycle proteins, type II are misfolded proteins degraded for clearance, and type III are long-lived proteins degraded as a result of a change in the cellular environment e.g. nutrient status. The proteasome can degrade type I and II proteins whereas autophagy degrades type II and type III proteins (Benbrook and Long, 2012). It is estimated that upwards of 30% of newly synthesised proteins are degraded through the proteasome (Schubert *et al.,* 2000) and over 80% of all cellular proteins (Rzymski *et al.*, 2009).

5.1.3 Bortezomib

Bortezomib is a first generation 26S proteasome inhibitor synthesised in 1995 and FDA approved for treatment of multiple myeloma just 7 years later. It specifically binds the catalytic site of the 26S proteasome with high affinity. Bortezomib treatment is associated with neuropathy in 30% of patients and most commonly with gastro-intestinal problems and muscle weakness (Gelman *et al.*, 2013). Despite being efficacious in the treatment of newly diagnosed and relapsed multiple myeloma, disease relapse is commonly bortezomib-resistant and is associated with autophagy. Research suggests the killing mechanism of bortezomib is firstly through an ER stress response, leading to calcium-dependent apoptosis (Escalante *et al.*, 2013). Multiple *in vitro* and *in vivo* studies have reported inhibition of survival pathways, including autophagy and NF-κB signalling, in sensitisation of multiple myeloma models to bortezomib treatment (Escalante *et al.*, 2013, Kawaguchi *et al.*, 2011, Kawabata *et al.*, 2012, Kraus *et al.*, 2013, Walsby *et al.*, 2010, Zhang *et al.*, 2015). Continuing research has found this principle to be successful in other cancer models including breast, cervical, and renal cancers, melanoma and leukaemia (Thaler *et al.*, 2014, Brüning *et al.*, 2013, Sato *et al.*, 2012, Selimovic *et al.*, 2013, Kraus *et al.*, 2014, Wang *et al.*, 2015).

Bortezomib has also been used in the context of TSC: In the ELT3 cell line, bortezomib was found to induce apoptosis through the ER stress pathway, primarily through ATF4 and CHOP expression. This was found to be mediated through mTORC1 induction of c-MYC, which was rescued by inhibition of mTORC1 with rapamycin (Babcock *et al.*,

2013). Conversely, in a *Tsc2*-/- mouse model, 1 month bortezomib treatment failed to significantly reduce kidney tumour volume despite achieving expected pharmacodynamic effects. This was compared to rapamycin treatment which achieved 99% tumour volume reduction (Auricchio *et al.*, 2012). This study highlights how drugs can behave differently *in vitro* to *in vivo* setting, but the authors did not try sensitising the tumour cells by combining bortezomib with other drugs, as described above.

5.1.4 Bortezomib in clinical trials

Studies using bortezomib have become increasingly popular and a number of clinical trials for its use in cancer treatment have recently been completed. However, these have not produced overly positive results: A phase I trial combining bortezomib with sorafenib (a small molecule inhibitor of several tyrosine protein kinases approved for treatment of kidney, liver and thyroid carcinoma) in patients with advanced malignant melanoma documented no observed response despite safe use of the drug combination (Sullivan *et al.*, 2015). Using the same combination of bortezomib and sorafenib, a phase II study was trialled in patients with metastatic or unresectable renal cell carcinoma. Similarly to the phase I trial, the drug combination was found to be well tolerated but yielded no additional efficacy to treatment with sorafenib alone and so the study was halted for futility (Rao and Lauer, 2015). In a phase II trial in paediatric patients with refractory/recurrent Hodgkin lymphoma, bortezomib was combined with an alkylating agent, ifosfamide, and an anti-mitotic chemotherapy, vinorelbine. The study was halted before completion due to poor trial design. Despite no reported statistically significant results, the authors stated that the drug combination held promise and showed 91% of patients achieved an overall response (Horton *et al.*, 2015). Perhaps the most relevant clinical trial utilising bortezomib combined it with NVP-AUY922, an experimental HSP90 inhibitor used in 28 cancer clinical trials to date. In patients with relapsed or refractory multiple melanoma, disease progression was stabilised using NVP-AUY922 alone and a maximum tolerated dose was not reached although patients experienced reversible ocular toxicity. However, inhibition of HSP90 was compensated for by an increase in HSP70 which may contribute to drug resistance. In patients receiving combination treatment, the standard recommended dose of bortezomib was not tolerated when combined with

NVP-AUY922 and 3 of 5 patients had to discontinue treatment due to toxicity issues (Seggewiss-Bernhardt *et al.*, 2015).

5.2 Aims of Chapter 5

Bortezomib has been shown to be an effective inducer of cell death in multiple cancer models and also in the context of TSC. Combination of bortezomib with inhibition of survival pathways sensitised cancer cells to treatment in preclinical models, but was not effective or not well tolerated in clinical trials. The main aims of this chapter were:

1. To determine whether bortezomib enhances nelfinavir-induced ER stress

2. To assess whether combination of nelfinavir and bortezomib is an effective and selective inducer of cell death in a panel of mTORC1-overactive cells

3. To identify the mechanism of nelfinavir-bortezomib-mediated cell death

5.3 Results

5.3.1 Bortezomib enhances nelfinavir-induced ER stress

Treatment with nelfinavir and bortezomib was assessed for effectiveness of ER stress induction (Fig 5.1). A western blot was used to detect ER stress markers BiP, CHOP, and GADD34, mTORC1 signalling through phosphorylation of S6K1 and rpS6, and proteasome activity through accumulation of ubiquitin protein in *Tsc2*+/+ and *Tsc2*-/- MEFs (Fig 5.1A). Nelfinavir treatment effects on ER stress and mTORC1 signalling shown in the previous chapters were replicated once more. Both MG132 and bortezomib increased expression of ER stress markers in *Tsc2*-/- MEFs, which was enhanced by nelfinavir co-treatment.

Of particular interest is that nelfinavir does not inhibit the 26S proteasome in either cell line. There are a minority of publications which support this finding in varying cell lines (Brüning *et al.*, 2010, Shim *et al.*, 2012). MG132 was used as a positive control for proteasome inhibition alongside the more clinically relevant bortezomib. Both MG132 and bortezomib induced robust inhibition of the proteasome, as indicated by accumulation of poly-ubiquitin protein in both cell lines. Interestingly, combination with nelfinavir and either MG132 or bortezomib reduced build-up of poly-ubiquitin protein in both cell lines. In *Tsc2*-/- MEFs, rapamycin was shown to inhibit the proteasome and could not be used to completely rescue the accumulation of ER stress proteins with combined treatment of nelfinavir and bortezomib, although some reduction in BiP and CHOP was observed. At the time these results were unexpected, but the observation that rapamycin inhibits proteasomal activity in *Tsc2*-/- MEFs was confirmed in the literature shortly afterwards (Zhang *et al.*, 2014). Previous research stated rapamycin allosterically inhibits the proteasome at high concentrations but was suggested to have little efficacy for proteasome inhibition when the drug is used at relatively low concentrations required for inhibition of mTORC1 (Osmulski and Gaczynska, 2013).

To support the increased ER stress markers following nelfinavir and bortezomib co-treatment shown in figure 5.1A, a PCR was performed to assess XBP1 splicing (Fig 5.1B). As shown previously, nelfinavir increases XBP1 splicing in both cell lines. Bortezomib did not appear to increase XBP1 splicing compared to untreated controls.

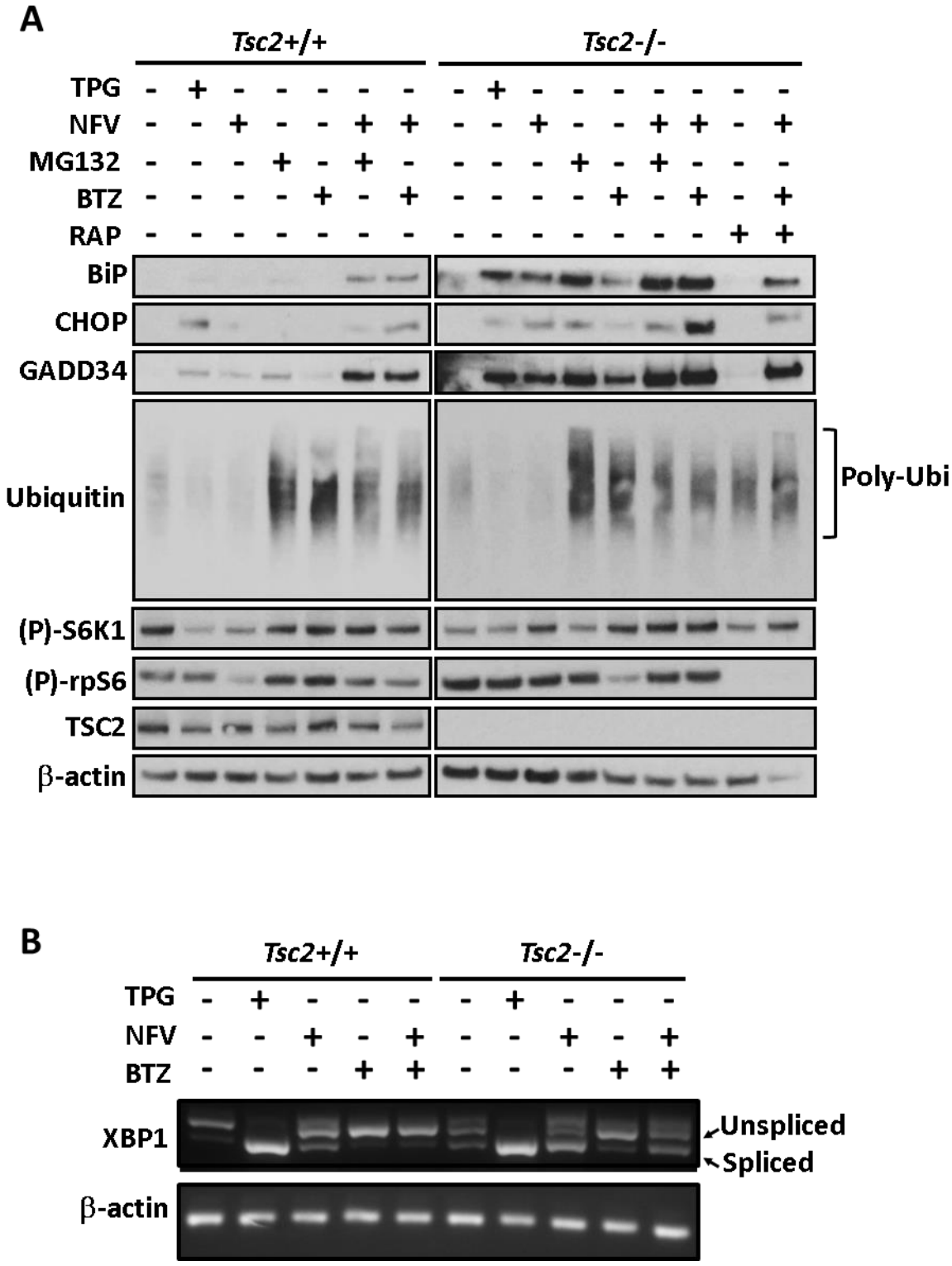

Figure 5.1: Nelfinavir does not inhibit the proteasome in MEFs but proteasome inhibition enhances nelfinavir-induced ER stress. *Tsc2*+/+ and *Tsc2*-/- MEFs were treated with either DMSO vehicle alone, 1 μM thapsigargin (TPG), 20 μM nelfinavir (NFV), 1 μM MG132, 50 nM bortezomib (BTZ), 100 nM rapamycin (RAP), or a combination of drugs as indicated for 6 h. A) Protein lysates were analysed for BiP, CHOP, GADD34, Ubiquitin, phosphorylated S6K1, phosphorylated rpS6, TSC2 and β-actin. B) PCR products for XBP1 mRNA were resolved on agarose gels (unspliced 480 bp [upper band], spliced 454 bp [lower band]). β-actin is shown as a control.

Indeed, combination of nelfinavir with bortezomib seemed to subtly reduce XBP1 splicing compared to nelfinavir treatment alone in both cell lines.

5.3.2 Nelfinavir and bortezomib co-treatment causes significant and selective cell death in multiple *in vitro* models with overactive mTORC1

A standard dose of 20 μM nelfinavir was combined with 50 nM bortezomib and assessed for cell death using flow cytometry with DRAQ7 staining over time (Appendix XII). After 24 h combined nelfinavir and bortezomib treatment, the *Tsc2*+/+ MEFs showed a significant increase in cell death from 13.3 % to 27.8 % (P=0.026) but this was significantly lower than the 75.2 % cell death in *Tsc2*-/- MEFs (P=0.0034), implying selectivity of the drug combination to induce cell death between cell lines. Indeed, synergy experiments performed in the Tee lab proved combination of nelfinavir with bortezomib is synergistic at induction of cell death (unpublished data).

The effect of nelfinavir and bortezomib co-treatment on cell death in *Tsc2*+/+ and *Tsc2*-/- MEFs was assessed by flow cytometry with DRAQ7 staining (Fig 5.2A/B). Etoposide, a topoisomerase inhibitor and DNA damage-inducing chemotherapeutic, was used as a positive control for cell death. Etoposide increased cell death in *Tsc2*+/+ MEFs from 10.7 % to 11.9% (P=0.736) and from 9.8 % to 26.7 % in *Tsc2*-/- MEFs (P=0.003). As a single agent, bortezomib induced significant and selective cell death in *Tsc2*-/- MEFs compared to *Tsc2*+/+ MEFs (mean 41% vs 11%, P=<0.001). Combination of nelfinavir with bortezomib produced a synergistic increase in cell death to 83% in *Tsc2*-/- MEFs whilst *Tsc2*+/+ MEFs only increased to 18% (P=0.029 and P=0.157, respectively). This effect could not be rescued by mTORC1 inhibition with rapamycin and cell death remained high at 87 % (P=0.882). Additionally, rapamycin treatment alone had no significant effect on cell death in *Tsc2*-/- MEFs (P=0.778).

Combination of nelfinavir and bortezomib was shown to effectively kill ELT3-V3 cells (Figure 5.3A/B) and NCI-H460 cells (Figure 5.4A/B), by 63.2 % (P=<0.001) and 58.1 % (P=<0.001), respectively. Cell death was not rescued by rapamycin treatment in either cell line (P=0.405 and P=0.882), which suggests that cell death through nelfinavir-

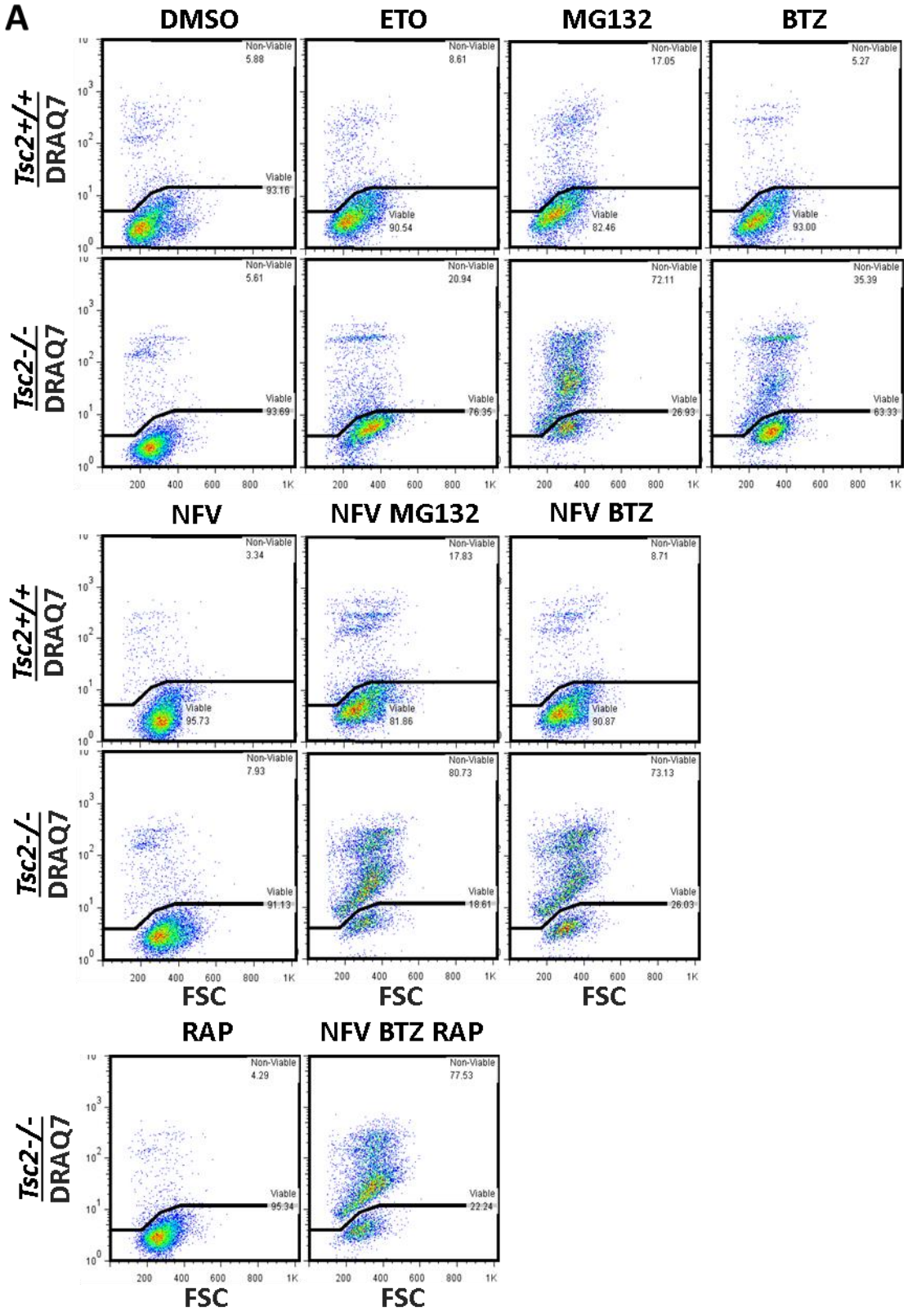
A
DMSO
ETO
MG132
BTZ
Tsc2+/+ DRAQ7
Tsc2-/- DRAQ7
Non-Viable 5.88
Viable 93.16
Non-Viable 8.61
Viable 90.54
Non-Viable 17.05
Viable 82.46
Non-Viable 5.27
Viable 93.00
Non-Viable 5.61
Viable 93.69
Non-Viable 20.94
Viable 76.35
Non-Viable 72.11
Viable 26.93
Non-Viable 35.39
Viable 63.33
NFV
NFV MG132
NFV BTZ
Non-Viable 3.34
Viable 95.73
Non-Viable 17.83
Viable 81.86
Non-Viable 8.71
Viable 90.87
Non-Viable 7.93
Viable 91.13
Non-Viable 80.73
Viable 18.61
Non-Viable 73.13
Viable 26.03
FSC
RAP
NFV BTZ RAP
Non-Viable 4.29
Viable 95.34
Non-Viable 77.53
Viable 22.24

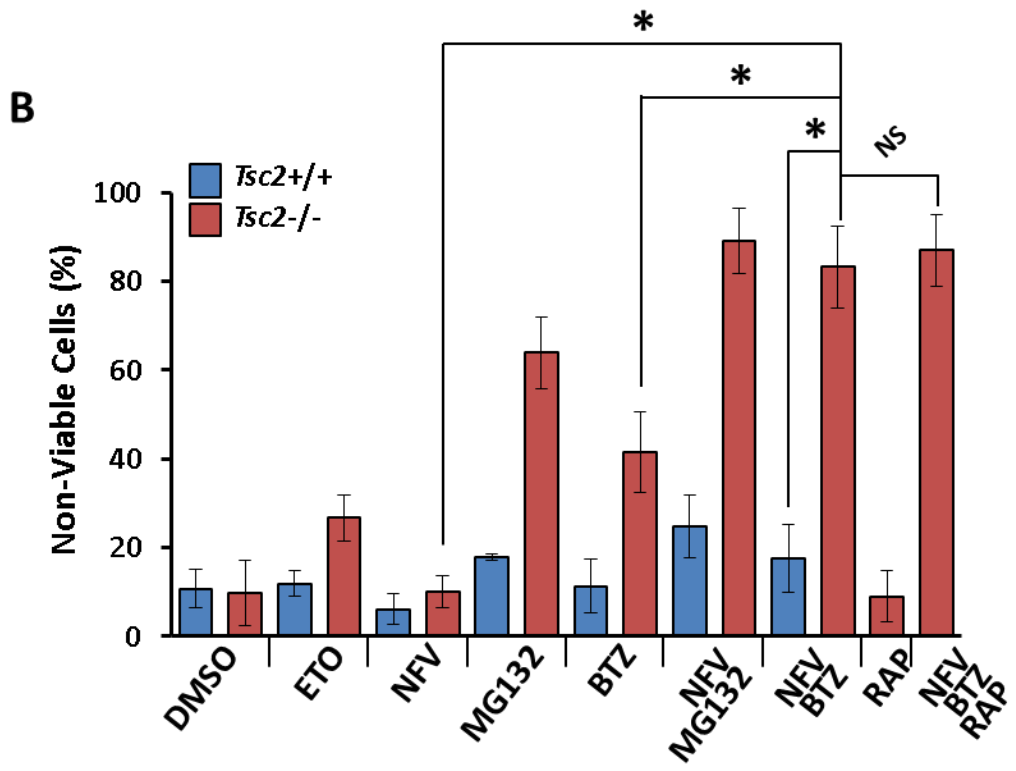

Figure 5.2: Combined nelfinavir and bortezomib causes significant and selective cell death in *Tsc2*-/- MEFs which cannot be rescued by rapamycin. *Tsc2*+/+ and *Tsc2*-/- MEFs were treated with either DMSO vehicle alone, 100 µM etoposide (ETO), 20 µM nelfinavir (NFV), 1 µM MG132, 50 nM bortezomib (BTZ), 100 nM rapamycin (RAP), or a combination of drugs as indicated for 24 h. A) Cells were subjected to flow cytometry analysis with DRAQ7 staining. The number of DRAQ7-stained cells are graphed in B. n=3, *P<0.05.

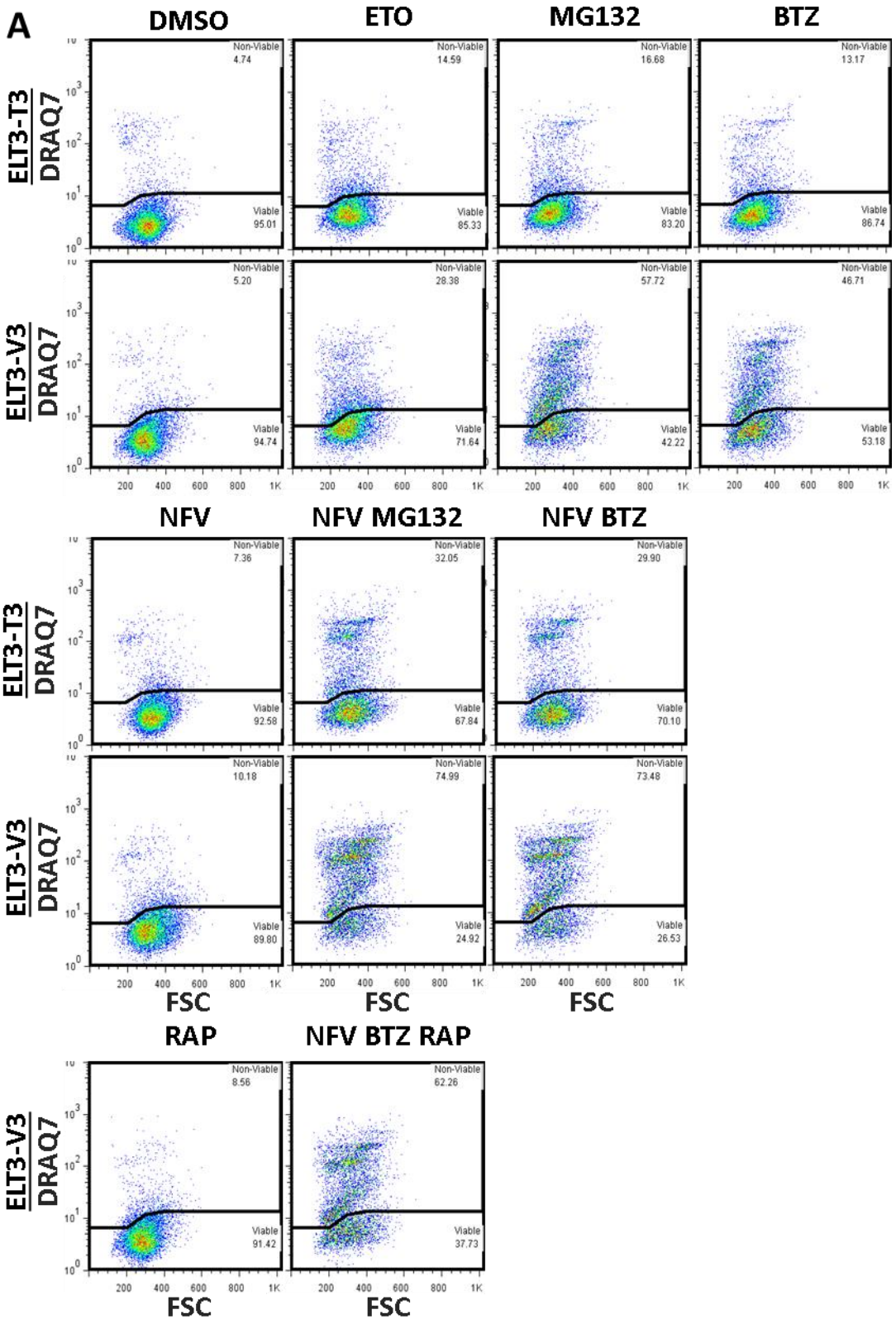
A
DMSO
ETO
MG132
BTZ
ELT3-T3 DRAQ7
ELT3-V3 DRAQ7
Non-Viable 4.74
Viable 95.01
Non-Viable 14.59
Viable 85.33
Non-Viable 16.68
Viable 83.20
Non-Viable 13.17
Viable 86.74
Non-Viable 5.20
Viable 94.74
Non-Viable 28.38
Viable 71.64
Non-Viable 57.72
Viable 42.22
Non-Viable 46.71
Viable 53.18
NFV
NFV MG132
NFV BTZ
Non-Viable 7.36
Viable 92.58
Non-Viable 32.05
Viable 67.84
Non-Viable 29.90
Viable 70.10
Non-Viable 10.18
Viable 89.80
Non-Viable 74.99
Viable 24.92
Non-Viable 73.48
Viable 26.53
FSC
RAP
NFV BTZ RAP
Non-Viable 8.56
Viable 91.42
Non-Viable 62.26
Viable 37.73
FSC

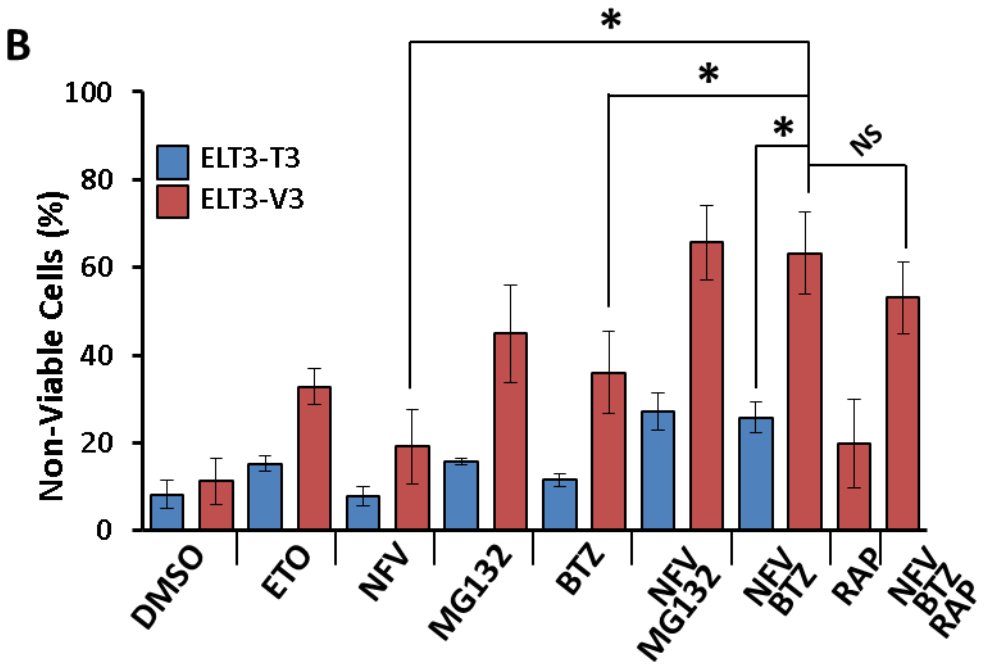

Figure 5.3: Combined nelfinavir and bortezomib causes significant and selective cell death in ELT3-V3 cells which cannot be rescued by rapamycin. ELT3-T3 and ELT3-V3 cells were treated with either DMSO vehicle alone, 100 µM etoposide (ETO), 20 µM nelfinavir (NFV), 1 µM MG132, 50 nM bortezomib (BTZ), 100 nM rapamycin (RAP), or a combination of drugs as indicated for 24 h. A) Cells were subjected to flow cytometry analysis with DRAQ7 staining. The number of DRAQ7-stained cells are graphed in B. n=3, *P<0.05.

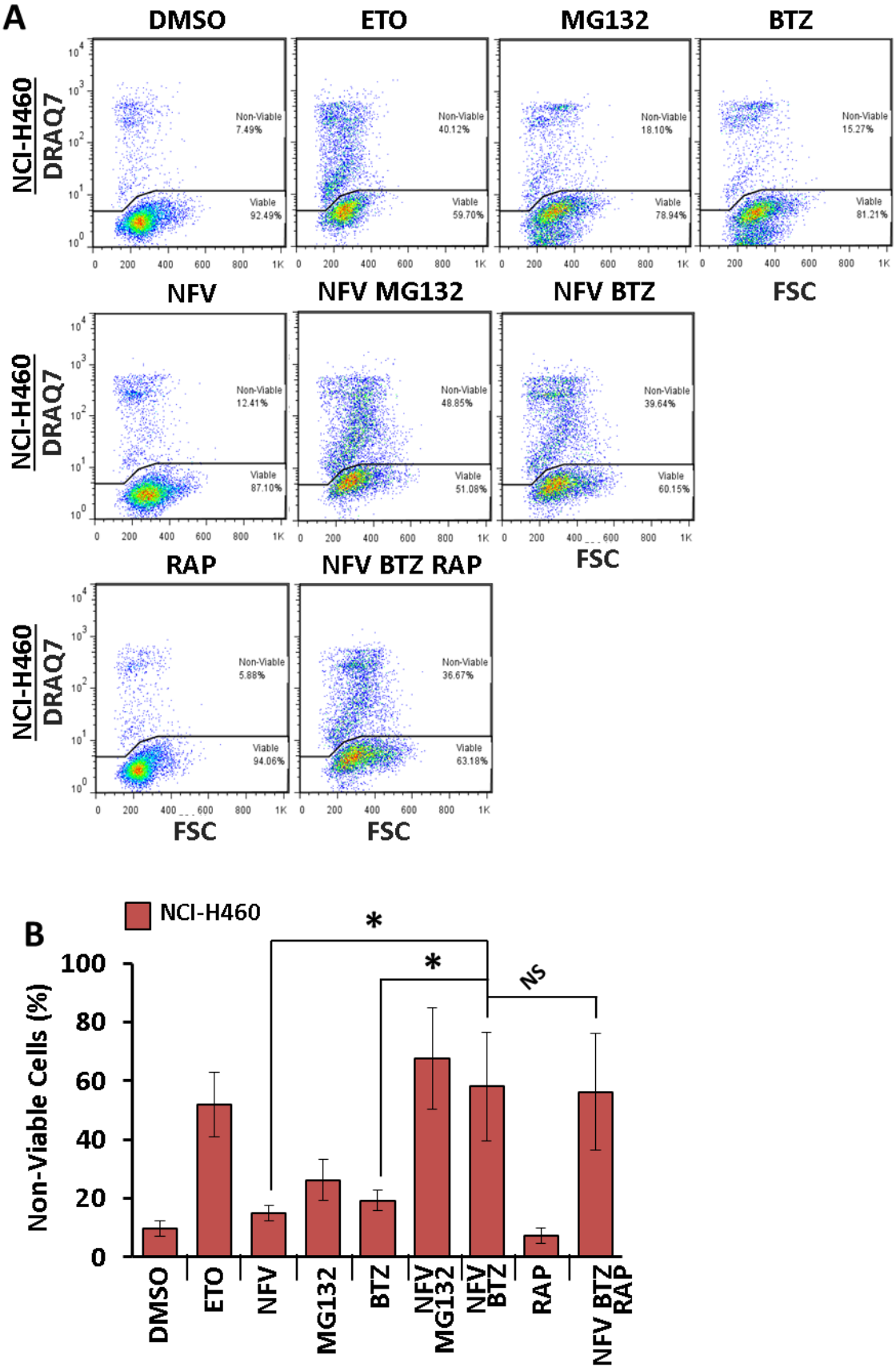
A
DMSO
ETO
MG132
BTZ
NFV
NFV MG132
NFV BTZ
RAP
NFV BTZ RAP
NCI-H460
DRAQ7
Non-Viable
Viable
FSC
B
NCI-H460
Non-Viable Cells (%)
*
NS
DMSO
ETO
NFV
MG132
BTZ
NFV MG132
NFV BTZ
RAP
NFV BTZ RAP

Figure 5.4: Combined nelfinavir and bortezomib causes significant and selective cell death in NCI-H460 cells which cannot be rescued by rapamycin. NCI-H460 cells were treated with either DMSO vehicle alone, 100 μM etoposide (ETO), 20 μM nelfinavir (NFV), 1 μM MG132, 50 nM bortezomib (BTZ), 100 nM rapamycin (RAP), or a combination of drugs as indicated for 24 h. A) Cells were subjected to flow cytometry analysis with DRAQ7 staining. The number of DRAQ7-stained cells are graphed in B. n=3, *P<0.05.

bortezomib treatment is unlikely to be mTORC1-dependent, but rather TSC2-dependent.

5.3.3 Nelfinavir-bortezomib treatment causes apoptosis which is not rescued by rapamycin

To identify the mechanism of cell death, *Tsc2*+/+ and *Tsc2*-/- MEFs were assessed by western blot following 24 h treatment (Fig 5.5). Cells were probed for the ER stress marker IRE1α, markers of apoptosis caspase-3, -8 and PARP, markers of autophagy flux SQSTM1 and LC3-I and –II, and phosphorylated rpS6 as a readout of mTORC1 signalling. IRE1α is primarily involved in a pro-survival response and is shown to be robustly increased with nelfinavir treatment in both cell lines. It is greatly reduced by etoposide treatment and similarly by combined nelfinavir and MG132 or bortezomib treatment in both cell lines. In *Tsc2*-/- MEFs, rapamycin treatment elevated levels of IRE1α but rapamycin was insufficient to rescue reduction by nelfinavir and bortezomib. Induction of apoptosis can occur through activation of the caspase cascade, which can be triggered through various signalling mechanisms. One such mechanism can occur at the level of caspase-8 proteins that are in close proximity to death receptors, which when cleaved can trigger the caspase cascade via cleavage of caspase-3, which in turn cleaves PARP. Cleaved protein products of caspase-3, -8, or PARP were not observed in *Tsc2*+/+ MEFs regardless of treatment. In *Tsc2*-/- MEFs, the only drug to not induce cleavage of any apoptosis markers was single nelfinavir drug treatment. Although MG132 did not induce caspase cleavage, modest PARP cleavage is evident. Where the initiator caspase-8 is cleaved, caspase-3 and PARP cleavage follows. Of interest, combination of nelfinavir and bortezomib induces strong cleavage of apoptosis markers to a similar extent to etopisode, despite causing a higher percentage of cell death in flow cytometry assays (Fig 5.2-5.4).

Inhibition of the proteasome with either MG132 or botezomib also caused autophagy inhibition, as indicated by a strong presence of SQSTM1 and LC3-II in both cell lines (Fig 5.5). Combination with nelfinavir had little effect and so it seems autophagy inhibition has little influence on the outcome of cell death. As seen throughout this chapter, it would appear that inhibition of mTORC1 with rapamycin also has little effect on the outcome of cell death despite effective inhibition of mTORC1 signalling as shown through reduced phosphorylation of rpS6.

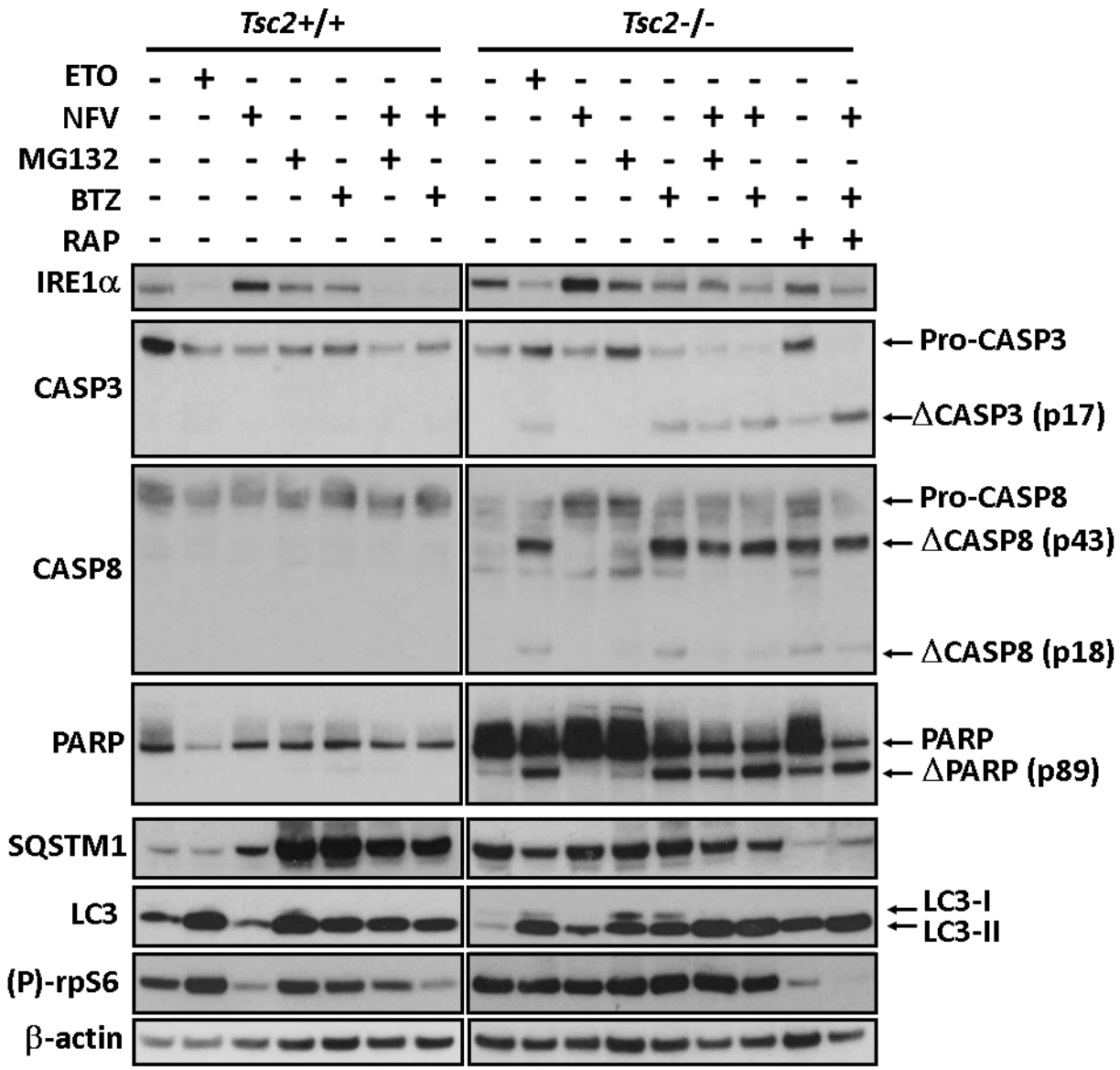

Figure 5.5: Nelfinavir and bortezomib-induced cell death may be through the intrinsic apoptosis pathway. *Tsc2*+/+ and *Tsc2*-/- MEFs were treated with either DMSO vehicle alone, 100 μM etoposide (ETO), 20 μM nelfinavir (NFV), 1 μM MG132, 50 nM bortezomib (BTZ), 100 nM rapamycin (RAP), or a combination of drugs as indicated for 24 h. Protein lysates were analysed for IRE1α, pro and cleaved caspase 3, pro and cleaved caspase 8, pro and cleaved PARP, SQSTM1, LC3-I and –II, phosphorylated rpS6 and β-actin.

5.3.4 Nelfinavir-bortezomib-induced cell death cannot be rescued by inhibition of mTORC1 or caspase 8 cleavage

To assess whether cell death was caspase- or mTOR-dependent, a caspase-8 inhibitor (Z-IETD-FMK) and the ATP-competative mTOR inhibitor (Ku0063794) were employed in a range of mTORC1-overactive cell lines (Fig 5.6A/B). Z-IETD-FMK is a peptide substrate for caspase-8 which acts as an inhibitor of caspase-8 via irreversible binding to the proteolytic active site. Ku0063794 is a more potent inhibitor of mTORC1 and mTORC2 than rapamycin. With the addition of *TSC2*-/- AML cells, combination treatment with nelfinavir and bortezomib induced significant cell death as seen previously in *Tsc2*-/- MEFs, ELT3-V3 and NCI-H460 cells. Z-IETD-FMK or Ku0063794 treatment was unable to rescue cell death in any cell line. Interestingly, Ku0063794 treatment significantly increased nelfinavir-bortezomib-induced cell death selectively in *Tsc2*-/- MEFs (from 48.2 % to 88.9 %, P=0.024). Complimentary western blots were performed to confirm drug effects on markers of apoptosis (Fig 5.7A/B). Figure 5.7A shows Z-IETD-FMK was able to prevent cleavage of caspase-8 and downstream caspase-3. However, cleavage of PARP was still evident. As the caspase-8 antibody is mouse-specific, it was unsuitable for use with the other cell lines, which were either human or rat. Figure 5.7B shows a reduction in caspase-3 and PARP cleavage following addition of Z-IETD-FMK treatment with nelfinavir and bortezomib compared to without, as would be expected from inhibition of upstream caspase-8 cleavage. In addition to these experiments, phase contrast microscopy images were taken at 8 h of treatment to assess whether a reduction in cell death by Z-IETD-FMK or Ku0063794 could be seen at an earlier time point. From visual assessment of cell density, no obvious reduction in cell death could be seen at the earlier time point of 8 h (Fig 5.8).

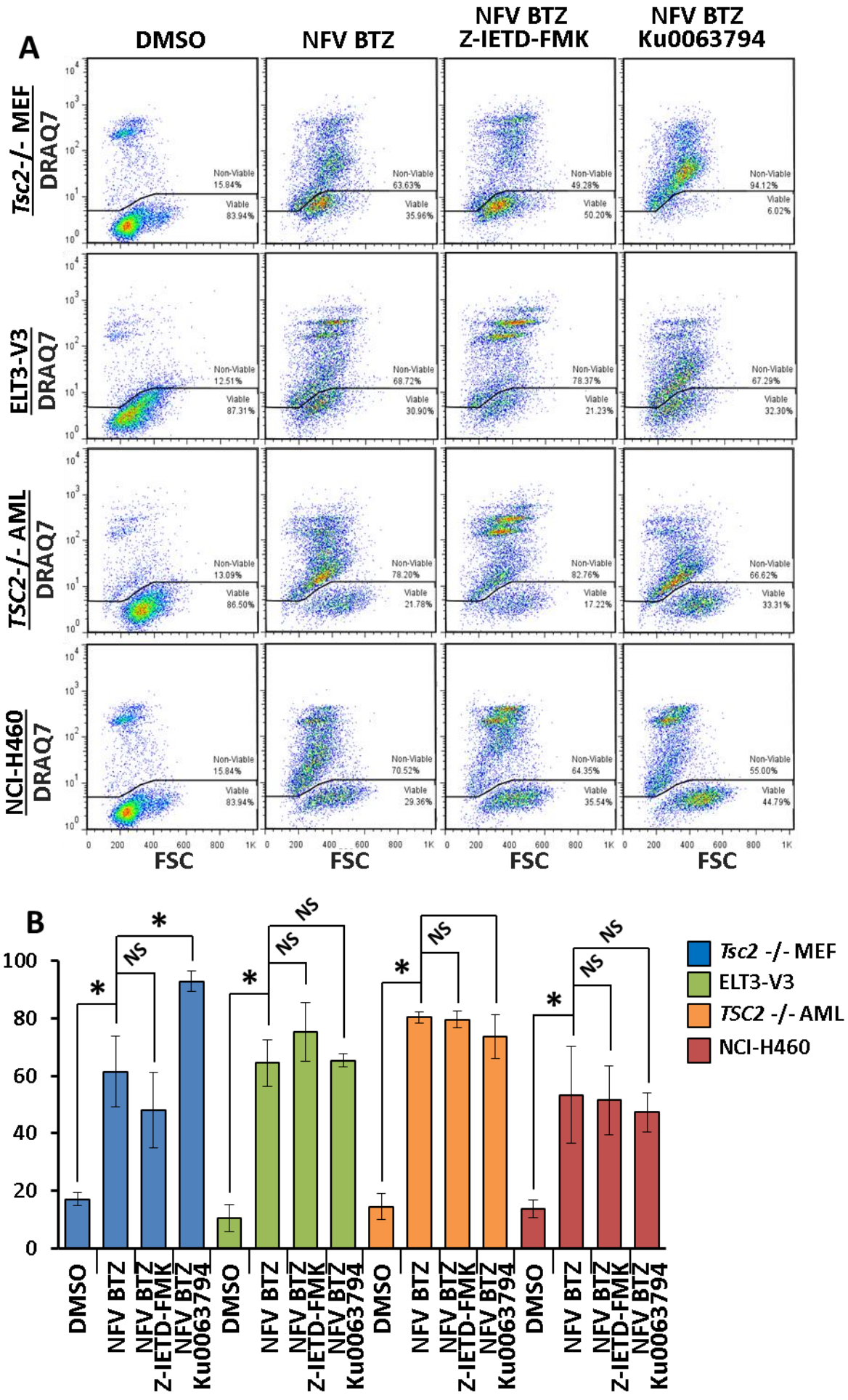
A
DMSO
NFV BTZ
NFV BTZ Z-IETD-FMK
NFV BTZ Ku0063794
Tsc2-/- MEF DRAQ7
ELT3-V3 DRAQ7
TSC2-/- AML DRAQ7
NCI-H460 DRAQ7
Non-Viable 15.84%
Viable 83.94%
Non-Viable 63.63%
Viable 35.96%
Non-Viable 49.28%
Viable 50.20%
Non-Viable 94.12%
Viable 6.02%
Non-Viable 12.51%
Viable 87.31%
Non-Viable 68.72%
Viable 30.90%
Non-Viable 78.37%
Viable 21.23%
Non-Viable 67.29%
Viable 32.30%
Non-Viable 13.09%
Viable 86.50%
Non-Viable 78.20%
Viable 21.78%
Non-Viable 82.76%
Viable 17.22%
Non-Viable 66.62%
Viable 33.31%
Non-Viable 15.84%
Viable 83.94%
Non-Viable 70.52%
Viable 29.36%
Non-Viable 64.35%
Viable 35.54%
Non-Viable 55.00%
Viable 44.79%
0 200 400 600 800 1K
FSC
B
100
80
60
40
20
0
*
NS
DMSO
NFV BTZ
NFV BTZ Z-IETD-FMK
NFV BTZ Ku0063794
Tsc2 -/- MEF
ELT3-V3
TSC2 -/- AML
NCI-H460

Figure 5.6: Nelfinavir and bortezomib-induced cell death cannot be rescued by inhibition of caspase 8 cleavage or inhibition of mTORC1. *Tsc2*-/- MEF, ELT3-V3, *TSC2*-/- AML and NCI-H460 cell lines were treated with either DMSO vehicle alone, combined 20 μM nelfinavir (NFV) and 50 nM bortezomib (BTZ), combined NFV-BTZ with 10 μM Z-IETD-FMK, or combined NFV-BTZ with 1 μM Ku0063794 for 24 h. A) Cells were subjected to flow cytometry analysis with DRAQ7 staining. The number of DRAQ7-stained cells are graphed in B. n=3, *P<0.05.

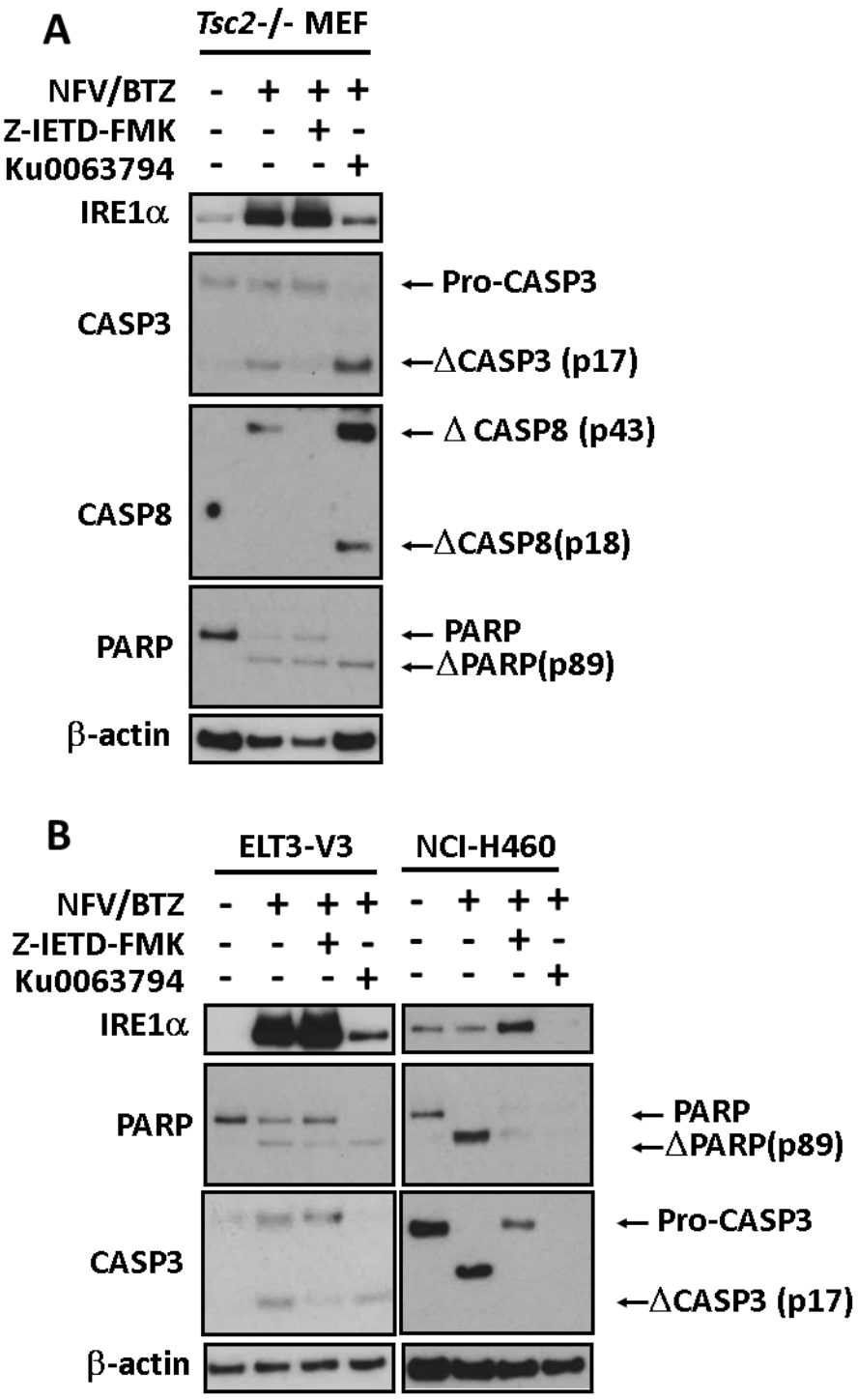

Figure 5.7: Nelfinavir and bortezomib-induced cell death is not mediated exclusively through caspase-dependent apoptosis. *Tsc2*-/- MEF, ELT3-V3 and NCI-H460 cell lines were treated with either DMSO vehicle alone, combined 20 μM nelfinavir (NFV) and 50 nM bortezomib (BTZ), combined NFV-BTZ with 10 μM Z-IETD-FMK, or combined NFV-BTZ with 1 μM Ku0063794 for 24 h before analysis of protein lysates. A) *Tsc2*-/- MEFs were analysed for IRE1α, pro and cleaved caspase 3, pro and cleaved caspase 8, pro and cleaved PARP and β-actin. B) ELT3-V3 and NCI-H460 cells were analysed for IRE1α, pro and cleaved caspase 3, pro and cleaved PARP and β-actin.

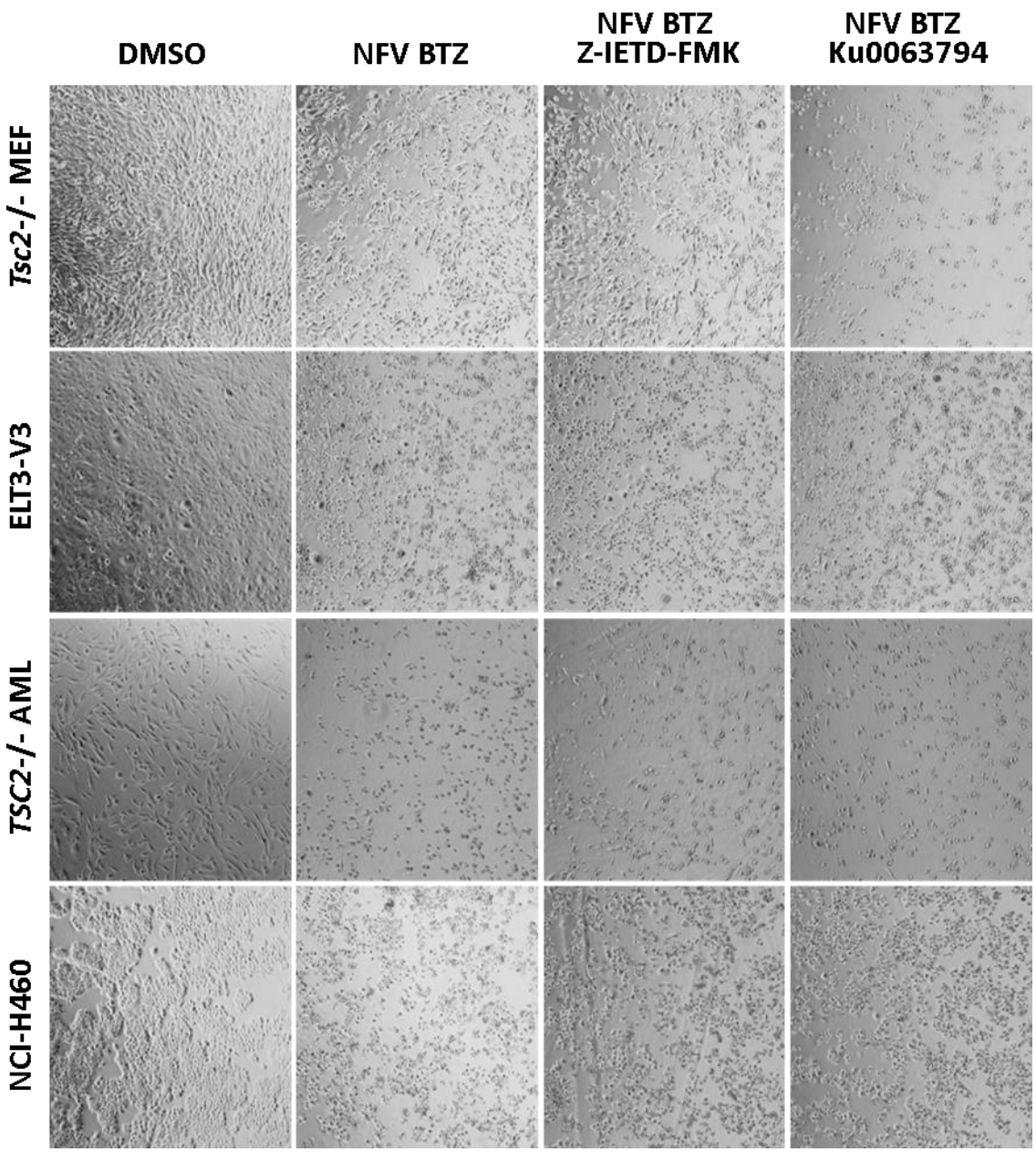

Figure 5.8: Nelfinavir and bortezomib-induced cell death is not rescued by competative caspase 8 or mTORC1 inhibitors, even after a shorter treatment length of 8 h. *Tsc2*-/- MEF, ELT3-V3, *TSC2*-/- AML and NCI-H460 cell lines were treated with either DMSO vehicle alone, combined 20 µM nelfinavir (NFV) and 50 nM bortezomib (BTZ), combined NFV-BTZ with 10 µM Z-IETD-FMK, or combined NFV-BTZ with 1 µM Ku0063794 for 24 h. Images were taken at x 40 magnification using phase contrast after 8 h treatment.

5.4 Discussion

5.4.1 Bortezomib enhances nelfinavir-induced ER stress

Combination of nelfinavir with either MG132 or bortezomib greatly increased levels of ER stress compared to treatment with either agent alone, as observed by increased BiP, CHOP, and GADD34 proteins, particularly in *Tsc2*-/- MEFs (Fig 5.1A). Of interest, nelfinavir-bortezomib was more effective at induction of CHOP protein than nelfinavir-MG132. In contrast to protein levels of ER stress markers, nelfinavir-bortezomib treatment appeared to be less effective at induction of XBP-1 splicing compared to nelfinavir treatment alone (Fig 5.1B).

Aside from the autophagy pathway, unfolded proteins in the ER are also removed by proteasomal degradation. Nelfinavir has been shown to inhibit the proteasome in multiple tumour types, including epithelial cancer and myeloma (Gupta *et al.*, 2007, Bono *et al.*, 2012), which suggests this is one method by which nelfinavir induces ER stress. However, the present study did not observe proteasome inhibition in *Tsc2*+/+ or *Tsc2*-/- MEFs following nelfinavir treatment (Fig 5.1A). Thus, it seems likely that proteasome inhibition by nelfinavir is cell type dependent, similar to that previously discussed regarding the action of nelfinavir on multiple other cellular functions.

Since mTORC1 activation suppresses the autophagy flux, malignant cells with overactive mTORC1 phenotypically have reduced basal autophagy activity. Autophagy downregulation results in a higher dependency on the proteasome for proteolytic breakdown of aberrant proteins and restoration of ER homeostasis to prevent cell death (Rubinsztein, 2006). This was recently highlighted by research detailing functional TSC2 loss enhanced proteasomal degradation in an mTORC1-dependent manner in *Tsc2*-/- MEFs (Zhang *et al.*, 2014). Therefore, inhibition of the preoteasome is a potential therapeutic strategy for treatment of mTORC1-driven tumours and cancers through enhancement of ER stress beyond a tolerated threshold. Indeed, multiple cancer cell lines with elevated mTORC1 signalling have shown selective cytotoxicity towards proteasome inhibitor treatment, including melanoma and breast cancer (Selimovic *et al.*, 2013, Thaler *et al.*, 2014), and cellular and murine models of TSC (Auricchio *et al.*, 2012, Siroky *et al.*, 2012, Babcock *et al.*, 2013).

5.4.2 Nelfinavir and bortezomib co-treatment causes significant and selective cell death in multiple *in vitro* models with overactive mTORC1

Despite being labelled as a proteasome inhibitor, nelfinavir has been shown to enhance the cytotoxic effects of bortezomib in multiple cancer cell models, likely through the action of nelfinavir on multiple cellular targets (Shim *et al.*, 2012, Kawabata *et al.*, 2012, Kraus *et al.*, 2013). Phase I and II clinical trials using combined nelfinavir and bortezomib have also begun, in the context of myeloma and leukaemia/lymphoma (ClinicalTrials.gov: NCT01164709, NCT02188537, NCT01555281). Thus far, no preclinical or clinical study has determined whether the cytotoxic effect of nelfinavir-bortezomib treatment is dependent on the TSC1/TSC2-mTORC1 pathway. Work performed in the Tee lab showed that combination of nelfinavir and bortezomib was synergistic at induction of cell death and treatment is selective towards *Tsc2*-/- cells (unpublished data). Similar to the combination of nelfinavir and chloroquine treatment in chapter 2, nelfinavir and bortezomib treatment appeared to induce elevated ER stress (Fig 5.1) which *Tsc2*+/+ cells were able to compensate for and survive, whereas in *Tsc2*-/- cells basal ER stress was higher and was pushed beyond survivable limits following drug treatment (Fig 5.2). These results are not confined to a single cell line and were replicated in other *in vitro* models with overactive mTORC1 (Fig 5.3-5.4).

5.4.3 Nelfinavir-bortezomib-induced cell death cannot be rescued by inhibition of mTORC1 or caspase 8 cleavage

Since neither mTORC1 inhibitor used (rapamycin or KU0063794) was able to reverse cell death, the mechanism may not be mTORC1-dependent (Fig 5.2-5.4, 5.6). However, TSC2 appears to be critical for cell survival which could be due to a number of reasons. In particular, the inhibitory action of TSC1/TSC2 on mTORC1 is much more dominant than direct mTORC1 inhibition by AMPK or SESN2, which have a comparatively weak suppression of mTORC1 activity.

In contrast to nelfinavir-chloroquine treatment, nelfinavir-bortezomib treatment caused definitive apoptosis, as shown by cleavage of caspase-8, -3 and PARP in 24 h treated samples (Fig 5.5). Although caspase-8 cleavage is part of the extrinsic apoptotic pathway (typically activated through death receptors on the cell surface), there are

several reports of caspase-8 cleavage being mediated through ER stress, specifically through CHOP upregulation of death receptor 5 (DR5) (Lu *et al.*, 2014, Liu *et al.*, 2012, Kim *et al.*, 2011). Additionally, bortezomib has been shown to enhance caspase-8 activation, which was implicated to be through UPR induction (Vaeteewoottacharn *et al.*, 2013) and was thought to be a mechanism for sensitising human renal cell carcinoma cells to further treatment (Brooks *et al.*, 2010). Although nelfinavir-bortezomib treatment caused increased CHOP protein (5.1A) and cleavage of caspase-8 (Fig 5.5), inhibition of caspase-8 cleavage by Z-IETD-FMK did not significantly rescue nelfinavir-bortezomib-mediated cell death in a range of mTORC1 overactive cell lines (Fig 5.6-5.7). This result implies cell death is not primarily through apoptosis, but an alternative mechanism, most likely necrosis. Further research is required to define the mode of cell death. However the mode, the mechanism of cell death is most likely mediated through elevated ER stress.

The IRE1α-TRAF2-ASK1 pathway activates JNK signalling and this feeds into NF-κB signalling. NF-κB is activated by many stimuli including ER stress (Deng *et al.*, 2004). The NF-κB complex is a transcription factor responsible for regulation of multiple cellular pathways including cell growth and survival. It is composed of the RelA, RelB, c-Rel, NF-κB1 and NF-κB2 subunits which collectively form hetero- or homodimers. The NF-κB complex itself is negatively regulated by IκB, which binds to and sequesters NF-κB in the cytoplasm. IκB activity is controlled by the IκB kinase (IKK), which phosphorylates IκB at $Ser^{32/36}$ residues to allow its ubiquitination at $Lys^{21/22}$ and subsequent 26S proteasomal degradation, leaving NF-κB free to translocate to the nucleus (Kim *et al.*, 2006, Lee *et al.*, 2013). Nuclear NF-κB has been detected in multiple cancer types, both solid tumours and hematological malignancies, and has been shown to be activated by oncogenic mutation of mitogenic pathways including EGF and PDGF receptors, and proteins within MAPK and PI3K signalling. Activation of NF-κB in cancers confers resistance to cell death and is associated with poor survival (Kim *et al.*, 2000). There are currently no clinically approved NF-κB inhibitors and the present convention for NF-κB inhibition is to prevent degradation of IκB by the use of proteasome inhibitors. Bortezomib is currently the only approved proteasome inhibitor for human use. The present study showed elevated basal levels of phosphorylated RelA (a post-translational modification required for NF-κB activation)

in *Tsc2*-/- MEFs compared to *Tsc2*+/+ MEFs, which was further increased by nelfinavir treatment, likely through increased ER stress signalling (Fig 3.4). Indirect inhibition of NF-κB by bortezomib coupled with high levels of ER stress from both proteasome inhibition by bortezomib, and nelfinavir treatment, is the likely cause of the observed high levels of cell death in mTORC1-overactive cells.

5.4.4 Summary of chapter 5

Combination of nelfinavir with bortezomib effectively induces selective cell death in cells with overactive mTORC1. This action is likely mediated through nelfinavir-induced ER stress in combination with bortezomib-induced proteasome inhibition, leading to reduction of NF-κB. Interestingly, nelfinavir was found to have no inhibitory effect on the proteasome in either *Tsc2*+/+ or *Tsc2*-/- MEFs. Nelfinavir-bortezomib-induced cell death caused caspase cleavage, suggesting apoptotic cell death. However, cell death was not rescued by drug inhibition of caspase cleavage, indicating death is not exclusively apoptotic. Similarly, drug inhibition of mTORC1 failed to rescue nelfinavir-bortezomib-induced cell death, indicating the mechanism of death may be more dependent on TSC2 than mTORC1.

6. Final Discussion and Conclusions

6.1 TSC2 is required for nelfinavir-mediated mTORC1 inhibition

It was not the purpose of this study to decipher the mechanism of nelfinavir-induced ER stress. However, it would appear that nelfinavir elicits a cytoprotective ER stress response in *Tsc2*+/+ cells. This study observed that nelfinavir did indeed elevate ER stress through increases in XBP1 splicing, CHOP mRNA, and increased levels of IRE1α and GADD34 proteins. Concurrently, nelfinavir increased phosphorylation of AMPK and reduced phosphoryation of rps6 and S6K1 proteins. This is suggestive that nelfinavir activates TSC2 through AMPK to inhibit mTORC1. This mechanism has been described by Brüning *et al.,* (2013), whereby nelfinavir-mediated ER stress activated ATF4 and increased SESN2 expression, which activated TSC2 through AMPK (Brüning *et al.*, 2013). These findings corroborate the observed increase in phosphorylated AMPK (Fig 3.4) in the present study and presents another explanation as to why phosphorylated rpS6 is decreased following nelfinavir treatment only in *Tsc2*+/+ MEFs (Fig 3.3). Another ATF4-mediated, TSC2-dependent mechanism of mTORC1 inhibition is through regulated in DNA damage and development 1 (REDD1). REDD1 was recently found to decrease Akt-mediated inhibitory phosphorylation of TSC2, specifically at Thr^{308} (Dennis *et al.*, 2014). SESN2 was recently shown to inhibit mTORC1 independently of TSC2 through regulation of GATOR1. The GATOR1 complex functions as a GAP for RagA/B, preventing mTORC1 recruitment to the lysosome (Bar-Peled *et al.*, 2013). SESN2 has been shown to inhibit the negative regulator of GATOR1, GATOR2, during times of stress (Parmigiani *et al.*, 2014). Never-the-less, this study did not observe decreases in mTORC1 signalling in *Tsc2*-/- cells, suggesting a TSC2-dependent mechanism. Inability of *Tsc2*-/- cells to reduce mTORC1 signalling resulted in accumulation of protein within the ER, but this was of an insufficient level to cause cell death with nelfinavir treatment alone.

6.2 Nelfinavir-chloroquine

6.2.1 Nelfinavir and chloroquine co-treatment causes cell death in mTORC1-overactive cells

This work also suggested the mechanism of chloroquine-induced cell death was independent of apoptosis, since caspase inhibition did not reduce levels of cytotoxicity (Maycotte *et al.*, 2012). This additionally supports the findings of the present study that nefinavir and chloroquine co-treatment did not induce cleavage of caspase-3 or PARP (Appendix VII). Theoretically, nelfinavir-chloroquine treatment should be at least partially rescued by an mTORC1 inhibitor such as rapamycin or Ku006379.

6.2.2 Cell death is not caused by autophagy inhibition

In this study, cell death was not attributed to autophagy inhibition. It is likely that inhibition of autophagy potentiates the ER stress and the effect of nelfinavir-chloroquine, but autophagy inhibition is not sufficient to cause cell death in combination with neflinavir (Fig 4.10). Instead, it would appear that the lysosome is a critical mediator of cell death in this context. This is supported by work showing chloroquine sensitised breast cancer cells to cisplatin treatment which was not replicated by other autophagy inhibitors, or knockdown of ATG12 or Beclin 1 (Maycotte *et al.*, 2012). Harhaji-Trajkovic *et al.,* (2012) did not observe cell death when using autophagy inhibitors other than chloroquine in combination with cell starvation.

Mefloquine did not inhibit autophagy but was more effective at causing cell death than chloroquine in combination with nelfinavir (Fig 4.10). Mefloquine accumulates within and disrupts lysosomes in the same manner as chloroquine (Glaumann *et al.*, 1992) but, contrastingly to chloroquine, was found to permeabilise the lysosome membrane in acute myeloid leukaemia cells (Sukhai *et al.*, 2013). This action of mefloquine could account for increased cytotoxicity observed in both *Tsc2*-/- and *Tsc2*+/+ MEFs and could be tested for using acridine orange staining and flow cytometry or fluorescence microscopy, or electron microscopy. If confirmed, mefloquine-mediated lysosomal membrane permeabilisation and subsequent release of lysosomal contents into the cytoplasm would most likely result in necrosis and an inflammatory response *in vivo* which may render this potential drug treatment too toxic for clinical use.

Cell death induction by nelfinavir and chloroquine appears to be relevant when mTORC1 is overactive due to upstream oncogenic mutation, even in cells with intact TSC2, as demonstrated by the present study in NCI-H460 cells (Fig 4.7).

6.2.2 Cell death is rescued by inhibition of the v-ATPase

The primary function of lysosomes is to degrade extra- and intracellular material by engulfment and subjection to the highly acidic environment within. The v-ATPase is responsible for maintenance of lysosomal acidity through its ATP-dependent proton pump activity. Importantly, the active v-ATPase is required for Ragulator-Rag-mTORC1 binding to the lysosome (Zoncu *et al.*, 2011). Recent research used chloroquine treatment to raise lysosomal pH in osteoclasts which had the effect of increasing phosphorylated mTORC1 protein levels through a lack of degradation via the lysosome (Hu *et al.*, 2015). In yeast, v-ATPase activity was found to be greatly increased by cell growth in pH 7 conditions compared to pH 5 and was insensitive to inhibition (Diakov and Kane, 2010). As chloroquine is alkaline, its accumulation within lysosomes increases pH which may stimulate activation of the v-ATPase, resulting in more robust mTORC1 recruitment to the lysosome. When Rheb is active, this would result in increased protein synthesis and elevated ER stress. Combined with nelfinavir in *Tsc2*-/- cells, we observed that chloroquine induces cell death which can be rescued to levels of *Tsc2*+/+ cells by bafilomycin-A1 inhibition of the v-ATPase (Fig 4.10). These results confirm previous findings by Harhaji-Trajkovic *et al.,* (2012) where cell death was not reversed by antioxidant agents, but was rescued by bafilomycin-A1 co-treatment. Taken together, these results suggest cytotoxic effects seen in co-treatment are mediated by lysosome dysfunction that involves the v-ATPase.

6.3 Nelfinavir-bortezomib

6.3.1 Potential involvement of NF-κB

Under conditions of ER stress, translation is repressed through PERK-mediated activation of eIF2α. This results in decreased levels of IκB which are further reduced by IRE1α-TRAF2-ASK1 and JNK-mediated IKK activity. This further allows an increase in free NF-κB which translocates to the nucleus and transcriptionally activates multiple pro-survival genes including those involved in the ER stress response and UPR (Tam *et*

al., 2012). ER stress-mediated NF-κB activation could explain some of the cytoprotective effects observed following nelfinavir treatment. Preliminary studies found JSH23, a drug which prevents NF-κB translocation to the nucleus, to be a deadly treatment in *Tsc2*-/- and *Tsc2*+/+ MEFs (Fig 3.7). Interestingly, combination of JSH23 with nelfinavir greatly reduced the observed cell death in *Tsc2*+/+ MEFs, whilst still producing a high level of cell death in *Tsc2*-/- MEFs. This differential result is worthy of further research to prove the effect and investigate the potential underlying mechanisms.

Tsc2-/- MEFs exhibited increased basal levels of phosphorylated RelA protein which was increased by nelfinavir treatment (Fig 3.4). This suggests increased activation of NF-κB in these cells which is most likely mediated through ER stress signalling. Bortezomib is known to decrease activity of NF-κB due to reduced proteasomal degradation of IκB. In combination with nelfinavir, bortezomib proved to be effective at causing selective cell death in mTORC1 overactive cells, which wild type cells were able to tolerate. Direct inhibition of proteasomal degradation using bortezomib treatment reduced the effectiveness of the UPR and increased ER stress.

6.3.2 Failure to rescue cell death with mTORC1 inhibition

Inhibition of mTORC1 with rapamycin or Ku0063794 failed to rescue nelfinavir-bortezomib-induced cell death. These findings confirm previous research showing rapamycin was not able to protect against ER stress-induced apoptosis in either *Tsc1*-/- or *Tsc2*-/- MEFs (Kang *et al.*, 2011). One potential explanation for this is that rapamycin was observed to cause proteasome inhibition in *Tsc2*-/- MEFs (Fig 5.1), which supports current findings (Zhang *et al.*, 2014). Another explanation is that rapamycin is a poor inhibitor of mTORC1, requiring FKBP12 binding to allosterically inhibit mTORC1, primarily preventing larger substrate binding, such as S6K1 (Yip *et al.*, 2010). Ku0063794 is more effective at inhibiting mTORC1 than rapamycin, but also has multiple off-target kinase effects (Garcia-Martinez *et al.*, 2009). Since inhibition of mTORC1 did not significantly rescue nelfinavir-bortezomib-induced cell death (Fig 5.2-5.4, 5.6), it might be suggested that the mechanism of cell death is not mTORC1-dependent, but rather TSC2-dependent. Since inhibition of caspase cleavage did not rescue cell death (Fig 5.7-5.8), the precise mechanism of cell death remains unknown. Further investigation is required.

6.4 Future study

Further study with nelfinavir and chloroquine should determine whether the lysosome is involved in treatment outcome and include intracellular lysosome tracking in live cells under both treated and untreated conditions. Immunofluorescence time lapse microscopy with lysotracker red, and co-staining of the nucleus (and actin or other cytoskeletal stain) would be an ideal technique for observing lysosome localisation. Additionally, acridine orange could be used in combination with flow cytometry to identify differences in number and stability of lysosomes between treatments and cell lines. This could be used in combination with fluorescence microscopy to determine whether rupture of lysosomes and resultant necrosis is the cause of cell death following nelfinavir-chloroquine treatment. Additionally, electron microscopy would be an effective way of determining the state of ER stress through ER expansion, for determining localisation and state of lysosomes, number and condition of mitochondria (relating to ROS), for confirming blockade of autophagy, and for detection of hallmarks of apoptosis/necrosis after nelfinavir-chloroquine treatment. Cell death should be replicated using an alternative lysosome inhibitor such as ammonium chloride and/or an alternative ER stress-inducer such as tunicamycin. v-ATPase activity could be measured using acridine orange staining with flow cytometry to measure fluorescence intensity following addition of ATP to cells.

Future study with nelfinavir and bortezomib should determine whether cell death is mediated through changes in NF-κB levels, which could be achieved through analysis of NF-κB-associated proteins through western blot, or through RNA-Seq screening for changes in NF-κB gene expression targets. As with nelfinavir-chloroquine, electron microscopy would be a useful tool for assessment of ER homeostasis, as cell death is more likely mediated primarily through excessive ER stress. This could be replicated using an alternative ER stress inducer, as mentioned above, combined with bortezomib.

6.5 Conclusions

This research aimed to identify a novel drug combination for treatment of a broad spectrum of cancer and disease with overactive mTORC1 signalling. This novel approach utilised several cellular models with overactive mTORC1 through either *Tsc2*

mutation or upstream oncogenic signalling incurring increased mTORC1 activation as part of targeted therapy. At the time the research was initiated, nelfinavir had not previously been investigated in these cell lines. This study reveals that mTORC1 overactive cells are sensitive to drug-induced increased ER stress burden. While wild-type cells tolerate drug combinations, cytotoxicity within the TSC2-null cells is evident at low drug concentrations and is likely attributable to their inability to manage ER stress burden in a timely and appropriate manner. This is evidenced by elevated protein and mRNA levels of ER stress markers such as GADD34, CHOP and spliced XBP1. This research shows that cells with overactive mTORC1, through either lack of functional TSC2 or through upstream oncogenic mutation, are compromised in their ability to efficiently sense ER stress burden and to restore ER homeostasis.

Unfolded proteins within the ER are removed via both the autophagy and proteasome pathways. The present research shows that it is not the inhibitory action of chloroquine on autophagy which enhances cell death when combined with nelfinavir. Neither is it the inhibitory action of nelfinavir on the proteasome which induces ER stress.

In the present study, cell death was only observed upon co-treatment with nelfinavir and another drug: nelfinavir-chloroquine treatment involved chloroquine entrapment within the lysosome, likely increasing pH and stimulating mTORC1 activity which could not be prevented by nelfinavir-mediated activation of TSC2 in *Tsc2*-/- cells, resulting in cell death. Nelfinavir-bortezomib treatment involved inhibition of the proteasome, reducing NF-κB activity and increasing ER stress which was further increased by nelfinavir. Cell death through nelfinavir-chloroquine or nelfinavir-bortezomib was greatly reduced in cells with active TSC2. Inactivation of TSC2 either through genetic mutation (*Tsc2*-/- MEF, ELT3-V3, *TSC2*-/- AML cell lines) or through oncogenic growth factor-mediated inhibition (NCI-H460 cell line) appears to be crucial for significant cell death.

Tsc2-null cells have also been shown to be sensitive to glucose starvation (Choo *et al.*, 2010) and have elevated levels of ROS (Suzuki *et al.*, 2008). Recent work utilised a similar approach to the present study, wherby chelerythrine chloride was used to increase ROS beyond a tollerated threshold. Chelerythrine treatment induced

necroptotic cell death selectively in *Tsc2*-/- MEFs and ELT3-V3 cells, which was rescued by NAC (Medvetz *et al.*, 2015). Medvetz *et al.* (2015) also saw 57 % tumour reduction in xenograft tumour models after 4 weeks of treatment compared to untreated tumours. No evidence of toxicity was observed.

By targeting ER stress, there is potential for treatment of many cancers known to have increased mTORC1 signalling including breast, renal and pancreatic cancers, as well as benign tumour diseases such as TSC. However, this combination of drugs was not tested in cells heterozygous for *Tsc2*. Should drug treatment be cytotoxic in *Tsc2*+/- cells, it would likely be unsuitable for treatment of TSC patients.

This work tested viable drug combinations that could be repositioned to the clinic. The focus was to identify an effective, cytotoxic drug combination which could be used for stratified treatment of multiple cell types with overactive mTORC1. The main limitation of this study was a lack of animal models, the use of which would have enabled testing of drug combinations in a more realistic model system and may have given insight into associated toxicities. Further research using animal models and, if successful, preclinical trials is warranted.

7. References

AEBI, M., BERNASCONI, R., CLERC, S. & MOLINARI, M. 2010. N-glycan structures: recognition and processing in the ER. *Trends Biochem Sci,* 35**,** 74-82.

AURICCHIO, N., MALINOWSKA, I., SHAW, R., MANNING, B. D. & KWIATKOWSKI, D. J. 2012. Therapeutic trial of metformin and bortezomib in a mouse model of tuberous sclerosis complex (TSC). *PLoS One,* 7**,** e31900.

B'CHIR, W., MAURIN, A. C., CARRARO, V., AVEROUS, J., JOUSSE, C., MURANISHI, Y., PARRY, L., STEPIEN, G., FAFOURNOUX, P. & BRUHAT, A. 2013. The eIF2alpha/ATF4 pathway is essential for stress-induced autophagy gene expression. *Nucleic Acids Res,* 41**,** 7683-99.

BABCOCK, J. T., NGUYEN, H. B., HE, Y., HENDRICKS, J. W., WEK, R. C. & QUILLIAM, L. A. 2013. Mammalian target of rapamycin complex 1 (mTORC1) enhances bortezomib-induced death in tuberous sclerosis complex (TSC)-null cells by a c-MYC-dependent induction of the unfolded protein response. *J Biol Chem,* 288**,** 15687-98.

BAE-HARBOE, Y. S. & GERONEMUS, R. G. 2013. Targeted topical and combination laser surgery for the treatment of angiofibromas. *Lasers Surg Med,* 45**,** 555-7.

BAR-PELED, L., CHANTRANUPONG, L., CHERNIACK, A. D., CHEN, W. W., OTTINA, K. A., GRABINER, B. C., SPEAR, E. D., CARTER, S. L., MEYERSON, M. & SABATINI, D. M. 2013. A Tumor suppressor complex with GAP activity for the Rag GTPases that signal amino acid sufficiency to mTORC1. *Science,* 340**,** 1100-6.

BARILLARI, G., SGADARI, C., TOSCHI, E., MONINI, P. & ENSOLI, B. 2003. HIV protease inhibitors as new treatment options for Kaposi's sarcoma. *Drug Resist Updat,* 6**,** 173-81.

BENBROOK, D. M. & LONG, A. 2012. Integration of autophagy, proteasomal degradation, unfolded protein response and apoptosis. *Exp Oncol,* 34**,** 286-97.

BHAUMIK, S. R. & MALIK, S. 2008. Diverse regulatory mechanisms of eukaryotic transcriptional activation by the proteasome complex. *Crit Rev Biochem Mol Biol,* 43**,** 419-33.

BISSLER, J. J., KINGSWOOD, J. C., RADZIKOWSKA, E., ZONNENBERG, B. A., FROST, M., BELOUSOVA, E., SAUTER, M., NONOMURA, N., BRAKEMEIER, S., DE VRIES, P. J., WHITTEMORE, V. H., CHEN, D., SAHMOUD, T., SHAH, G., LINCY, J., LEBWOHL, D. & BUDDE, K. 2013. Everolimus for angiomyolipoma associated with tuberous sclerosis complex or sporadic lymphangioleiomyomatosis (EXIST-2): a multicentre, randomised, double-blind, placebo-controlled trial. *Lancet,* 381**,** 817-24.

BLUM, L., PELLET, C., AGBALIKA, F., BLANCHARD, G., MOREL, P., CALVO, F. & LEBBE, C. 1997. Complete remission of AIDS-related Kaposi's sarcoma associated with undetectable human herpesvirus-8 sequences during anti-HIV protease therapy. *AIDS,* 11**,** 1653-5.

BLUMENTHAL, G. M., GILLS, J. J., BALLAS, M. S., BERNSTEIN, W. B., KOMIYA, T., DECHOWDHURY, R., MORROW, B., ROOT, H., CHUN, G., HELSABECK, C., STEINBERG, S. M., LOPICCOLO, J., KAWABATA, S., GARDNER, E. R., FIGG, W. D. & DENNIS, P. A. 2014. A phase I trial of the HIV protease inhibitor nelfinavir in adults with solid tumors. *Oncotarget,* 5**,** 8161-72.

BONO, C., KARLIN, L., HAREL, S., MOULY, E., LABAUME, S., GALICIER, L., APCHER, S., SAUVAGEON, H., FERMAND, J. P., BORIES, J. C. & ARNULF, B. 2012. The human immunodeficiency virus-1 protease inhibitor nelfinavir impairs proteasome

activity and inhibits the proliferation of multiple myeloma cells in vitro and in vivo. *Haematologica,* 97**,** 1101-9.

BROOKS, A. D., JACOBSEN, K. M., LI, W., SHANKER, A. & SAYERS, T. J. 2010. Bortezomib sensitizes human renal cell carcinomas to TRAIL apoptosis through increased activation of caspase-8 in the death-inducing signaling complex. *Mol Cancer Res,* 8**,** 729-38.

BRÜNING, A. 2011. Analysis of nelfinavir-induced endoplasmic reticulum stress. *Methods Enzymol,* 491**,** 127-42.

BRÜNING, A., BURGER, P., VOGEL, M., RAHMEH, M., GINGELMAIERS, A., FRIESE, K., LENHARD, M. & BURGES, A. 2009. Nelfinavir induces the unfolded protein response in ovarian cancer cells, resulting in ER vacuolization, cell cycle retardation and apoptosis. *Cancer Biol Ther,* 8**,** 226-32.

BRÜNING, A., FRIESE, K., BURGES, A. & MYLONAS, I. 2010. Tamoxifen enhances the cytotoxic effects of nelfinavir in breast cancer cells. *Breast Cancer Res,* 12**,** R45.

BRÜNING, A. & JÜCKSTOCK, J. 2015. Misfolded proteins: from little villains to little helpers in the fight against cancer. *Front Oncol,* 5**,** 47.

BRÜNING, A., RAHMEH, M. & FRIESE, K. 2013. Nelfinavir and bortezomib inhibit mTOR activity via ATF4-mediated sestrin-2 regulation. *Mol Oncol*.

BUDANOV, A. V. & KARIN, M. 2008. p53 Target Genes Sestrin1 and Sestrin2 Connect Genotoxic Stress and mTOR Signaling. *Cell,* 134**,** 451-460.

CHOI, J., CHEN, J., SCHREIBER, S. L. & CLARDY, J. 1996. Structure of the FKBP12-rapamycin complex interacting with the binding domain of human FRAP. *Science,* 273**,** 239-42.

CHOO-WING, R., SYED, M. A., HARIJITH, A., BOWEN, B., PRYHUBER, G., JANÉR, C., ANDERSSON, S., HOMER, R. J. & BHANDARI, V. 2013. Hyperoxia and Interferon-γ–Induced Injury in Developing Lungs Occur via Cyclooxygenase-2 and the Endoplasmic Reticulum Stress–Dependent Pathway. *Am J Respir Cell Mol Biol,* 48**,** 749-57.

CHOO, A. Y., KIM, S. G., VANDER HEIDEN, M. G., MAHONEY, S. J., VU, H., YOON, S. O., CANTLEY, L. C. & BLENIS, J. 2010. Glucose addiction of TSC null cells is caused by failed mTORC1-dependent balancing of metabolic demand with supply. *Mol Cell,* 38**,** 487-99.

CLEMENTS, D., DONGRE, A., KRYMSKAYA, V. P. & JOHNSON, S. R. 2015. Wild type mesenchymal cells contribute to the lung pathology of lymphangioleiomyomatosis. *PLoS One,* 10**,** e0126025.

CONANT, M. A., OPP, K. M., PORETZ, D. & MILLS, R. G. 1997. Reduction of Kaposi's sarcoma lesions following treatment of AIDS with ritonovir. *AIDS,* 11**,** 1300-1.

DAZERT, E. & HALL, M. N. 2011. mTOR signaling in disease. *Curr Opin Cell Biol,* 23**,** 744-55.

DENG, J., LU, P. D., ZHANG, Y., SCHEUNER, D., KAUFMAN, R. J., SONENBERG, N., HARDING, H. P. & RON, D. 2004. Translational repression mediates activation of nuclear factor kappa B by phosphorylated translation initiation factor 2. *Mol Cell Biol,* 24**,** 10161-8.

DENNIS, M. D., COLEMAN, C. S., BERG, A., JEFFERSON, L. S. & KIMBALL, S. R. 2014. REDD1 enhances protein phosphatase 2A-mediated dephosphorylation of Akt to repress mTORC1 signaling. *Sci Signal,* 7**,** ra68.

DEWAN, M. Z., TOMITA, M., KATANO, H., YAMAMOTO, N., AHMED, S., YAMAMOTO, M., SATA, T., MORI, N. & YAMAMOTO, N. 2009. An HIV protease inhibitor,

ritonavir targets the nuclear factor-kappaB and inhibits the tumor growth and infiltration of EBV-positive lymphoblastoid B cells. *Int J Cancer,* 124**,** 622-9.

DIAKOV, T. T. & KANE, P. M. 2010. Regulation of vacuolar proton-translocating ATPase activity and assembly by extracellular pH. *J Biol Chem,* 285**,** 23771-8.

DIBBLE, C. C., ELIS, W., MENON, S., QIN, W., KLEKOTA, J., ASARA, J. M., FINAN, P. M., KWIATKOWSKI, D. J., MURPHY, L. O. & MANNING, B. D. 2012. TBC1D7 is a third subunit of the TSC1-TSC2 complex upstream of mTORC1. *Mol Cell,* 47**,** 535-46.

ESCALANTE, A. M., MCGRATH, R. T., KAROLAK, M. R., DORR, R. T., LYNCH, R. M. & LANDOWSKI, T. H. 2013. Preventing the autophagic survival response by inhibition of calpain enhances the cytotoxic activity of bortezomib in vitro and in vivo. *Cancer Chemother Pharmacol,* 71**,** 1567-76.

FEDORKO, M. 1967. Effect of chloroquine on morphology of cytoplasmic granules in maturing human leukocytes--an ultrastructural study. *J Clin Invest,* 46**,** 1932-42.

FRAND, A. R., CUOZZO, J. W. & KAISER, C. A. 2000. Pathways for protein disulphide bond formation. *Trends Cell Biol,* 10**,** 203-10.

FRANZ, D. N., BISSLER, J. J. & MCCORMACK, F. X. 2010. Tuberous sclerosis complex: neurological, renal and pulmonary manifestations. *Neuropediatrics,* 41**,** 199-208.

FRANZ, D. N., LEONARD, J., TUDOR, C., CHUCK, G., CARE, M., SETHURAMAN, G., DINOPOULOS, A., THOMAS, G. & CRONE, K. R. 2006. Rapamycin causes regression of astrocytomas in tuberous sclerosis complex. *Ann Neurol,* 59**,** 490-8.

FRANZ, D. N. & WEISS, B. D. 2012. Molecular therapies for tuberous sclerosis and neurofibromatosis. *Curr Neurol Neurosci Rep,* 12**,** 294-301.

GANTT, S., CASPER, C. & AMBINDER, R. F. 2013. Insights into the broad cellular effects of nelfinavir and the HIV protease inhibitors supporting their role in cancer treatment and prevention. *Curr Opin Oncol,* 25**,** 495-502.

GARCIA-MARTINEZ, J. M., MORAN, J., CLARKE, R. G., GRAY, A., COSULICH, S. C., CHRESTA, C. M. & ALESSI, D. R. 2009. Ku-0063794 is a specific inhibitor of the mammalian target of rapamycin (mTOR). *Biochem J,* 421**,** 29-42.

GELMAN, J. S., SIRONI, J., BEREZNIUK, I., DASGUPTA, S., CASTRO, L. M., GOZZO, F. C., FERRO, E. S. & FRICKER, L. D. 2013. Alterations of the intracellular peptidome in response to the proteasome inhibitor bortezomib. *PLoS One,* 8**,** e53263.

GENG, Y., KOHLI, L., KLOCKE, B. J. & ROTH, K. A. 2010. Chloroquine-induced autophagic vacuole accumulation and cell death in glioma cells is p53 independent. *Neuro Oncol,* 12**,** 473-81.

GETHING, M. J. & SAMBROOK, J. 1992. Protein folding in the cell. *Nature,* 355**,** 33-45.

GILLS, J. J., LOPICCOLO, J., TSURUTANI, J., SHOEMAKER, R. H., BEST, C. J., ABU-ASAB, M. S., BOROJERDI, J., WARFEL, N. A., GARDNER, E. R., DANISH, M., HOLLANDER, M. C., KAWABATA, S., TSOKOS, M., FIGG, W. D., STEEG, P. S. & DENNIS, P. A. 2007. Nelfinavir, A lead HIV protease inhibitor, is a broad-spectrum, anticancer agent that induces endoplasmic reticulum stress, autophagy, and apoptosis in vitro and in vivo. *Clin Cancer Res,* 13**,** 5183-94.

GLAUMANN, H., MOTAKEFI, A. M. & JANSSON, H. 1992. Intracellular distribution and effect of the antimalarial drug mefloquine on lysosomes of rat liver. *Liver,* 12**,** 183-90.

GOLDEN, E. B., CHO, H. Y., HOFMAN, F. M., LOUIE, S. G., SCHONTHAL, A. H. & CHEN, T. C. 2015. Quinoline-based antimalarial drugs: a novel class of autophagy inhibitors. *Neurosurg Focus,* 38**,** E12.

GROENEWOUD, M. J. & ZWARTKRUIS, F. J. 2013. Rheb and Rags come together at the lysosome to activate mTORC1. *Biochem Soc Trans,* 41**,** 951-5.

GROSSO, G., SGADARI, C., BARILLARI, G., TOSCHI, E., BACIGALUPO, I., CARLEI, D., PALLADINO, C., BACCARINI, S., MALAVASI, L., MORACCI, G., LEONE, P., CHIOZZINI, C., MONINI, P. & ENSOLI, B. 2003. [HIV protease inhibitors for the treatment of Kaposi's sarcoma]. *Recenti Prog Med,* 94**,** 69-74.

GU, Z. C. & ENENKEL, C. 2014. Proteasome assembly. *Cell Mol Life Sci,* 71**,** 4729-45.

GUAN, M., FOUSEK, K. & CHOW, W. A. 2012. Nelfinavir inhibits regulated intramembrane proteolysis of sterol regulatory element binding protein-1 and activating transcription factor 6 in castration-resistant prostate cancer. *FEBS J,* 279**,** 2399-411.

GUAN, M., SU, L., YUAN, Y. C., LI, H. & CHOW, W. A. 2015. Nelfinavir and nelfinavir analogs block site-2 protease cleavage to inhibit castration-resistant prostate cancer. *Sci Rep,* 5**,** 9698.

GUO, Y., CHEKALUK, Y., ZHANG, J., DU, J., GRAY, N. S., WU, C. L. & KWIATKOWSKI, D. J. 2013. TSC1 involvement in bladder cancer: diverse effects and therapeutic implications. *J Pathol,* 230**,** 17-27.

GUPTA, A. K., LI, B., CERNIGLIA, G. J., AHMED, M. S., HAHN, S. M. & MAITY, A. 2007. The HIV protease inhibitor nelfinavir downregulates Akt phosphorylation by inhibiting proteasomal activity and inducing the unfolded protein response. *Neoplasia,* 9**,** 271-8.

HAAS, I. G. & WABL, M. 1983. Immunoglobulin heavy chain binding protein. *Nature,* 306**,** 387-9.

HANAHAN, D. & WEINBERG, R. A. 2011. Hallmarks of cancer: the next generation. *Cell,* 144**,** 646-74.

HARHAJI-TRAJKOVIC, L., ARSIKIN, K., KRAVIC-STEVOVIC, T., PETRICEVIC, S., TOVILOVIC, G., PANTOVIC, A., ZOGOVIC, N., RISTIC, B., JANJETOVIC, K., BUMBASIREVIC, V. & TRAJKOVIC, V. 2012. Chloroquine-mediated lysosomal dysfunction enhances the anticancer effect of nutrient deprivation. *Pharm Res,* 29**,** 2249-63.

HARTL, F. U., BRACHER, A. & HAYER-HARTL, M. 2011. Molecular chaperones in protein folding and proteostasis. *Nature,* 475**,** 324-32.

HEALY, S. J., GORMAN, A. M., MOUSAVI-SHAFAEI, P., GUPTA, S. & SAMALI, A. 2009. Targeting the endoplasmic reticulum-stress response as an anticancer strategy. *Eur J Pharmacol,* 625**,** 234-46.

HORTON, T. M., DRACHTMAN, R. A., CHEN, L., COLE, P. D., MCCARTEN, K., VOSS, S., GUILLERMAN, R. P., BUXTON, A., HOWARD, S. C., HOGAN, S. M., SHEEHAN, A. M., LOPEZ-TERRADA, D., MRAZEK, M. D., AGRAWAL, N., WU, M. F., LIU, H., DE ALARCON, P. A., TRIPPET, T. M. & SCHWARTZ, C. L. 2015. A phase 2 study of bortezomib in combination with ifosfamide/vinorelbine in paediatric patients and young adults with refractory/recurrent Hodgkin lymphoma: a Children's Oncology Group study. *Br J Haematol*.

HOWE, S. R., GOTTARDIS, M. M., EVERITT, J. I., GOLDSWORTHY, T. L., WOLF, D. C. & WALKER, C. 1995. Rodent model of reproductive tract leiomyomata. Establishment and characterization of tumor-derived cell lines. *Am J Pathol,* 146**,** 1568-79.

HOYER-HANSEN, M. & JAATTELA, M. 2007. Connecting endoplasmic reticulum stress to autophagy by unfolded protein response and calcium. *Cell Death Differ,* 14**,** 1576-82.

HU, Y., CARRARO-LACROIX, L. R., WANG, A., OWEN, C., BAJENOVA, E., COREY, P. N., BRUMELL, J. H. & VORONOV, I. 2015. Lysosomal pH Plays a Key Role in Regulation of mTOR Activity in Osteoclasts. *J Cell Biochem*.

HUYNH, H., HAO, H. X., CHAN, S. L., CHEN, D., ONG, R., SOO, K. C., POCHANARD, P., YANG, D., RUDDY, D., LIU, M., DERTI, A., BALAK, M. N., PALMER, M. R., WANG, Y., LEE, B. H., SELLAMI, D., ZHU, A. X., SCHLEGEL, R. & HUANG, A. 2015. Loss of Tuberous Sclerosis Complex 2 (TSC2) Is Frequent in Hepatocellular Carcinoma and Predicts Response to mTORC1 Inhibitor Everolimus. *Mol Cancer Ther,* 14**,** 1224-35.

JAGER, R., BERTRAND, M. J., GORMAN, A. M., VANDENABEELE, P. & SAMALI, A. 2012. The unfolded protein response at the crossroads of cellular life and death during endoplasmic reticulum stress. *Biol Cell,* 104**,** 259-70.

JIANG, W., MIKOCHIK, P. J., RA, J. H., LEI, H., FLAHERTY, K. T., WINKLER, J. D. & SPITZ, F. R. 2007. HIV protease inhibitor nelfinavir inhibits growth of human melanoma cells by induction of cell cycle arrest. *Cancer Res,* 67**,** 1221-7.

JOZWIAK, J., JOZWIAK, S. & OLDAK, M. 2006. Molecular activity of sirolimus and its possible application in tuberous sclerosis treatment. *Med Res Rev,* 26**,** 160-80.

KANG, Y. J., LU, M. K. & GUAN, K. L. 2011. The TSC1 and TSC2 tumor suppressors are required for proper ER stress response and protect cells from ER stress-induced apoptosis. *Cell Death Differ,* 18**,** 133-44.

KATAOKA, K., FUJIMOTO, K., ITO, D., KOIZUMI, M., TOYODA, E., MORI, T., KAMI, K. & DOI, R. 2005. Expression and prognostic value of tuberous sclerosis complex 2 gene product tuberin in human pancreatic cancer. *Surgery,* 138**,** 450-5.

KAWABATA, S., GILLS, J. J., MERCADO-MATOS, J. R., LOPICCOLO, J., WILSON, W., 3RD, HOLLANDER, M. C. & DENNIS, P. A. 2012. Synergistic effects of nelfinavir and bortezomib on proteotoxic death of NSCLC and multiple myeloma cells. *Cell Death Dis,* 3**,** e353.

KAWAGUCHI, T., MIYAZAWA, K., MORIYA, S., OHTOMO, T., CHE, X. F., NAITO, M., ITOH, M. & TOMODA, A. 2011. Combined treatment with bortezomib plus bafilomycin A1 enhances the cytocidal effect and induces endoplasmic reticulum stress in U266 myeloma cells: crosstalk among proteasome, autophagy-lysosome and ER stress. *Int J Oncol,* 38**,** 643-54.

KIM, B. M., MAENG, K., LEE, K. H. & HONG, S. H. 2011. Combined treatment with the Cox-2 inhibitor niflumic acid and PPARgamma ligand ciglitazone induces ER stress/caspase-8-mediated apoptosis in human lung cancer cells. *Cancer Lett,* 300**,** 134-44.

KIM, H. J., HAWKE, N. & BALDWIN, A. S. 2006. NF-kappaB and IKK as therapeutic targets in cancer. *Cell Death Differ,* 13**,** 738-47.

KIM, J. H., CHOI, A. R., KIM, Y. K. & YOON, S. 2013. Co-treatment with the anti-malarial drugs mefloquine and primaquine highly sensitizes drug-resistant cancer cells by increasing P-gp inhibition. *Biochem Biophys Res Commun,* 441**,** 655-60.

KIM, J. Y., LEE, S., HWANGBO, B., LEE, C. T., KIM, Y. W., HAN, S. K., SHIM, Y. S. & YOO, C. G. 2000. NF-kappaB activation is related to the resistance of lung cancer cells to TNF-alpha-induced apoptosis. *Biochem Biophys Res Commun,* 273**,** 140-6.

KLIONSKY, D. J., ELAZAR, Z., SEGLEN, P. O. & RUBINSZTEIN, D. C. 2008. Does bafilomycin A1 block the fusion of autophagosomes with lysosomes? *Autophagy,* 4**,** 849-50.

KOENIG, M. K., HEBERT, A. A., ROBERSON, J., SAMUELS, J., SLOPIS, J., WOERNER, A. & NORTHRUP, H. 2012. Topical rapamycin therapy to alleviate the cutaneous

manifestations of tuberous sclerosis complex: a double-blind, randomized, controlled trial to evaluate the safety and efficacy of topically applied rapamycin. *Drugs R D,* 12**,** 121-6.

KOHRMAN, M. H. 2012. Emerging treatments in the management of tuberous sclerosis complex. *Pediatr Neurol,* 46**,** 267-75.

KOVACS, A. L. & SEGLEN, P. O. 1982. Inhibition of hepatocytic protein degradation by inducers of autophagosome accumulation. *Acta Biol Med Ger,* 41**,** 125-30.

KRAUS, M., BADER, J., OVERKLEEFT, H. & DRIESSEN, C. 2013. Nelfinavir augments proteasome inhibition by bortezomib in myeloma cells and overcomes bortezomib and carfilzomib resistance. *Blood Cancer J,* 3**,** e103.

KRAUS, M., MULLER-IDE, H., RUCKRICH, T., BADER, J., OVERKLEEFT, H. & DRIESSEN, C. 2014. Ritonavir, nelfinavir, saquinavir and lopinavir induce proteotoxic stress in acute myeloid leukemia cells and sensitize them for proteasome inhibitor treatment at low micromolar drug concentrations. *Leuk Res,* 38**,** 383-92.

KUCEJOVA, B., PENA-LLOPIS, S., YAMASAKI, T., SIVANAND, S., TRAN, T. A., ALEXANDER, S., WOLFF, N. C., LOTAN, Y., XIE, X. J., KABBANI, W., KAPUR, P. & BRUGAROLAS, J. 2011. Interplay between pVHL and mTORC1 pathways in clear-cell renal cell carcinoma. *Mol Cancer Res,* 9**,** 1255-65.

KUO, L. J. & YANG, L. X. 2008. Gamma-H2AX - a novel biomarker for DNA double-strand breaks. *In Vivo,* 22**,** 305-9.

KUSHCHAYEVA, Y., JENSEN, K., RECUPERO, A., COSTELLO, J., PATEL, A., KLUBO-GWIEZDZINSKA, J., BOYLE, L., BURMAN, K. & VASKO, V. 2014. The HIV protease inhibitor nelfinavir down-regulates RET signaling and induces apoptosis in medullary thyroid cancer cells. *J Clin Endocrinol Metab,* 99**,** E734-45.

LAPLANTE, M. & SABATINI, D. M. 2012. mTOR signaling in growth control and disease. *Cell,* 149**,** 274-93.

LEE, A. S. 1987. Coordinated regulation of a set of genes by glucose and calcium ionophores in mammalian cells. *Trends Biochem Sci,* 12**,** 20-23.

LEE, K. H., JEONG, J. & YOO, C. G. 2013. Long-term incubation with proteasome inhibitors (PIs) induces IkappaBalpha degradation via the lysosomal pathway in an IkappaB kinase (IKK)-dependent and IKK-independent manner. *J Biol Chem,* 288**,** 32777-86.

LIN, J. H., LI, H., YASUMURA, D., COHEN, H. R., ZHANG, C., PANNING, B., SHOKAT, K. M., LAVAIL, M. M. & WALTER, P. 2007. IRE1 signaling affects cell fate during the unfolded protein response. *Science,* 318**,** 944-9.

LIU, G., SU, L., HAO, X., ZHONG, N., ZHONG, D., SINGHAL, S. & LIU, X. 2012. Salermide up-regulates death receptor 5 expression through the ATF4-ATF3-CHOP axis and leads to apoptosis in human cancer cells. *J Cell Mol Med,* 16**,** 1618-28.

LIU, Y., SHOJI-KAWATA, S., SUMPTER, R. M., JR., WEI, Y., GINET, V., ZHANG, L., POSNER, B., TRAN, K. A., GREEN, D. R., XAVIER, R. J., SHAW, S. Y., CLARKE, P. G., PUYAL, J. & LEVINE, B. 2013. Autosis is a Na+,K+-ATPase-regulated form of cell death triggered by autophagy-inducing peptides, starvation, and hypoxia-ischemia. *Proc Natl Acad Sci U S A,* 110**,** 20364-71.

LU, M., LAWRENCE, D. A., MARSTERS, S., ACOSTA-ALVEAR, D., KIMMIG, P., MENDEZ, A. S., PATON, A. W., PATON, J. C., WALTER, P. & ASHKENAZI, A. 2014. Opposing unfolded-protein-response signals converge on death receptor 5 to control apoptosis. *Science,* 345**,** 98-101.

MA, Y. & HENDERSHOT, L. M. 2004. ER chaperone functions during normal and stress conditions. *J Chem Neuroanat,* 28**,** 51-65.

MAHONEY, E., MADDOCKS, K., FLYNN, J., JONES, J., COLE, S. L., ZHANG, X., BYRD, J. C. & JOHNSON, A. J. 2013. Identification of endoplasmic reticulum stress-inducing agents by antagonizing autophagy: a new potential strategy for identification of anti-cancer therapeutics in B-cell malignancies. *Leuk Lymphoma,* 54**,** 2685-92.

MARCU, M. G., DOYLE, M., BERTOLOTTI, A., RON, D., HENDERSHOT, L. & NECKERS, L. 2002. Heat shock protein 90 modulates the unfolded protein response by stabilizing IRE1alpha. *Mol Cell Biol,* 22**,** 8506-13.

MAYCOTTE, P., ARYAL, S., CUMMINGS, C. T., THORBURN, J., MORGAN, M. J. & THORBURN, A. 2012. Chloroquine sensitizes breast cancer cells to chemotherapy independent of autophagy. *Autophagy,* 8**,** 200-12.

MCCORMACK, P. L. 2011. Celecoxib: a review of its use for symptomatic relief in the treatment of osteoarthritis, rheumatoid arthritis and ankylosing spondylitis. *Drugs,* 71**,** 2457-89.

MEDVETZ, D., SUN, Y., LI, C., KHABIBULLIN, D., BALAN, M., PARKHITKO, A., PRIOLO, C., ASARA, J. M., PAL, S., YU, J. & HENSKE, E. P. 2015. High-throughput drug screen identifies chelerythrine as a selective inducer of death in a TSC2-null setting. *Mol Cancer Res,* 13**,** 50-62.

MICEL, L. N., TENTLER, J. J., SMITH, P. G. & ECKHARDT, G. S. 2013. Role of ubiquitin ligases and the proteasome in oncogenesis: novel targets for anticancer therapies. *J Clin Oncol,* 31**,** 1231-8.

MITSCHER, L. A. 2005. Bacterial topoisomerase inhibitors: quinolone and pyridone antibacterial agents. *Chem Rev,* 105**,** 559-92.

MURPHY, M., ARMSTRONG, D., SEPKOWITZ, K. A., AHKAMI, R. N. & MYSKOWSKI, P. L. 1997. Regression of AIDS-related Kaposi's sarcoma following treatment with an HIV-1 protease inhibitor. *AIDS,* 11**,** 261-2.

NGIAM, T. L. & GO, M. L. 1987. Stereospecific inhibition of cholinesterases by mefloquine enantiomers. *Chem Pharm Bull (Tokyo),* 35**,** 409-12.

OHOKA, N., YOSHII, S., HATTORI, T., ONOZAKI, K. & HAYASHI, H. 2005. TRB3, a novel ER stress-inducible gene, is induced via ATF4-CHOP pathway and is involved in cell death. *EMBO J,* 24**,** 1243-55.

OSMULSKI, P. A. & GACZYNSKA, M. 2013. Rapamycin allosterically inhibits the proteasome. *Mol Pharmacol,* 84**,** 104-13.

OZCAN, U., OZCAN, L., YILMAZ, E., DUVEL, K., SAHIN, M., MANNING, B. D. & HOTAMISLIGIL, G. S. 2008. Loss of the tuberous sclerosis complex tumor suppressors triggers the unfolded protein response to regulate insulin signaling and apoptosis. *Mol Cell,* 29**,** 541-51.

PAI, V. B. & NAHATA, M. C. 1999. Nelfinavir mesylate: a protease inhibitor. *Ann Pharmacother,* 33**,** 325-39.

PAN, J., MOTT, M., XI, B., HEPNER, E., GUAN, M., FOUSEK, K., MAGNUSSON, R., TINSLEY, R., VALDES, F., FRANKEL, P., SYNOLD, T. & CHOW, W. A. 2012. Phase I study of nelfinavir in liposarcoma. *Cancer Chemother Pharmacol,* 70**,** 791-9.

PARKHITKO, A. A., PRIOLO, C., COLOFF, J. L., YUN, J., WU, J. J., MIZUMURA, K., XU, W., MALINOWSKA, I. A., YU, J., KWIATKOWSKI, D. J., LOCASALE, J. W., ASARA, J. M., CHOI, A. M., FINKEL, T. & HENSKE, E. P. 2014. Autophagy-dependent metabolic reprogramming sensitizes TSC2-deficient cells to the antimetabolite 6-aminonicotinamide. *Mol Cancer Res,* 12**,** 48-57.

PARMIGIANI, A., NOURBAKHSH, A., DING, B., WANG, W., KIM, Y. C., AKOPIANTS, K., GUAN, K. L., KARIN, M. & BUDANOV, A. V. 2014. Sestrins inhibit mTORC1 kinase activation through the GATOR complex. *Cell Rep,* 9**,** 1281-91.

PIVA, R., BELARDO, G. & SANTORO, M. G. 2006. NF-kappaB: a stress-regulated switch for cell survival. *Antioxid Redox Signal,* 8**,** 478-86.

PORE, N., GUPTA, A. K., CERNIGLIA, G. J., JIANG, Z., BERNHARD, E. J., EVANS, S. M., KOCH, C. J., HAHN, S. M. & MAITY, A. 2006a. Nelfinavir down-regulates hypoxia-inducible factor 1alpha and VEGF expression and increases tumor oxygenation: implications for radiotherapy. *Cancer Res,* 66**,** 9252-9.

PORE, N., GUPTA, A. K., CERNIGLIA, G. J. & MAITY, A. 2006b. HIV protease inhibitors decrease VEGF/HIF-1alpha expression and angiogenesis in glioblastoma cells. *Neoplasia,* 8**,** 889-95.

PORTER, K. R. 1953. Observations on a submicroscopic basophilic component of cytoplasm. *J Exp Med,* 97**,** 727-50.

POUS, C. & CODOGNO, P. 2011. Lysosome positioning coordinates mTORC1 activity and autophagy. *Nat Cell Biol,* 13**,** 342-4.

RAO, A. & LAUER, R. 2015. Phase II Study of Sorafenib and Bortezomib for First-Line Treatment of Metastatic or Unresectable Renal Cell Carcinoma. *Oncologist,* 20**,** 370-1.

RITOSSA, F. 1962. A new puffing pattern induced by temperature shock and DNP in drosophila. *Experientia,* 18**,** 571-573.

RUBINSZTEIN, D. C. 2006. The roles of intracellular protein-degradation pathways in neurodegeneration. *Nature,* 443**,** 780-6.

RUTISHAUSER, J. & SPIESS, M. 2002. Endoplasmic reticulum storage diseases. *Swiss Med Wkly,* 132**,** 211-22.

RZYMSKI, T., MILANI, M., SINGLETON, D. C. & HARRIS, A. L. 2009. Role of ATF4 in regulation of autophagy and resistance to drugs and hypoxia. *Cell Cycle,* 8**,** 3838-47.

SANO, R. & REED, J. C. 2013. ER stress-induced cell death mechanisms. *Biochim Biophys Acta,* 1833**,** 3460-70.

SATO, A., ASANO, T., ITO, K. & ASANO, T. 2012. Ritonavir interacts with bortezomib to enhance protein ubiquitination and histone acetylation synergistically in renal cancer cells. *Urology,* 79**,** 966 e13-21.

SCHLEICHER, S. M., MORETTI, L., VARKI, V. & LU, B. 2010. Progress in the unraveling of the endoplasmic reticulum stress/autophagy pathway and cancer: implications for future therapeutic approaches. *Drug Resist Updat,* 13**,** 79-86.

SCHRODER, M. & KAUFMAN, R. J. 2005. ER stress and the unfolded protein response. *Mutat Res,* 569**,** 29-63.

SEGGEWISS-BERNHARDT, R., BARGOU, R. C., GOH, Y. T., STEWART, A. K., SPENCER, A., ALEGRE, A., BLADE, J., OTTMANN, O. G., FERNANDEZ-IBARRA, C., LU, H., PAIN, S., AKIMOV, M. & IYER, S. P. 2015. Phase 1/1B trial of the heat shock protein 90 inhibitor NVP-AUY922 as monotherapy or in combination with bortezomib in patients with relapsed or refractory multiple myeloma. *Cancer*.

SELIMOVIC, D., PORZIG, B. B., EL-KHATTOUTI, A., BADURA, H. E., AHMAD, M., GHANJATI, F., SANTOURLIDIS, S., HAIKEL, Y. & HASSAN, M. 2013. Bortezomib/proteasome inhibitor triggers both apoptosis and autophagy-dependent pathways in melanoma cells. *Cell Signal,* 25**,** 308-18.

SGADARI, C., MONINI, P., BARILLARI, G. & ENSOLI, B. 2003. Use of HIV protease inhibitors to block Kaposi's sarcoma and tumour growth. *Lancet Oncol,* 4**,** 537-47.

SHACKA, J. J., KLOCKE, B. J., SHIBATA, M., UCHIYAMA, Y., DATTA, G., SCHMIDT, R. E. & ROTH, K. A. 2006. Bafilomycin A1 inhibits chloroquine-induced death of cerebellar granule neurons. *Mol Pharmacol,* 69**,** 1125-36.

SHARMA, N., THOMAS, S., GOLDEN, E. B., HOFMAN, F. M., CHEN, T. C., PETASIS, N. A., SCHONTHAL, A. H. & LOUIE, S. G. 2012. Inhibition of autophagy and induction of breast cancer cell death by mefloquine, an antimalarial agent. *Cancer Lett,* 326**,** 143-54.

SHIBATA, Y., VOELTZ, G. K. & RAPOPORT, T. A. 2006. Rough sheets and smooth tubules. *Cell,* 126**,** 435-9.

SHIM, J. S., RAO, R., BEEBE, K., NECKERS, L., HAN, I., NAHTA, R. & LIU, J. O. 2012. Selective inhibition of HER2-positive breast cancer cells by the HIV protease inhibitor nelfinavir. *J Natl Cancer Inst,* 104**,** 1576-90.

SHIN, H. M., KIM, M. H., KIM, B. H., JUNG, S. H., KIM, Y. S., PARK, H. J., HONG, J. T., MIN, K. R. & KIM, Y. 2004. Inhibitory action of novel aromatic diamine compound on lipopolysaccharide-induced nuclear translocation of NF-kappaB without affecting IkappaB degradation. *FEBS Lett,* 571**,** 50-4.

SHIN, J. H., PARK, S. J., JO, Y. K., KIM, E. S., KANG, H., PARK, J. H., LEE, E. H. & CHO, D. H. 2012. Suppression of autophagy exacerbates Mefloquine-mediated cell death. *Neurosci Lett,* 515**,** 162-7.

SIROKY, B. J., YIN, H., BABCOCK, J. T., LU, L., HELLMANN, A. R., DIXON, B. P., QUILLIAM, L. A. & BISSLER, J. J. 2012. Human TSC-associated renal angiomyolipoma cells are hypersensitive to ER stress. *Am J Physiol Renal Physiol,* 303**,** F831-44.

SJODAHL, G., LAUSS, M., GUDJONSSON, S., LIEDBERG, F., HALLDEN, C., CHEBIL, G., MANSSON, W., HOGLUND, M. & LINDGREN, D. 2011. A systematic study of gene mutations in urothelial carcinoma; inactivating mutations in TSC2 and PIK3R1. *PLoS One,* 6**,** e18583.

SOLOMON, V. R. & LEE, H. 2009. Chloroquine and its analogs: a new promise of an old drug for effective and safe cancer therapies. *Eur J Pharmacol,* 625**,** 220-33.

SUKHAI, M. A., PRABHA, S., HURREN, R., RUTLEDGE, A. C., LEE, A. Y., SRISKANTHADEVAN, S., SUN, H., WANG, X., SKRTIC, M., SENEVIRATNE, A., CUSIMANO, M., JHAS, B., GRONDA, M., MACLEAN, N., CHO, E. E., SPAGNUOLO, P. A., SHARMEEN, S., GEBBIA, M., URBANUS, M., EPPERT, K., DISSANAYAKE, D., JONET, A., DASSONVILLE-KLIMPT, A., LI, X., DATTI, A., OHASHI, P. S., WRANA, J., ROGERS, I., SONNET, P., ELLIS, W. Y., COREY, S. J., EAVES, C., MINDEN, M. D., WANG, J. C., DICK, J. E., NISLOW, C., GIAEVER, G. & SCHIMMER, A. D. 2013. Lysosomal disruption preferentially targets acute myeloid leukemia cells and progenitors. *J Clin Invest,* 123**,** 315-28.

SULLIVAN, R. J., IBRAHIM, N., LAWRENCE, D. P., ALDRIDGE, J., GIOBBIE-HURDER, A., HODI, F. S., FLAHERTY, K. T., CONLEY, C., MIER, J. W., ATKINS, M. B. & MCDERMOTT, D. F. 2015. A Phase I Trial of Bortezomib and Sorafenib in Advanced Malignant Melanoma. *Oncologist*.

SUN, L., NIU, L., ZHU, X., HAO, J., WANG, P. & WANG, H. 2012. Antitumour effects of a protease inhibitor, nelfinavir, in hepatocellular carcinoma cancer cells. *J Chemother,* 24**,** 161-6.

SUZUKI, T., DAS, S. K., INOUE, H., KAZAMI, M., HINO, O., KOBAYASHI, T., YEUNG, R. S., KOBAYASHI, K., TADOKORO, T. & YAMAMOTO, Y. 2008. Tuberous sclerosis complex 2 loss-of-function mutation regulates reactive oxygen species production through Rac1 activation. *Biochem Biophys Res Commun,* 368**,** 132-7.

TAM, A. B., MERCADO, E. L., HOFFMANN, A. & NIWA, M. 2012. ER stress activates NF-kappaB by integrating functions of basal IKK activity, IRE1 and PERK. *PLoS One,* 7**,** e45078.

TAURA, M., KARIYA, R., KUDO, E., GOTO, H., IWAWAKI, T., AMANO, M., SUICO, M. A., KAI, H., MITSUYA, H. & OKADA, S. 2013. Comparative analysis of ER stress response into HIV protease inhibitors: lopinavir but not darunavir induces potent ER stress response via ROS/JNK pathway. *Free Radic Biol Med,* 65**,** 778-88.

TEE, A. R., BLENIS, J. & PROUD, C. G. 2005. Analysis of mTOR signaling by the small G-proteins, Rheb and RhebL1. *FEBS Lett,* 579**,** 4763-8.

THALER, S., THIEDE, G., HENGSTLER, J. G., SCHAD, A., SCHMIDT, M. & SLEEMAN, J. P. 2014. The proteasome inhibitor Bortezomib (Velcade) as potential inhibitor of estrogen receptor-positive breast cancer. *Int J Cancer*.

THOMAS, S., SHARMA, N., GOLDEN, E. B., CHO, H., AGARWAL, P., GAFFNEY, K. J., PETASIS, N. A., CHEN, T. C., HOFMAN, F. M., LOUIE, S. G. & SCHONTHAL, A. H. 2012. Preferential killing of triple-negative breast cancer cells in vitro and in vivo when pharmacological aggravators of endoplasmic reticulum stress are combined with autophagy inhibitors. *Cancer Lett,* 325**,** 63-71.

TROUT, J. J., STAUBER, W. T. & SCHOTTELIUS, B. A. 1981. Increased autophagy in chloroquine-treated tonic and phasic muscles: an alternative view. *Tissue Cell,* 13**,** 393-401.

UDDIN, M. N., ITO, S., NISHIO, N., SUGANYA, T. & ISOBE, K. 2011. Gadd34 induces autophagy through the suppression of the mTOR pathway during starvation. *Biochem Biophys Res Commun,* 407**,** 692-8.

VAETEEWOOTTACHARN, K., KARIYA, R., MATSUDA, K., TAURA, M., WONGKHAM, C., WONGKHAM, S. & OKADA, S. 2013. Perturbation of proteasome function by bortezomib leading to ER stress-induced apoptotic cell death in cholangiocarcinoma. *J Cancer Res Clin Oncol,* 139**,** 1551-62.

VOELTZ, G. K., ROLLS, M. M. & RAPOPORT, T. A. 2002. Structural organization of the endoplasmic reticulum. *EMBO Rep,* 3**,** 944-50.

WALSBY, E. J., PRATT, G., HEWAMANA, S., CROOKS, P. A., BURNETT, A. K., FEGAN, C. & PEPPER, C. 2010. The NF-kappaB inhibitor LC-1 has single agent activity in multiple myeloma cells and synergizes with bortezomib. *Mol Cancer Ther,* 9**,** 1574-82.

WANG, Z., ZHU, S., ZHANG, G. & LIU, S. 2015. Inhibition of autophagy enhances the anticancer activity of bortezomib in B-cell acute lymphoblastic leukemia cells. *Am J Cancer Res,* 5**,** 639-50.

WATANABE, R., TAMBE, Y., INOUE, H., ISONO, T., HANEDA, M., ISOBE, K., KOBAYASHI, T., HINO, O., OKABE, H. & CHANO, T. 2007. GADD34 inhibits mammalian target of rapamycin signaling via tuberous sclerosis complex and controls cell survival under bioenergetic stress. *Int J Mol Med,* 19**,** 475-83.

WEISS, E. T. & GERONEMUS, R. G. 2010. New technique using combined pulsed dye laser and fractional resurfacing for treating facial angiofibromas in tuberous sclerosis. *Lasers Surg Med,* 42**,** 357-60.

WHITE, E. & DIPAOLA, R. S. 2009. The double-edged sword of autophagy modulation in cancer. *Clin Cancer Res,* 15**,** 5308-16.

WLODAWER, A. 2002. Rational approach to AIDS drug design through structural biology. *Annu Rev Med,* 53**,** 595-614.

WU, Y. T., TAN, H. L., SHUI, G., BAUVY, C., HUANG, Q., WENK, M. R., ONG, C. N., CODOGNO, P. & SHEN, H. M. 2010. Dual role of 3-methyladenine in modulation of autophagy via different temporal patterns of inhibition on class I and III phosphoinositide 3-kinase. *J Biol Chem,* 285**,** 10850-61.

XIANG, T., DU, L., PHAM, P., ZHU, B. & JIANG, S. 2015. Nelfinavir, an HIV protease inhibitor, induces apoptosis and cell cycle arrest in human cervical cancer cells via the ROS-dependent mitochondrial pathway. *Cancer Lett,* 364**,** 79-88.

XIE, L., EVANGELIDIS, T., XIE, L. & BOURNE, P. E. 2011. Drug discovery using chemical systems biology: weak inhibition of multiple kinases may contribute to the anti-cancer effect of nelfinavir. *PLoS Comput Biol,* 7**,** e1002037.

YAN, K. H., LIN, Y. W., HSIAO, C. H., WEN, Y. C., LIN, K. H., LIU, C. C., HSIEH, M. C., YAO, C. J., YAN, M. D., LAI, G. M., CHUANG, S. E. & LEE, L. M. 2013a. Mefloquine induces cell death in prostate cancer cells and provides a potential novel treatment strategy. *Oncol Lett,* 5**,** 1567-1571.

YAN, K. H., YAO, C. J., HSIAO, C. H., LIN, K. H., LIN, Y. W., WEN, Y. C., LIU, C. C., YAN, M. D., CHUANG, S. E., LAI, G. M. & LEE, L. M. 2013b. Mefloquine exerts anticancer activity in prostate cancer cells via ROS-mediated modulation of Akt, ERK, JNK and AMPK signaling. *Oncol Lett,* 5**,** 1541-1545.

YANG, H., RUDGE, D. G., KOOS, J. D., VAIDIALINGAM, B., YANG, H. J. & PAVLETICH, N. P. 2013. mTOR kinase structure, mechanism and regulation. *Nature,* 497**,** 217-23.

YANG, Y., IKEZOE, T., NISHIOKA, C., BANDOBASHI, K., TAKEUCHI, T., ADACHI, Y., KOBAYASHI, M., TAKEUCHI, S., KOEFFLER, H. P. & TAGUCHI, H. 2006. NFV, an HIV-1 protease inhibitor, induces growth arrest, reduced Akt signalling, apoptosis and docetaxel sensitisation in NSCLC cell lines. *Br J Cancer,* 95**,** 1653-62.

YIP, C. K., MURATA, K., WALZ, T., SABATINI, D. M. & KANG, S. A. 2010. Structure of the human mTOR complex I and its implications for rapamycin inhibition. *Mol Cell,* 38**,** 768-74.

YOSHIDA, H., OKU, M., SUZUKI, M. & MORI, K. 2006. pXBP1(U) encoded in XBP1 pre-mRNA negatively regulates unfolded protein response activator pXBP1(S) in mammalian ER stress response. *J Cell Biol,* 172**,** 565-75.

ZHANG, H., CICCHETTI, G., ONDA, H., KOON, H. B., ASRICAN, K., BAJRASZEWSKI, N., VAZQUEZ, F., CARPENTER, C. L. & KWIATKOWSKI, D. J. 2003. Loss of Tsc1/Tsc2 activates mTOR and disrupts PI3K-Akt signaling through downregulation of PDGFR. *J Clin Invest,* 112**,** 1223-33.

ZHANG, M., HE, J., LIU, Z., LU, Y., ZHENG, Y., LI, H., XU, J., LIU, H., QIAN, J., ORLOWSKI, R. Z., KWAK, L. W., YI, Q. & YANG, J. 2015. Anti-beta2-microglobulin monoclonal antibodies overcome bortezomib resistance in multiple myeloma by inhibiting autophagy. *Oncotarget,* 6**,** 8567-78.

ZHANG, Y., NICHOLATOS, J., DREIER, J. R., RICOULT, S. J., WIDENMAIER, S. B., HOTAMISLIGIL, G. S., KWIATKOWSKI, D. J. & MANNING, B. D. 2014. Coordinated regulation of protein synthesis and degradation by mTORC1. *Nature,* 513**,** 440-3.

ZHU, X., ZHANG, J., SUN, H., JIANG, C., DONG, Y., SHAN, Q., SU, S., XIE, Y., XU, N., LOU, X. & LIU, S. 2014. Ubiquitination of inositol-requiring enzyme 1 (IRE1) by the E3 ligase CHIP mediates the IRE1/TRAF2/JNK pathway. *J Biol Chem,* 289**,** 30567-77.

ZONCU, R., BAR-PELED, L., EFEYAN, A., WANG, S., SANCAK, Y. & SABATINI, D. M. 2011. mTORC1 senses lysosomal amino acids through an inside-out mechanism that requires the vacuolar H(+)-ATPase. *Science,* 334**,** 678-83.

8. Appendices

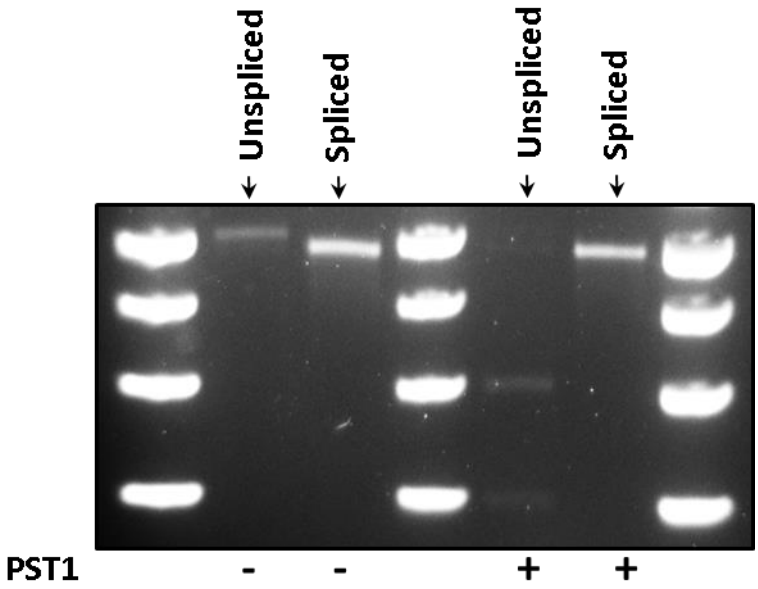

Appendix I: Confirmation of XBP1 spliced and unspliced product using PST1 digest. Spliced and unspliced PCR products were isolated from agarose gels and subjected to either PST1 digest or negative control before re-running on agarose gels for detection of 312 bp and 289 bp products detectable only in unspliced XBP1 extractions.

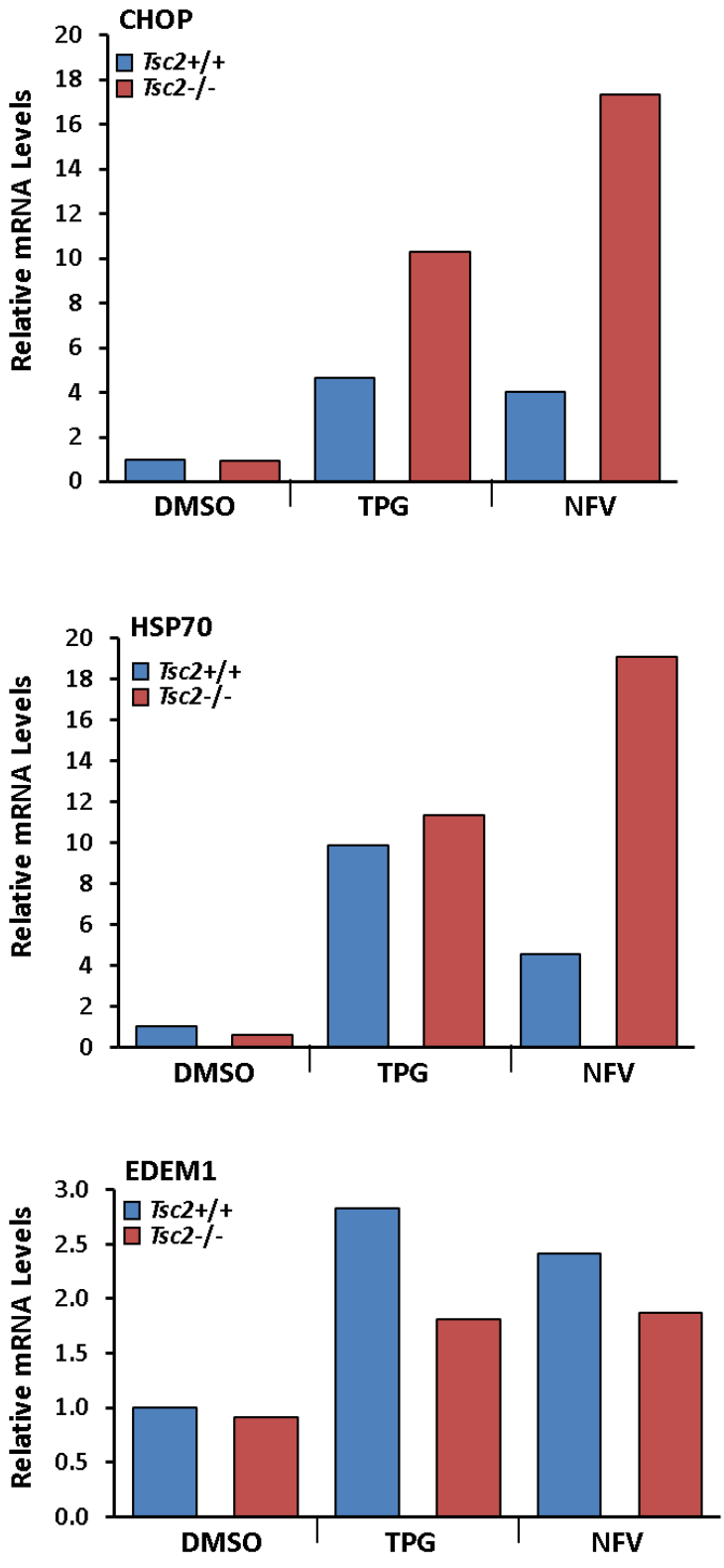

Appendix II: Establishment of CHOP as a reliable mRNA marker for early ER stress detection. *Tsc2*+/+ and *Tsc2*-/- MEFs were treated with either DMSO vehicle alone, 1 µM thapsigargin (TPG), 10µ, 20 µM, or 30µM of nelfinavir (NFV) for 3 h. A) CHOP mRNA, B) HSP70 mRNA, and C) EDEM1 mRNA was analysed and standardised against β-actin. n=1.

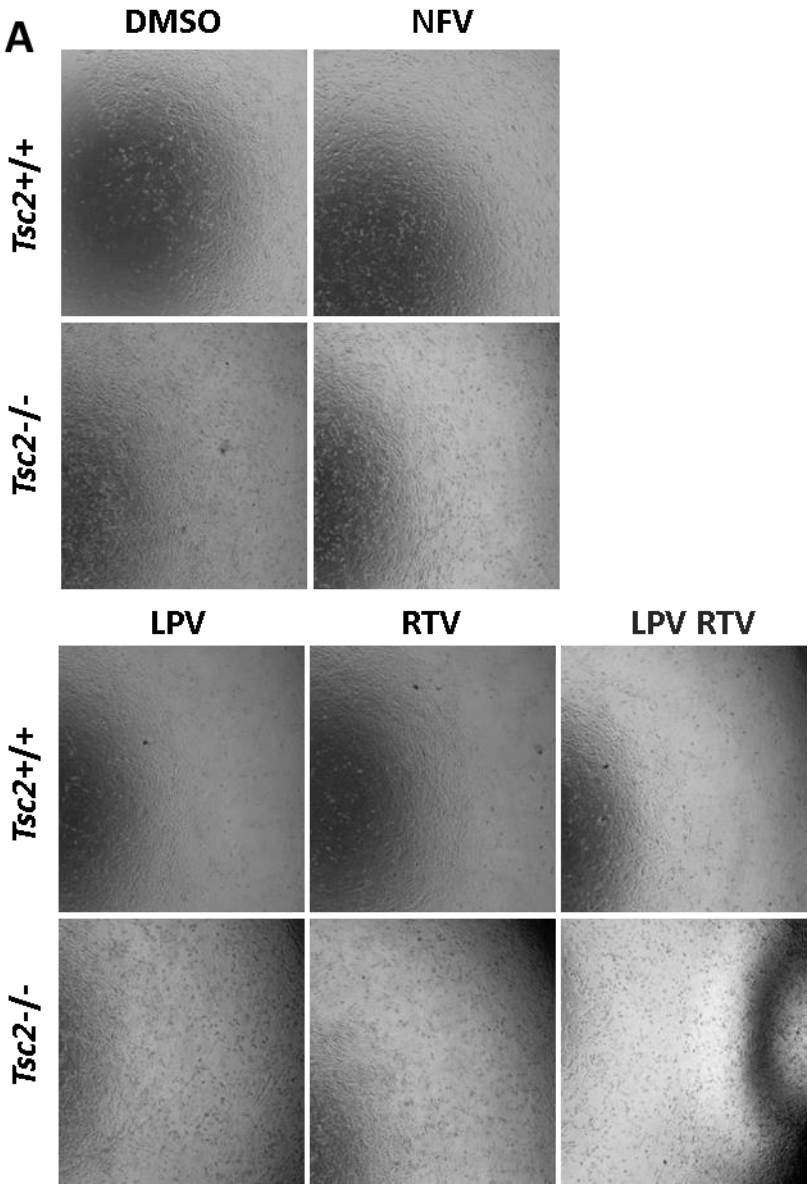
A
DMSO
NFV
Tsc2+/+
Tsc2-/-
LPV
RTV
LPV RTV
Tsc2+/+
Tsc2-/-

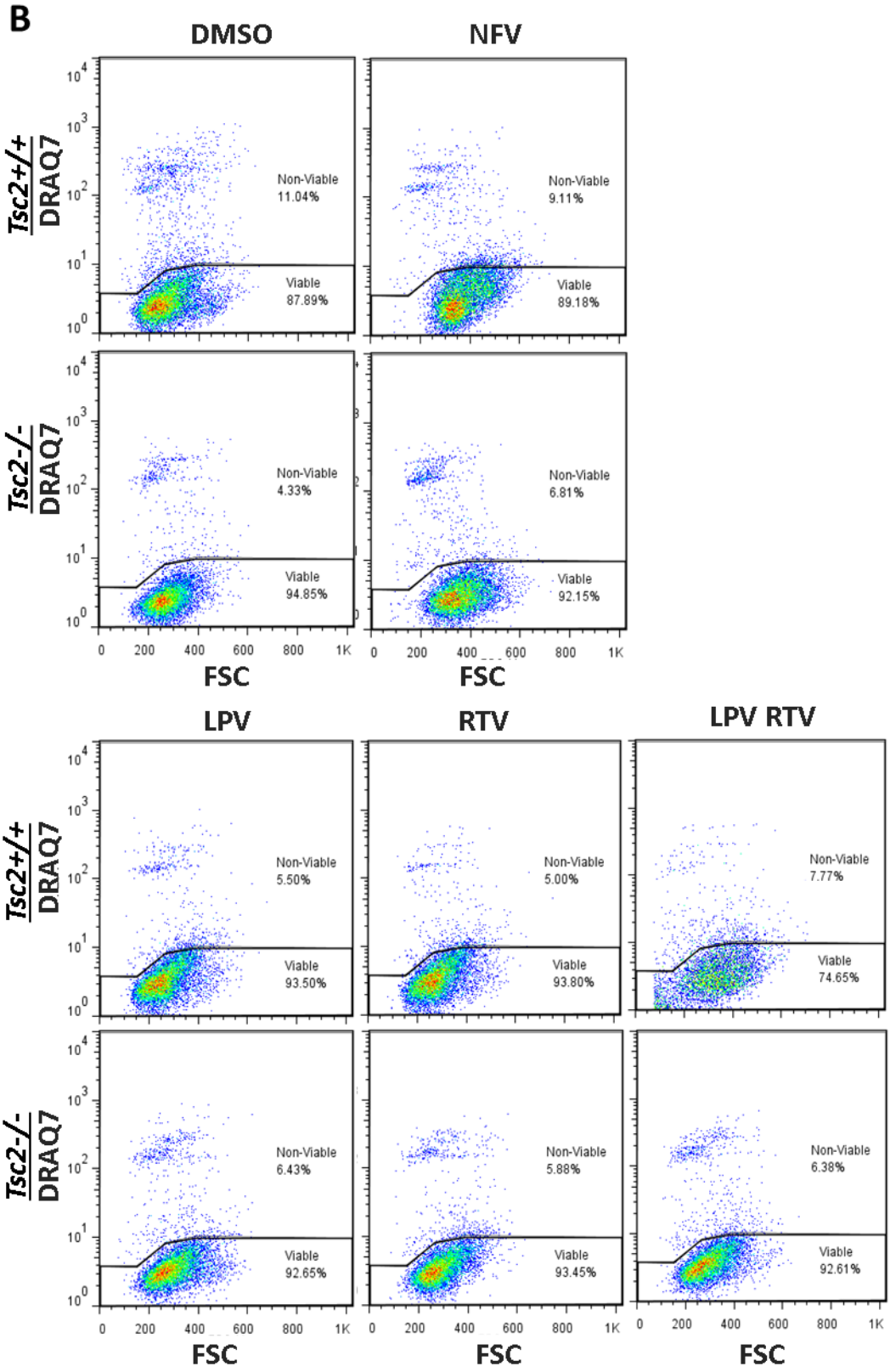

Appendix III: Ritonavir and lopinavir do not induce cell death at 24 h treatment. *Tsc2*+/+ and *Tsc2*-/- MEFs were treated with either DMSO vehicle alone, 1 µM thapsigargin (TPG), 20 µM of either lopinavir or ritonavir for 24 h. A) Phase contrast images were taken at x40 magnification and B) cells were analysed using flow cytometry and DRAQ7 staining. n=1.

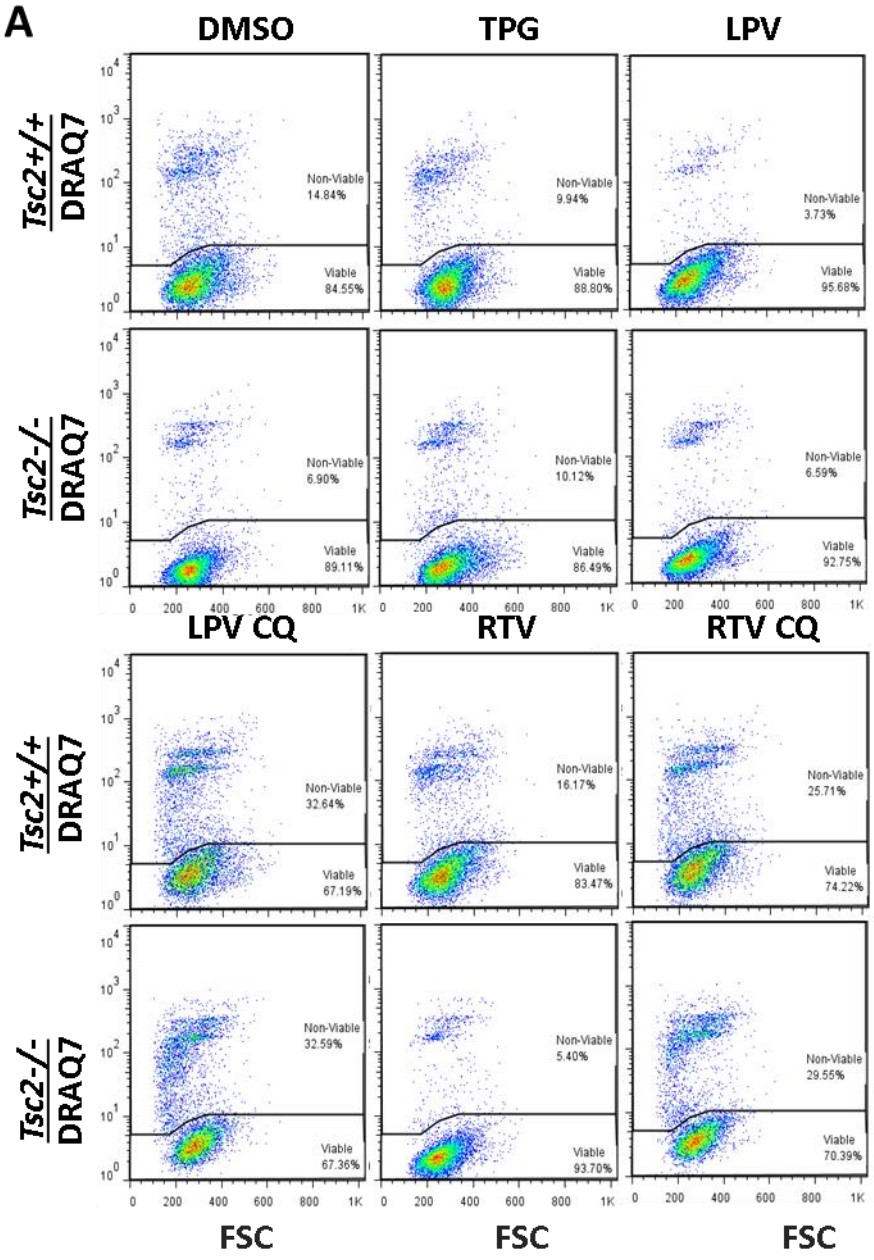
A
DMSO
TPG
LPV
Tsc2+/+ DRAQ7
Tsc2-/- DRAQ7
Non-Viable 14.84%
Viable 84.55%
Non-Viable 9.94%
Viable 88.80%
Non-Viable 3.73%
Viable 95.68%
Non-Viable 6.90%
Viable 89.11%
Non-Viable 10.12%
Viable 86.49%
Non-Viable 6.59%
Viable 92.75%
LPV CQ
RTV
RTV CQ
Non-Viable 32.64%
Viable 67.19%
Non-Viable 16.17%
Viable 83.47%
Non-Viable 25.71%
Viable 74.22%
Non-Viable 32.59%
Viable 67.36%
Non-Viable 5.40%
Viable 93.70%
Non-Viable 29.55%
Viable 70.39%
FSC
FSC
FSC

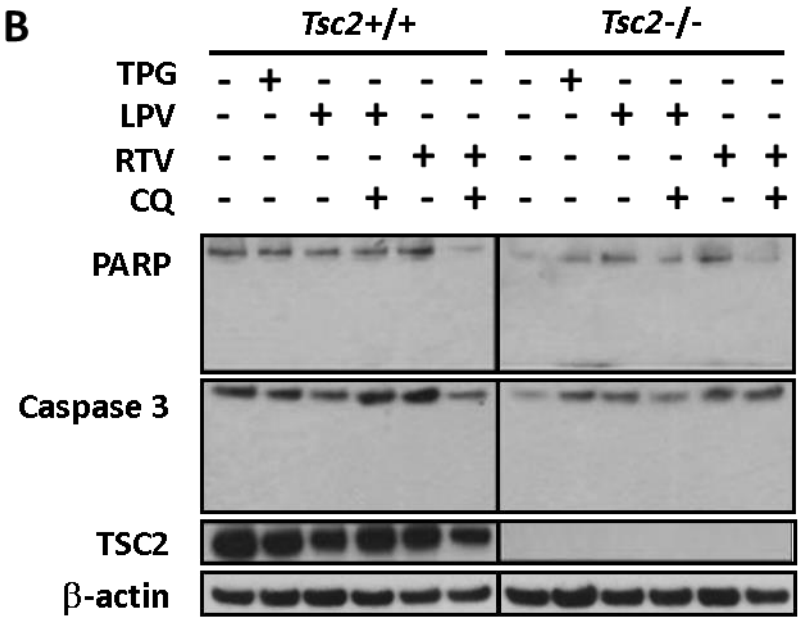

Appendix IV: Lopinavir and ritonavir cause caspase-independent cell death when combined with chloroquine in both *Tsc2+/+* and *Tsc2-/-* MEFs. Tsc2+/+ and *Tsc2*-/- MEFs were treated with either DMSO vehicle alone, 1 μM thapsigargin (TPG), 20 μM lopinavir, 20 μM ritonavir, or combined lopinavir or ritonavir with 20 μM chloroquine for 24 h. Protein extracts were analysed for PARP, caspase-3, TSC2 and β-actin. n=1.

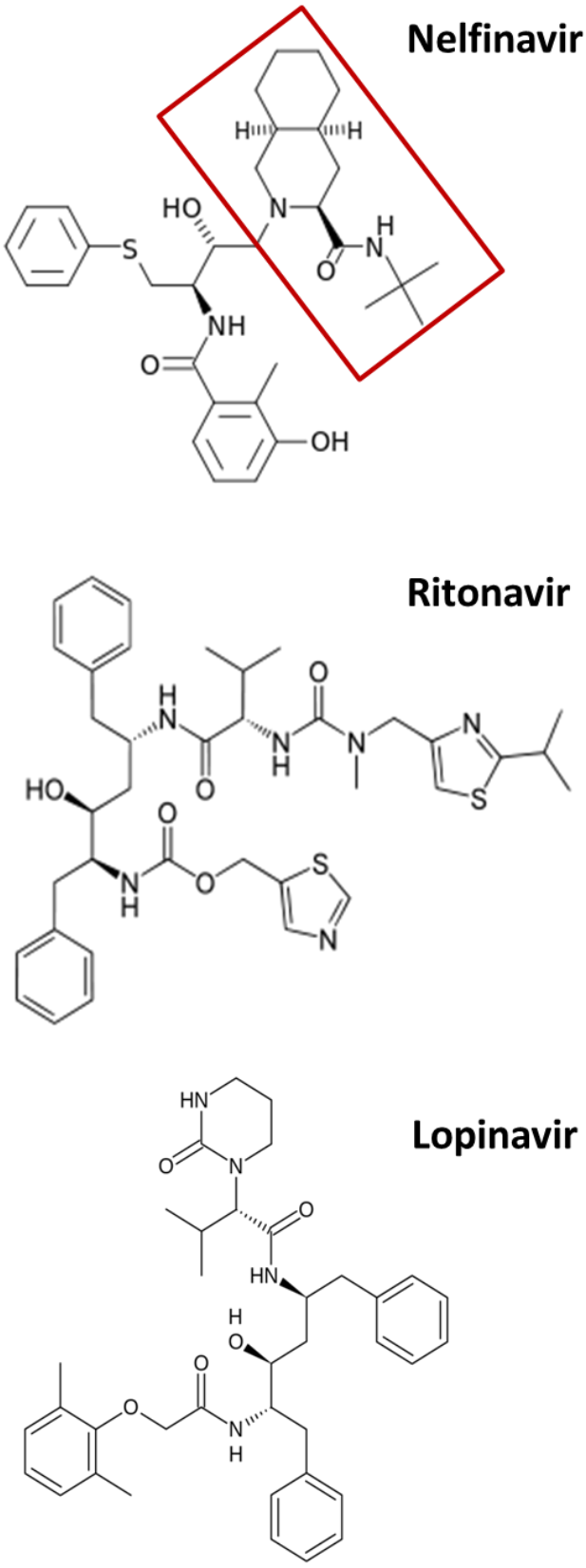

Appendix V: Structure of nelfinavir, ritonavir and lopinavir.

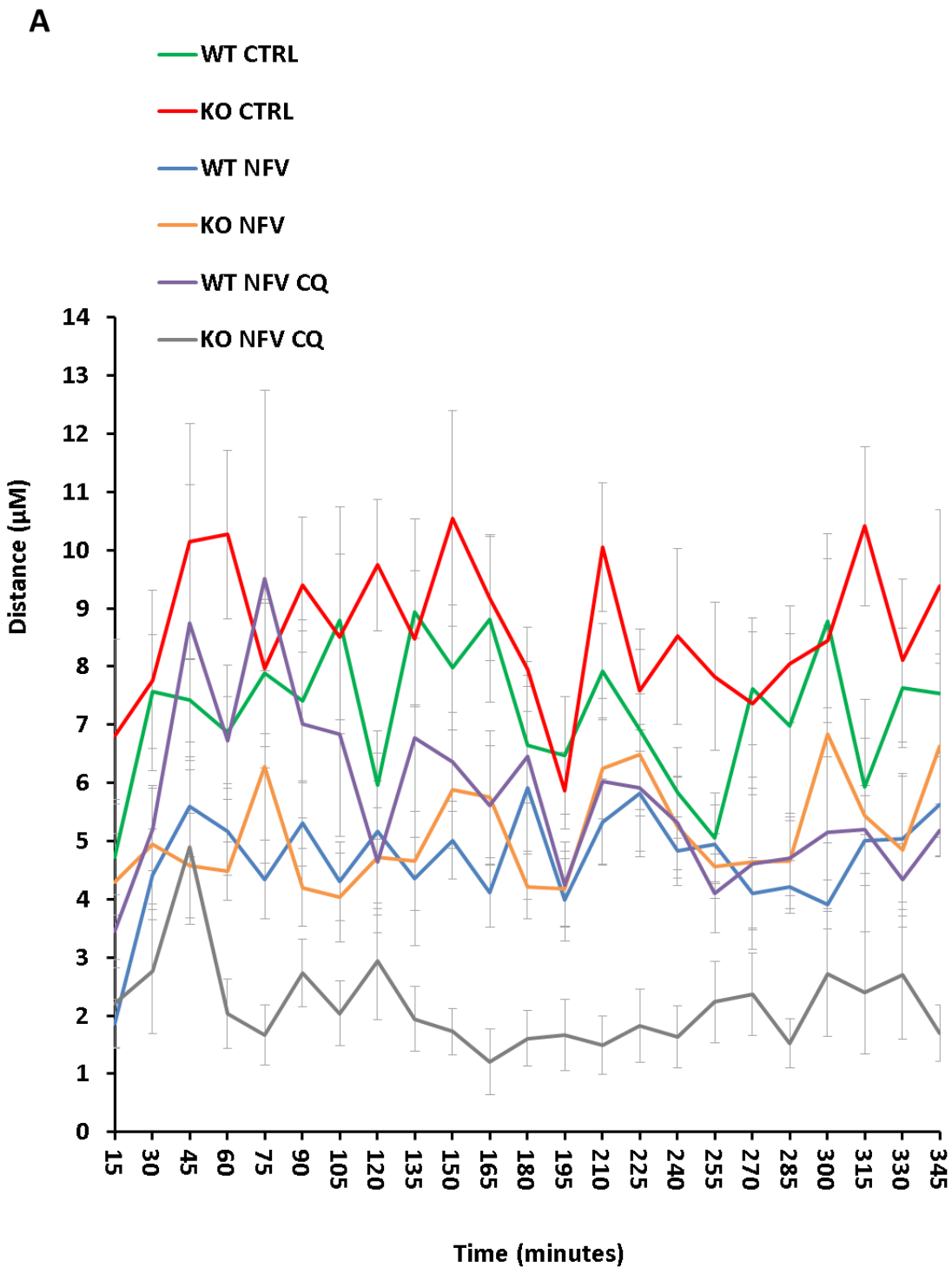
A
WT CTRL
KO CTRL
WT NFV
KO NFV
WT NFV CQ
KO NFV CQ
Distance (µM)
0
1
2
3
4
5
6
7
8
9
10
11
12
13
14
15
30
45
60
75
90
105
120
135
150
165
180
195
210
225
240
255
270
285
300
315
330
345
Time (minutes)

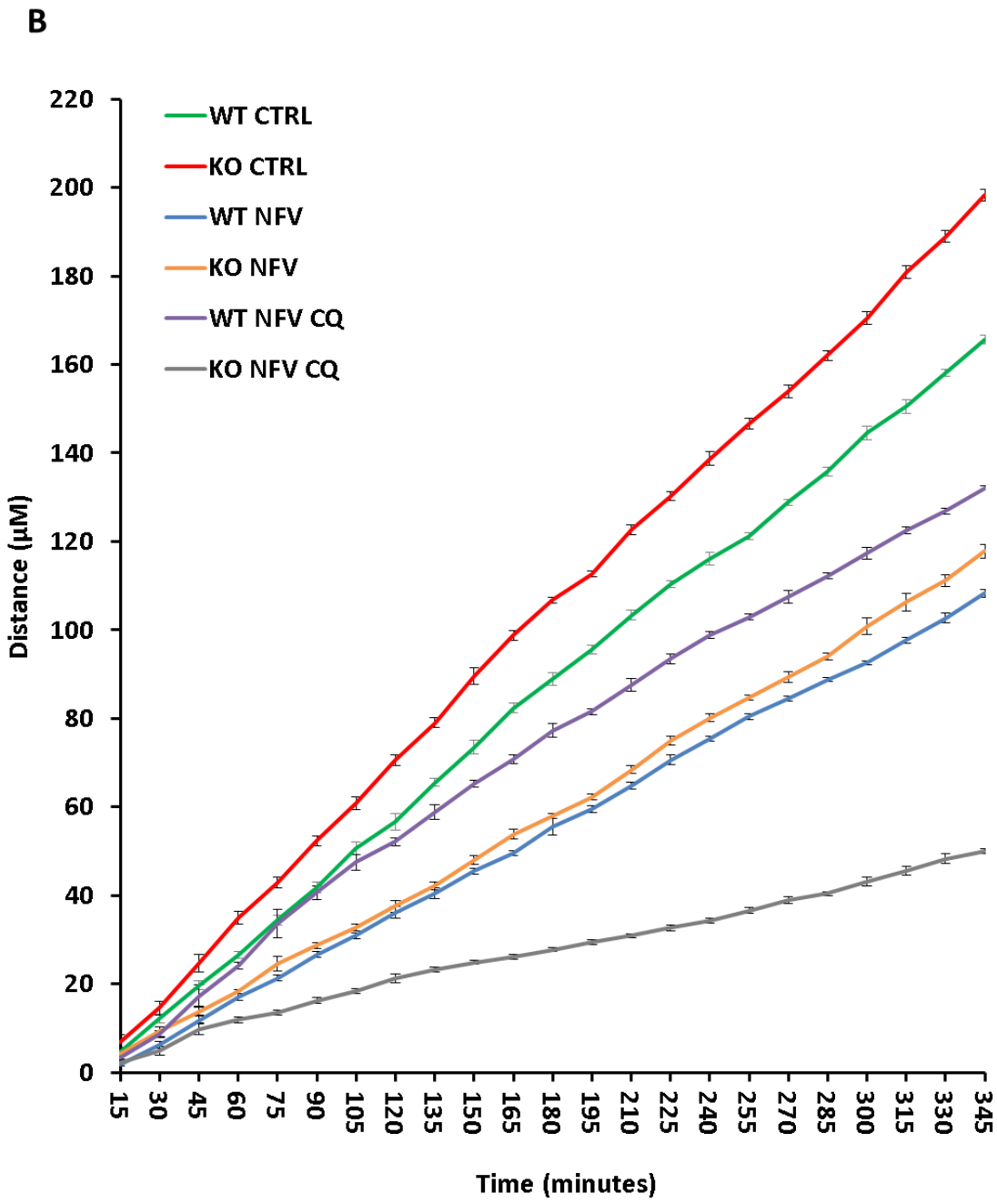

Appendix VI: *Tsc2*-/- MEFs are significantly more motile than *Tsc2*+/+ MEFs, which is reduced with nelfinavir and chloroquine treatment. Movement analysis of MEFs from figure 4.3 was performed between 15 minute intervals over the first 6 h of treatment and is displayed in µM distance moved A) per 15 minute interval, and B) cumulatively over the 6 h period. n=3 ± SEM.

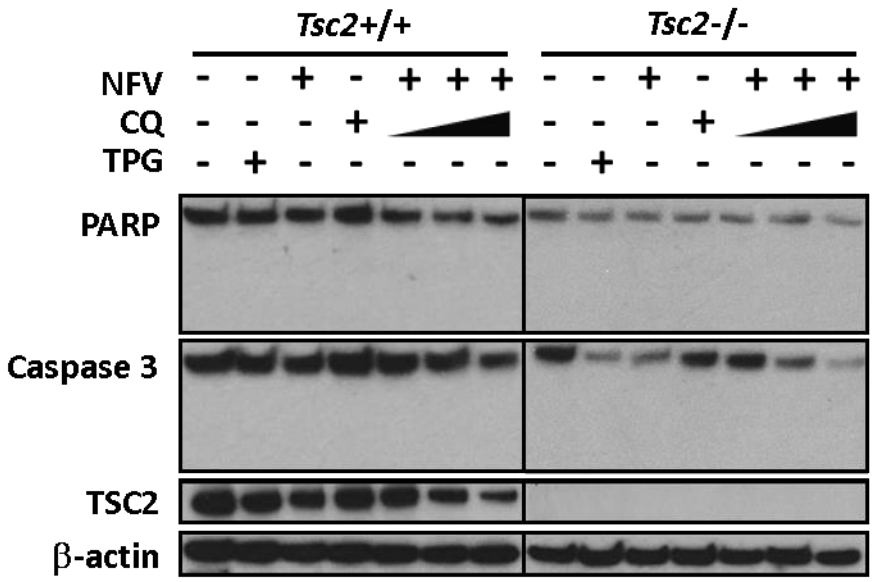

Appendix VII: Combination of nelfinavir and chloroquine does not kill cells through apoptosis, even at higher doses. *Tsc2*+/+ and *Tsc2*-/- MEFs were treated with either DMSO vehicle alone, 1 μM thapsigargin (TPG), 20 μM nelfinavir (NFV), 20 μM chloroquine (CQ) or a combination of NFV and 5 μM, 20 μM or 50 μM CQ for 24 h. A) Protein lysates were analysed for total and cleaved PARP, total and cleaved caspase-3, TSC2 and β-actin. B) Cells were subjected to flow cytometry analysis with DRAQ7 staining.

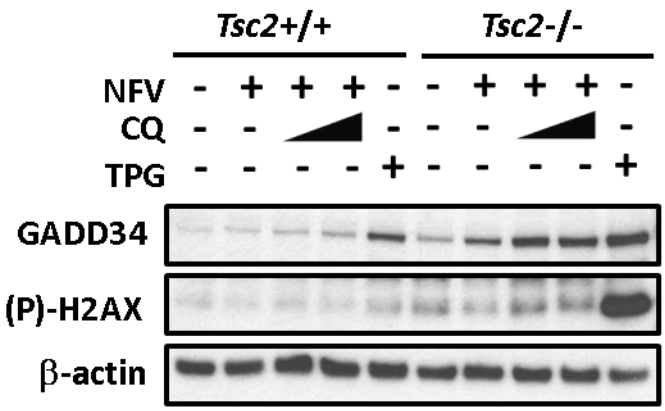

Appendix VIII: Nelfinavir and chloroquine-mediated cell death is unlikely through DNA double strand breaks. *Tsc2*+/+ and *Tsc2*-/- MEFs were treated with either DMSO vehicle alone, 1 μM thapsigargin (TPG), 20 μM nelfinavir (NFV), or nelfinavir combined with either 10 μM or 20 μM chloroquine for 24 h. Protein lysates were analysed for GADD34, phosphorylated H2AX or β-actin. n=1.

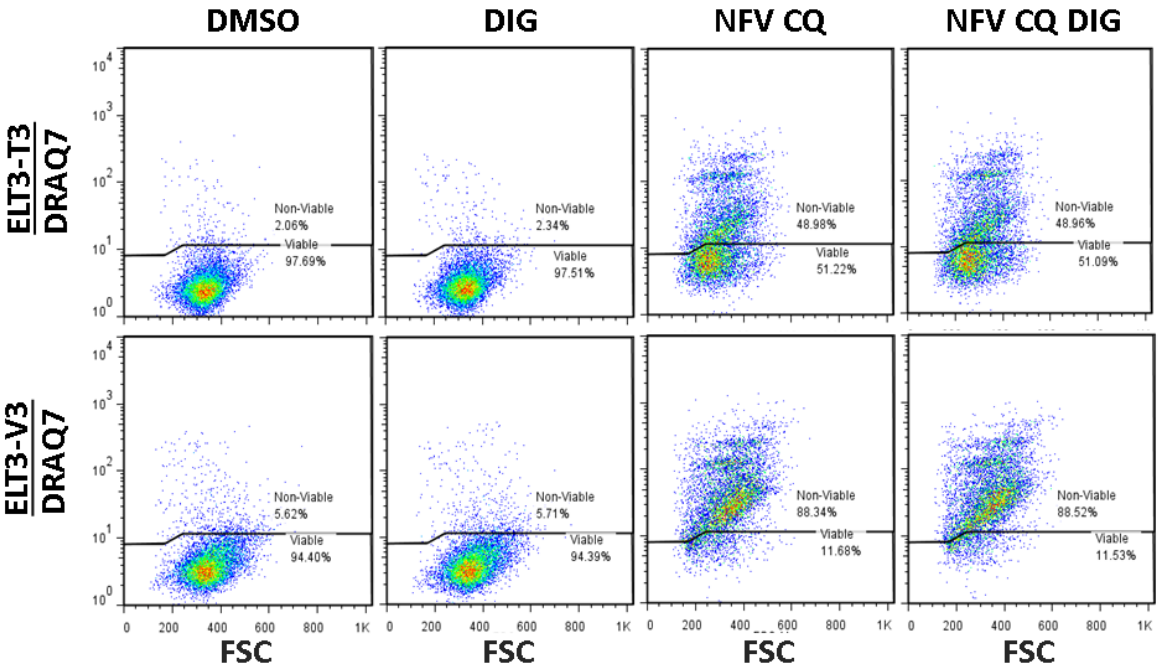

Appendix IVIII: Nelfinavir and chloroquine-mediated cell death is not rescued by Na+/K+ ATPase inhibition with digoxin. ELT3-T3 and ELT3-V3 cells were treated with DMSO vehicle alone, 5 digoxin (DIG), 20 µM nelfinavir (NFV) and 20 µM chloroquine (CQ), or combined digoxin, nelfinavir and chloroquine for 48 h before analysis by flow cyometry with DRAQ7 staining (n=1).

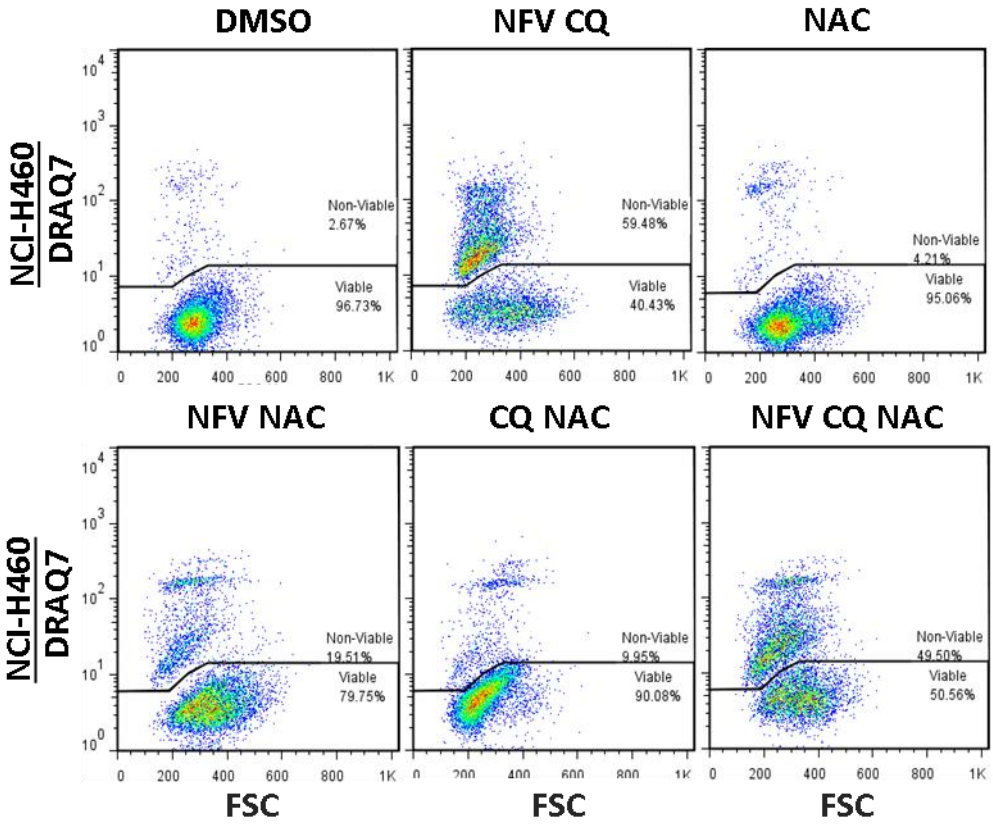

Appendix X: Nelfinavir and chloroquine-mediated cell death is unlikely through ROS in NCI-H460 cells. NCI-H460 cells were treated with either DMSO vehicle alone, 20 µM nelfinavir (NFV), 20 µM chloroquine (CQ), 20 µM N-acetyl-cysteine (NAC) or a combination as shown, for 24 h. Cells were subjected to flow cytometry analysis with DRAQ7 staining (n=1).

Chloroquine

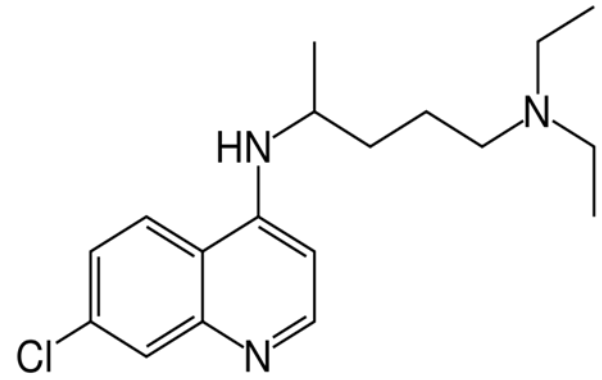

Mefloquine

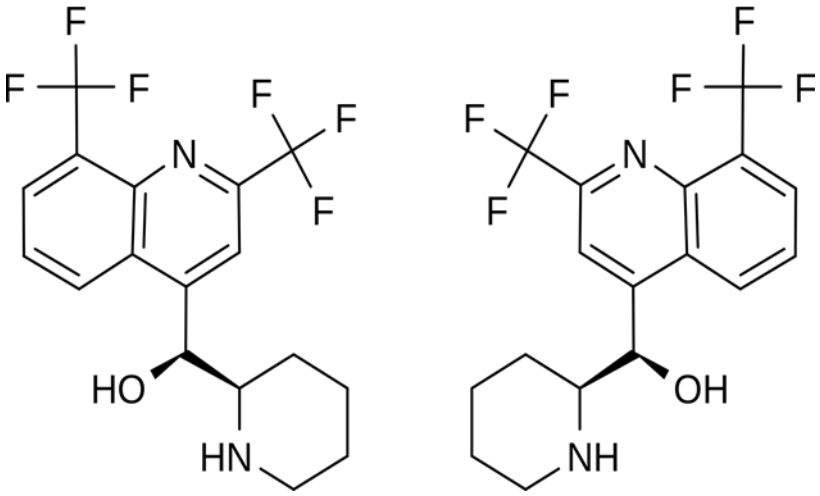

Appendix IX: Structure of chloroquine and mefloquine.

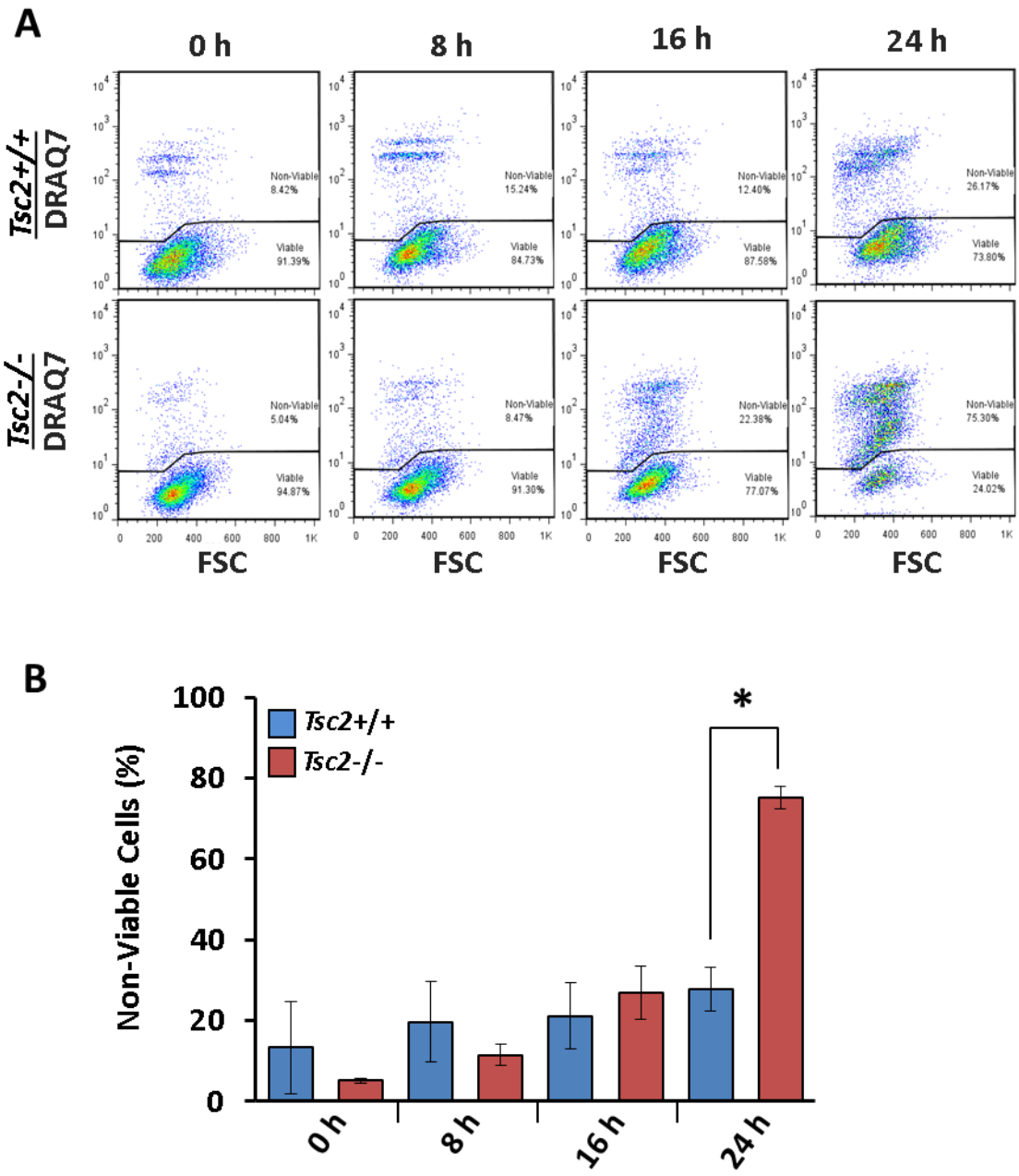

Appendix X: Combined nelfinavir and bortezomib causes significant and selective cell death at 24 h in *Tsc2-/-* MEFs. *Tsc2*+/+ and *Tsc2*-/- MEFs were treated with either DMSO vehicle alone or combination of 20 µM nelfinavir (NFV) and 50 nM bortezomib (BTZ) over 24 h. A) Cells were subjected to flow cytometry analysis with DRAQ7 staining at multiple time points over 24 h. The number of DRAQ7-stained cells are graphed in B. n=3, *P<0.05.